TÉCNICO LISBOA

Comparison of Space Propulsion Methods for a Manned Mission to Mars

André Gomes da Costa Guerra

Thesis to obtain the Master of Science Degree in

Aerospace Engineering

Examination Committee

Chairperson:	Prof. Fernando José Parracho Lau
Supervisor:	Prof. Paulo Jorge Soares Gil
Co-supervisor:	Prof. Orfeu Bertolami Neto
Members of the Committee:	Prof. João Manuel Gonçalves de Sousa Oliveira
	Prof. Jorge Tiago Almeida Páramos

November 2012

Cover photo ("Ariane VA209 liftoff") taken from ESA website: http://www.esa.int/esa-mmg/mmg.pl?b=b&type=I&collection=Launchers&single=y&start=37&size=b

In memory of my grandfather António Gomes...

Acknowledgements

During my college years many people gave me their support and/or transmitted their knowledge. Without them this path would have certainly been much more difficult. Although impractical to mention everyone they all have my truest gratitude.

Firstly I would like to thank my supervisor, Professor Paulo Gil, for his advice throughout the work and his help in reviewing this document. I would also like to thank my co-supervisor, Professor Orfeu Bertolami, for sharing his views with me, and helping me to review this thesis. Without him this project would probably not exist.

Secondly, I would like to show my appreciation to all my teachers. In particular to Professor Ana Mourão, for sharing her ideas, for her help in some of my projects and in particular when I shared my doubts with her, and to Professor Relógio Ribeiro, for his advices during the course and about future endeavours.

I would also like to express my thanks to my friends, and colleagues, for their support, advices and friendship. A special thanks to Ana Carvalho for her patience when listening to all my problems, and doubts, and her advices which have showed to be always accurate. I also have to mention Mariana Mota and Tiago Saúde for their fellowship during my years in Lisbon. Still today both of you have showed to be good friends.

Last but not least, my deep gratitude to all my family for their support during these many years. To my mother, Diana Guerra, for her patience and support during my entire life a huge thank you. Without her continuous incentive none of this would ever be possible. A special acknowledgement to my brother, Diogo Guerra, for his help, his support, his companionship and the numerous hours spent reading the many versions of this document time and time again.

Resumo

Neste trabalho desenvolve-se uma comparação de diferentes sistemas de propulsão no âmbito de uma missão tripulada a Marte. O principal objectivo é minimizar o tempo de viagem, mantendo limitada a massa à partida.

Os sistemas em comparação são o clássico motor químico (CECE), o motor nuclear térmico (NERVA), o motor iónico (PPS 1350-G) e o conceito de "*Pure Electro-Magnetic Thrust*" (PEMT) usando um motor nuclear, proposto por Carlo Rubbia.

A minimização do tempo de viagem é um aspecto importante em naves tripuladas dado que prolongadas exposições ao ambiente espacial causam problemas severos para a saúde, podendo levar à morte.

Uma arquitectura de missão é apresentada bem como um *mass budget* da nave tripulada e de carga, baseados em propostas anteriores de missões para Marte.

A trajectória da nave na partida e chegada aos planetas é calculada usando as órbitas de Kepler. Na fase interplanetária é efectuada uma integração numérica usando os métodos de *Runge-Kutta-Fehlberg*. Todos os cálculos são programados em MATLAB®.

Chega-se à conclusão que o motor iónico associado ao clássico motor químico é a solução que permite tempos de viagem mais curtos com menor massa. Os resultados obtidos com o PEMT sugerem que este poderá ser uma solução mais interessante apenas para destinos mais longínquos da Terra do que Marte.

Palavras-chave: Missão Tripulada, Marte, Propulsão Química, Propulsão Termo Nuclear, Propulsão Eléctrica, Propulsão Electro-Magnética Pura, Trajectória Interplanetária, Motor CECE, Motor NERVA, Motor PPS 1350-G.

Abstract

In this work we develop a comparison of different propulsion systems on a manned mission to Mars. The main objective is the minimisation of travel time, keeping the mass at departure in bounds.

The systems being compared here are the chemical engine (CECE), the nuclear thermal engine (NERVA), the ion engine (PPS 1350-G) and Rubbia's "Pure Electro-Magnetic Thrust" (PEMT) concept, using a nuclear engine.

The minimisation of travel time is an important aspect in a manned spacecraft since long stays in space cause severe health problems and might lead to death.

A mission architecture is developed as well as a mass budget for the cargo and manned spacecraft, based on previous mission proposals to Mars.

The trajectory of the spacecraft at departure and arrival is computed using Keplerian orbits. In the interplanetary phase we use a numerical integration (Runge-Kutta-Fehlberg methods). All calculations are programmed in MATLAB®.

We reach the conclusion that the ion engine combined with the classical chemical engine is the solution which has shorter travel times with the lowest mass. The results obtained using the PEMT suggest it would be a better solution for farther destinations from Earth than Mars.

Keywords: Manned Mission, Mars, Chemical Propulsion, Nuclear Thermal Propulsion, Electrical Propulsion, Pure Electro-Magnetic Propulsion, Interplanetary Trajectory, CECE Engine, NERVA Engine, PPS 1350-G Engine.

Contents

List of Tables

List of Figures

Acronyms & Nomenclature

Acronyms

AODCS Attitude and Orbit Determination and Control System

CECE Common Extensible Cryogenic Engine

CM Command Module

DRM Design Reference Mission

ERV Earth Return Vehicle

ESA European Space Agency

EtM Earth-to-Mars

EVA Extra-Vehicular Activity

HAB Human Habitat Module

ISAS Institute of Space and Astronautical Science

ISRU In-Situ Resource Utility

JAXA Japan Aerospace Exploration Agency

LEO Low Earth Orbit

LEV Lunar Excursion Vehicle

MAV Mars Ascent Vehicle

MEMS Microelectromechanical Systems

MtE Mars-to-Earth

NASA National Aeronautics and Space Administration

NERVA Nuclear Engine for Rocket Vehicle Application

NEXT NASA's Evolutionary Xenon Thruster

NSTAR NASA Solar Electric Propulsion Technology Application Readiness

PEMT Pure Electro-Magnetic Thrust

RK Runge-Kutta

RKF Runge-Kutta-Fehlberg

RTG Radioisotope Thermoelectric Generator

SM Service Module

SMART Small Missions for Advanced Research in Technology

SOI Sphere of Influence

TOF Time of Flight

Greek symbols

β Fractional Burnup

ΔV Change in Velocity [m/s]

ϵ Efficiency

λ Wavelength [μm]

μ Gravitational Parameter [m^3/s^2]

Φ_{rad} Radiated Power [W/m^2]

ρ Density [kg/m^3]

ρ_A Areal Density [kg/m^2]

σ Stefan-Boltzmann Constant = $5.670373e^{-8}\,W/m^2K^4$ [1]

θ_V Angle of Velocity Direction [rad]

θ_{F_T} Angle of Thrust Direction [rad]

ε Emissivity of a Body ≤ 1

Roman symbols

a Semimajor Axis [m]

A_w Atomic Weight

B Total Burnup [GW.d]

b Conjugate Axis [m]

c Light Speed in Vacuum = $299,792,458\,m/s$ [2]

C_3 Characteristic Energy [m^2/s^2]

CH_4 Methane

e Eccentricity

$\vec{F_g}$ Gravity Force [N]

F_T Thrust [N]

g_0 Standard Acceleration due to Gravity = $9.80665\,m/s^2$ [2]

h Angular Momentum [$kg.m^2/s$]

I_{sp} Specific Impulse [s]

LH_2	Liquid Hydrogen
LOX	Liquid Oxygen
M	Mass [kg]
$\dot{m}$	Mass Flow Rate [kg/s]
n_P	Angular Velocity of a Planet [rad/s]
O_2	Oxygen
$\vec{\boldsymbol{r}}$	Position Vector [m]
r	Modulus of Position Vector [m]
R	Propellant Ratio
R^i	Rotation Matrix
$\dot{\vec{\boldsymbol{r}}}$	Velocity Vector [m/s]
V	Modulus of Velocity Vector [m/s]
$\ddot{\vec{\boldsymbol{r}}}$	Acceleration Vector [m/s^2]
S	Surface Area [m^2]
sb	Specific Burnup [GW.d/t]
S_0	Solar Irradiance [W/m^2]
T	Temperature [K]
t	Time
t_w	Waiting Time [s]
$\vec{u}$	Unitary Vector
U	Uranium
^{235}U	Uranium-235 (Uranium Isotope)
^{238}U	Uranium-238 (Uranium Isotope)
UO_2	Uranium Dioxide
v	Volume [m^3]
W	Power [W]
w	Weight [kg]

Subscripts

a	Apoapsis
En	Engine
ex	Exhaust
P	Propellant

Pn	Nuclear Material Propellant
SC	Spacecraft
T	Tank
$\oplus$	Earth
♂	Mars
$\odot$	Sun
x, y, z	Cartesian components

Superscripts

C	Capture
D	Departure
DC	Departure & Capture
HT	Hohmann Transfers
I	Interplanetary
PP	Propellant Payload
RR	Radiator & Reflector
SP	Solar Panels
T	Total
TC	Transport Capsule

Chapter 1

Introduction

1.1 Objectives

In the present work a comparison of the performance of different propulsion systems is developed, in the context of a manned mission to Mars. With the objective of minimising travel time, we use a single mission architecture, while changing the propulsion system implemented. We start with the classical chemical solution, test the nuclear thermal option, analyse the modern electrical propulsion system and end with the proposal of Carlo Rubbia of a pure electro-magnetic thrust, using a nuclear reactor [3].

Mars is the selected destination since it is the next logical step in human exploration of the Solar System, considering that it is the closest body to Earth, other than the Moon, where landing is feasible (discarding Venus due to its harsh environment). Many unanswered questions (some of these dating back to the beginnings of astronomy) have always fuelled humankind curiosity and wonder for Mars. Some of these, most likely, can only be answered if a Human sets foot on Martian soil, e.g. to search for life on Mars (present or past). Another pressing reason for this choice is the extensive research in space missions to Mars that has been undertaken, and serves as comparison to our design.

1.2 Manned Missions

This work focus on a comparison of the propulsion systems. However, this is not independent of the mission design since the comparison is done within a mission to Mars. A research of previous missions and mission proposals to Mars was undertaken to establish a baseline mission architecture, providing also estimates of some mission design drivers (e.g. the mass of the human habitat module).

Many missions have been developed with Mars as a target; these included robotic surface exploration (e.g. NASA's Opportunity and Spirit missions [4]), satellite observation (e.g. ESA's Mars Express mission [5]) and sample return missions (e.g. iMars [6]). However, these types of missions are not suitable as baselines to the present work due to their different aims and most importantly for not being manned missions.

Manned missions have only gone as far as the Moon on the Apollo project, but there are several proposals of manned missions to Mars (which we use to built our mission architecture).

1.2.1 Mars Direct & Design Reference Mission

Among all the mission proposals developed we emphasise "Mars Direct" [7] and "Design Reference Mission" [8].

Mars Direct This proposal was developed by Robert Zubrin in 1990 and it consisted of a 25 billion American dollars (of 1990) program [7]. One of the objectives of the proposal is to use the minimum mass possible with the simplest architecture. It is argued in reference [7] that the total mission mass must be below $1,000\,\mathrm{t}$ and aims to use the technology available at the time. The proposal is comprised of two Saturn V type launchers, one bearing a 45 tonne unmanned cargo module and the other a 25 tonne human habitat module, and a crew of four astronauts per mission. The modules use the chemical upper stage of the rockets to launch to a 180 day transfer to Mars. Upon arrival the modules execute aerocapture (i.e. capture without the use of engines, just using the Martian atmosphere [9]). For the return the crew uses fuel produced from Mars' atmosphere and a chemical engine, executing a direct launch from the surface. Again a 180 day transfer is used. In total the mission takes 910 days to execute.

The mission proposed is composed by the following phases:

1. A launch of the unmanned cargo module which goes to and lands on Mars. Among other components it carries a nuclear powered fuel factory and an Earth Return Vehicle (ERV). After landing, the factory starts producing fuel from the Martian atmosphere.
2. In the next minimum-energy Mars transfer opportunity two more modules are launched, one of which is the human habitat module, HAB. This is done only if everything goes according to plan with the first module. The other launch is another unmanned cargo module, equal to the first.
3. Upon arrival both modules land on the planet's surface. The manned habitat lands near the first cargo module; the second cargo at travelling distance of the habitat, while establishing a new mission site for a future crew.
4. After a year and a half at the Martian surface the crew enters the ERV (fuelled by the nuclear factory) and leaves Mars using a direct transfer to Earth (i.e. the interplanetary injection manoeuvre is performed from the surface).

Some important characteristics of the mission are shown in table 1.1, and the mass budget for both modules in table 1.2. Figure 1.1 is a schematic of Mars Direct program.

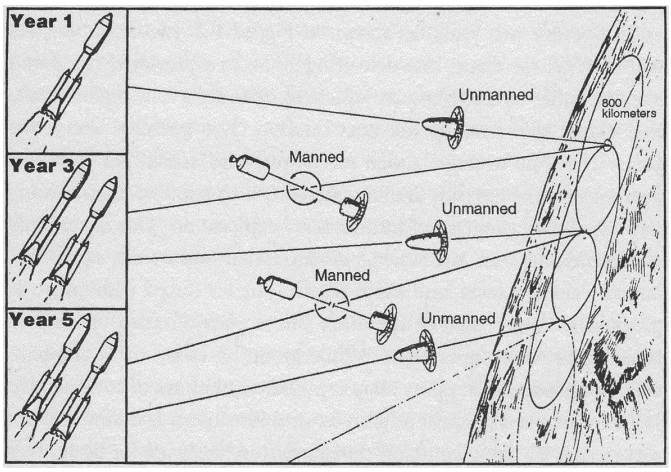

Figure 1.1 Mission sequence for the Mars Direct program [7].

Table 1.1 Characteristics of the Mars Direct mission (data from reference [7]).

Characteristic	Value
Outbound and Inbound Trajectory	180 days each
Mars Stay	550 days
Mission Propulsive ΔV	6.0 km/s
Time of Free Return Trajectory	2 years
Average Mission Radiation Dose	52 rem

Table 1.2 Mass budget of the Mars Direct mission (data from reference [7]).

Earth Return Vehicle	Tonnes	HAB	Tonnes
ERV cabin structure	3.0	HAB structure	5.0
Life-support system	1.0	Life-support system	3.0
Consumables	3.4	Consumables	7.0
Electrical power (5 kWe solar)	1.0	Electric power (5 kWe solar)	1.0
Reaction control system	0.5	Reaction control system	0.5
Communications and information management	0.1	Communications and information management	0.2
Furniture and interior	0.5	Furniture and interior	1.0
EVA suits (4)	0.4	EVA suits (4)	0.4
Spares and margin (16%)	1.6	Lab equipment	0.5
ERV cabin total	11.5	Field science equipment	0.5
Aeroshell	1.8	Crew	0.4
Light truck	0.5	Open rovers (2)	0.8
Hydrogen feedstock	6.3	Pressurized rover	1.4
ERV propulsion stages	4.5	Spares and margin (16%)	3.5
Propellant production plant	0.5		
Power reactor (80 kWe)	3.5		
ERV total	28.6	HAB total	25.2

Design Reference Mission In 1992-1993, in a workshop held at NASA, called Mars Exploration Study, a new proposal was developed for a manned mission to Mars named "Design Reference Mission" (DRM) [10]. Robert Zubrin acting as a consultant had some influence in the final design. This new proposal was built on Mars Direct. It is comprised of four Saturn V type launchers, the first three carrying a cargo lander, an ERV and an habitat lander and the last a manned habitat, and a crew of six astronauts. Each module uses the nuclear thermal upper stage of the rockets as the propulsion system and has a mass range between 60 to 70 tonnes.

The proposal main features are:

1. No need for a launch platform around Earth, e.g. a space station;
2. No need for a lunar outpost;
3. Requires a heavy-lift rocket (e.g. 240 tonnes to Low Earth Orbit);
4. Fast interplanetary transfers and long surface stays;
5. A crew of six elements;
6. Application of the ISRU (In-Situ Resource Utilization) concept;
7. Similar designs for both surface and space habitats.

The first two points were added to the proposal to initiate the "process of expunging the perception that a Mars mission must be conducted in a costly way" [10], which arose from early NASA designs. In particular,

NASA's "90-Day Report" which is a $450 billion American dollars mission, including an assembly of a 1,000 tonnes spacecraft in a space station in Low Earth Orbit (LEO) [11].

1.2.2 A Discussion on the Missions Proposals to Mars

Although at first glance both missions presented seem feasible, they are not without challenges.

The most significant differences between Mars Direct and DRM are the need for four launches per mission in the latter, instead of the two of the former. DRM has an extra two crew members and, instead of a unique Earth Return Vehicle, it has the Mars Ascent Vehicle (MAV) (fuelled by the ISRU factory) and the orbiting ERV (resulting in a rendezvous on Mars between the MAV and the ERV before returning to Earth).

One of the most important drawbacks of these proposals is the mission duration (in particular the 180 day interplanetary transfers). In mission design the human factor is an extremely important aspect and brings the minimisation of the transfer time to the list of top objectives. Space is not a complete vacuum and is a stern environment, as a result of weightlessness and all the electromagnetic radiation and debris. While a person is in space it is subjected to all those hazards which, among other problems, cause loss of bone/muscle mass and an increase in the probability of developing cancer [12–14]. So, even with an expected radiation dose of 52 rem (representing a 0.905% increase of developing cancer for a female astronaut, and a 0.68% for a male astronaut)[7], having 180 day transfers is a great risk, in view of the unpredictability of the solar cycle and the amount of bone/muscle mass that astronauts would lose (whose effects would be felt as soon as they land on Mars). Even around Earth we have not yet tried such a long mission duration.

Another problem present in Mars Direct is the aerocapture at the end of the interplanetary transfer. This option was later scratched in the DRM mission. Martian atmosphere is thinner than Earth's and, albeit it has been already tested for robotic missions, it poses an added risk for a 45 tonne spacecraft. Robotic spacecraft are smaller and can support greater impacts. The human habitat cannot suffer impacts above the human resistance and has bigger dimensions. This would imply that the HAB must start braking at greater speeds (possibly hypersonic) using bigger aeroshells, which is a solution not yet fully understood.

One of the other problems with Mars Direct, that was later diminished in DRM, is the ISRU concept. It is a good idea to have fuel produced on location, since it will save mass when leaving Earth. However, this is an added risk and should only be considered for a later mission, i.e. we should follow Apollo's example and try one step at a time, instead of everything at once.

After the concepts presented above, new mission proposals were developed, as the DRM 5.0 [15] and the "Austere Human Missions to Mars" [16]. These ones are mainly variants of the DRM, with updated technology and including or not options such as ISRU and aerocapture.

1.2.3 Apollo - The Only Manned Mission to Another Celestial Body

Apollo was a series of missions which took a crew of three astronauts to the Moon. The lessons learned constitute a knowledge base for any manned mission that follows.

The mission architecture used was the lunar orbit rendezvous option. It was chosen in detriment of other two options (direct launch and Earth rendezvous). The mission profile was divided into ten different phases (seen in figure 1.2) which were: launch; Earth parking orbit; Earth to lunar transit (and lunar to Earth transit); entry into lunar orbit (and departure from it); operations in lunar orbit; descent and landing on the Moon; surface operations; ascent from the Moon surface; lunar rendezvous; and Earth re-entry [17]. Although it seems

more complicated, and hazardous, it was designed to have the lowest mass upon launch, thus making it "highly attractive in engineering and cost terms" [17].

The idea was to discard every component as soon as it had fulfilled its function. For example, instead of landing the entire spacecraft on the Moon, only a lunar module (or lunar excursion vehicle, LEV, seen in figure 1.2) performed the landing, and it was discarded upon returning the astronauts to the mother ship (the command and service modules). Even the LEV was optimised and divided into: the descent stage, which performed the landing and remained on the surface (constituted by the main engine, fuel tanks and landing gear); and the ascent stage, with the crew quarters, a small rocket (with its fuel tanks), four thruster packages and all the paraphernalia needed to perform the surface mission. During the entire Apollo project this module weighted from 13,941.2 kg to 16,448.2 kg (from Apollo 9 to Apollo 17 missions) [18]. As stated in David Woods book: "The result was a remarkable manned spacecraft that was perhaps aesthetically ugly, yet whose form was well matched to the function it had to perform." [17].

Apart from the LEV the Apollo spacecraft had a command module (CM) and a service module (SM), also seen in figure 1.2. The CM carried the crew to the Moon and back, and was used also for Earth re-entry. It weighted 5,556.5 kg to 5,839.6 kg [18]. The SM served as support for the command module, and had a chemical propulsion system, a reaction control system and fuel cells. It weighted a maximum of 24,522.6 kg, where 18,412.7 kg was propellent, on the Apollo 15 mission [18].

Apollo had a circular parking orbit of 170 to 185 km high, with a lifetime of almost three hours. This is an important aspect when performing a manoeuvre like the translunar injection since it is best to be as close to the central body as possible in order to save fuel. Having a parking orbit also allowed astronauts to perform checkouts to the spacecraft.

Another important aspect of the mission is the forces felt by astronauts. During most of the time astronauts were in a weightlessness environment. The only times the crew was subject to the acceleration/deceleration forces were during launch, from landing to departure from the Moon, and finally in the re-entry. The peak occurred during the latter, when accelerations could reach 7.19 g [17]. During the re-entry the spacecraft command module was travelling at a velocity of 7 km/s, which led to the formation of a shock wave ahead of the module and the heating (and subsequently ionization) of the gases around it.

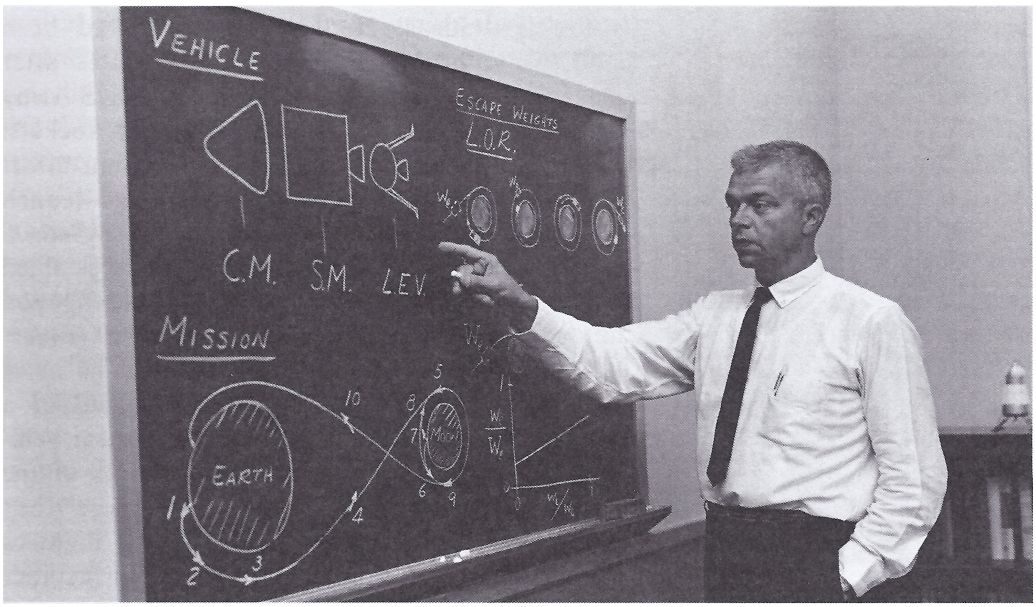

Figure 1.2 John Houbolt explaining the Lunar Orbit Rendezvous mission architecture [17].

1.3 Spacecraft Propulsion Types

Travelling in space usually means determining an optimum trajectory that reaches the target using the available propulsion. Trajectories improvements (including the possibility of having less travel time) are usually bound to propulsion advances. Several types of propulsion systems have been used in different missions [9, 19–22]. From the conventional chemical engine, passing through the electrical, to new state-of-the-art solar sails we have a wide range of propulsion systems already at our disposal or in the near future.

Before discussing the available propulsion types, we introduce some useful concepts.

F_T **- Thrust** The thrust is obtained from a momentum analysis to an engine, using Newton's 2nd and 3rd laws. Integrating the equations for an engine expelling a fluid with a velocity V_{ex} and with a pressure p_e, we obtain the expression for thrust

$$F_T = \dot{m}V_{ex} + A_e(p_e - p_a), \tag{1.1}$$

where $\dot{m}$ is the fuel rate, A_e the exit nozzle area and p_a the ambient pressure [19]. The term $A_e(p_e - p_a)$ can be neglected for $p_e \approx p_a$.

$\mathbf{I_{sp}}$ **- Specific Impulse** The specific impulse is used as a comparison factor between engines. It depends only on the fluid exhaust velocity (V_{ex}), which is an intrinsic characteristic of the engine. One of the main reasons for the importance of $\mathrm{I_{sp}}$ is its unit, seconds, which is transversal to the system of units in use [19]. From the definition of specific impulse (as the impulse given by unit weight of propellant) we can derive

$$I_{\mathrm{sp}} = \frac{F_T dt}{\dot{m} g_0 dt} = \frac{V_{ex}}{g_0}, \tag{1.2}$$

where g_0 represents the standard acceleration of gravity on Earth's surface.

From the above formulae we can extract the relation between thrust and $\mathrm{I_{sp}}$ (for $p_e \approx p_a$)

$$F_T = \dot{m} g_0 I_{\mathrm{sp}}. \tag{1.3}$$

F_T/w **- Thrust-to-Weight Ratio** The thrust-to-weight ratio is an also important concept when comparing different systems [19]. When an engine is working it propels the mass of the spacecraft plus its own mass. One aims to have the minimum engine mass so to have the maximum velocity change, assuming that the mass of the spacecraft is fixed. One maximises then the coefficient F_T/w, to have a larger thrust for the minimum weight of the engine.

1.3.1 Chemical Propulsion

Chemical propulsion is one of the most developed method of space propulsion, and the first to be used in extraterrestrial exploration. The usual chemical engine is comprised of fuel tanks, a combustion chamber, a nozzle and all the paraphernalia linking those components [19].

The propellants, usually a fuel (liquid hydrogen, LH_2) and an oxidant (liquid oxygen, LOX), are combined in the combustion chamber and undergo a chemical combustion reaction. The products of the reaction expand and are expelled through the nozzle. The high pressure and the velocity at which the gases are expelled produces the thrust, as can be seen by equation (1.1).

Engines using LH_2 and LOX as the fuel and oxidant are classified as cryogenic systems (since both propellants must be kept at cryogenic temperatures). The combustion reaction of these engines is very efficient and yields

thrusts of the order of the hundreds of kilo newton, with values of specific impulse exceeding 460 s [9]. For the present work only cryogenic systems are considered.

Other types of chemical engines are:

- Storable systems - Which use a nitrogen tetroxide oxidiser combined with a hydrazine (or a dimethyl hydrazine) as the fuel. Although they can be easily stored, they are toxic and corrosive. This type can only have a I_{sp} less than 330 s, and thrust from the tens to hundreds of newton [9].
- Monopropellant systems - This type of engines burns a hydrazine fuel which makes them simpler but with a specific impulse of less than 220 s (or simply expels a pressurised gas yielding a specific impulse of 70 s) [9].
- Solid propellant systems - Usually have a solid propellant (fuel and oxidiser) on a cylinder with a central hole (which controls the burn rate). The specific impulse of these systems are of the order of 250 s, with very high thrusts [9]. However, this type of systems can only be used once since the reaction cannot be stopped.

Due to their relatively low I_{sp} (compared with other methods) chemical engines are normally use as impulsive ones, i.e. it is assumed that the velocity change is condensed in a single moment. To have such engines (with I_{sp} commonly lower than $1,000$ s) to work for long periods of time implies a theoretical fuel expenditure too great. Another reason for using chemical engines in this manner is the gravity loss. Gravity losses occur when the spacecraft is not at the optimal position for the manoeuvre, and the velocity vector does not have the optimal direction. The amount of gravity loss is directly proportional to the time it takes to execute a manoeuvre, increasing the real fuel expenditure.

1.3.2 Nuclear Thermal Propulsion

Nuclear engines have been developed since the 1940s, although the idea had already been presented in the beginning of the twentieth century. There were even suggestions to include a nuclear upper stage, on the Nova rocket, for the lunar direct launch mission [19].

The principle is similar to chemical engines. A single propellant, usually hydrogen, is heated by the nuclear core and is expelled through a nozzle while expanding. The core, usually an uranium derivative (like dioxide or carbide) or plutonium, releases heat due to the nuclear reaction, which is limited by the melting point of the materials [9].

A quantity defining nuclear fuel performance is the burnup. This is defined as "The total energy released in fission by a given amount of nuclear fuel" [23]. A derivation of this is the specific burnup, which is the energy per unit mass (GW.day/tonne or simply GW.d/t). The maximum theoretical burnup of a ^{235}U fuel has a value of 950 GW.d/t. In nuclear power plants reactors usually only 1% of the nuclear fuel is transformed into energy [23, 24].

This type of engines have a higher I_{sp} and thrust when compared to chemical ones. However, due to political and environmental concerns, they have never been used for space missions and only ground tests were conducted. Several engines, within the Nuclear Engine for Rocket Vehicle Application (NERVA) program of NASA, were designed, constructed and tested until its end in 1972.

These engines are used as impulsive ones, due to their high thrust and $I_{sp} \approx 900$ s.

1.3.3 Electrical Propulsion

As stated above, chemical engines use the propellants as the energy source (through the chemical reaction) and, at the same time, to produce the thrust. When combining both functions, working fluid and energy source, the thrust and exhaust velocity are limited by thermodynamic relations of the propellants [19]. Electric propulsion overcomes this limitation by acquiring the energy by other means, separating the working fluid from the energy source.

Common sources of energy are solar, nuclear power generation and radioisotope thermal generators (RTG) [9]. Solar power is limited by the efficiency of current technology to convert solar energy into electrical power and where it is used (since solar energy is proportional to the inverse square of the distance from the Sun). Nuclear power systems do not present those limitations but represent a large increase of engine mass. The RTG technology can only achieve specific powers of 5 W/kg and is still being perfected [9].

There are three main types of electrical engines. The first is the gridded ion thrusters, whose principle is to accelerate ions through an electrical field maintained by two grids. Ionised Xenon is the propellant typically used. These engines have values of thrust from the 10 to 200 mN, having I_{sp} greater that 3,000 s [9].

The second engine is the so called Hall-effect thruster. It uses a rotating plasma which, due to the configuration of the engine, creates an electrical-magnetic field accelerating the propellant. Usually the forces produced are in the order of 100 mN, and a specific impulse of 1,500 s.

The other type of engine is the arcjet. These engines commonly use hydrazine heated by an electric arc discharge. This configuration is capable of greater thrusts (1 N) but have lower I_{sp} ($\approx$ 500 s) [9].

The thrust produced is then very small when compared to chemical engines, limited by the power supplied to the engine. As stated in reference [9] "achieving a twin objective of high specific impulse and high thrust is a particularly demanding task in terms of the energy that must be imparted to the propellant". However, these greater I_{sp} allow the engine to be running for longer periods of time with less fuel. To achieve the same velocity increment as the chemical engine, the electrical one does not use the impulsive approximation and are treated as non-impulsive engines.

Missions With Electrical Propulsion

Some missions already use non-impulsive technology. For example, the Deep Space 1 of NASA and the SMART-1 (Small Missions for Advanced Research in Technology) from ESA used the ion propulsion as the primary technology [25].

SMART-1 was a mission to the Moon launched on the 27th of September 2003. Its trajectory was very complex due to the low thrust these systems provide [25]. Deep Space 1 was launched earlier, in 24th October 1998. The purpose of the mission was also to test several technologies. It flew by Mars-crossing near-Earth asteroid 9969 Braille, in 1999, and by the comet Borrelly in 2001.

1.3.4 New Concept Engines

New types of engines, using revolutionary concepts, are constantly being presented. For instance Electrodynamic Tethers, MagSails, Plasma Sails and Solar Sails [22]. Electrodynamic Tethers uses the interaction between Earth's magnetic field and an electrical cable to produce thrust. MagSails and Plasma Sails produce a magnetic field that interacts with the solar wind ions. MagSails are also being proposed to be applied as a protection shield for astronauts in deep space missions.

The Solar Sail concept has already been tested with some success in laboratory and in space by NASA, ESA and by the Institute of Space and Astronautical Science (ISAS) mission of the Japan Aerospace Exploration Agency (JAXA) [9, 22].

Other types of propulsion aim to alter or control gravity. However, it has been shown even if gravity could be controlled for propulsion purposes, the gain will be minor when compared to current chemical options [26, 27]. Other systems use existing concepts like the "magnetized ion plasma system" [28], which separates the engine from the payload, or the "MicroThrust" project [29], which aims to reduce the system mass and size using microelectromechanical systems (MEMS).

The method to be examined in the present work is the "Pure Electro-Magnetic Thrust" (PEMT) [3], presented in 2002 by Carlo Rubbia. This engine produces thrust as a Solar Sail but uses a nuclear reactor as the power source.

Solar Sail Thurst Principle The Solar Sail uses the sunlight (photons), which can be considered constant along the year, to produce thrust. Photons have a dual particle-wave nature, and a photon with a frequency ν, moving at the speed of light c, has an energy (E_p) and a momentum (P_p):

$$E_p = h\nu = cP_p \quad \Rightarrow \quad P_p = \frac{h\nu}{c},$$

where h is Planck's constant [3]. Momentum conservation implies that: if a photon is absorbed by a surface it transfers its momentum to it; if it is emitted it also transfers a momentum to the source with the same magnitude (in the opposite direction); and if it is reflected, after hitting the surface with an angle α with respect to the normal vector of the surface, the momentum gained by the surface is $2P_v \sin\alpha$. Applying this to photons in a parallel beam ($P = \sum P_v$) and the Newton's 2nd law ($F = \frac{d}{dt}(P)$), yields

$$F = \frac{d}{dt}\left(\sum P_v\right) = \frac{1}{c}\frac{dE}{dt} = \frac{W}{c}, \tag{1.4}$$

for the case of a source of photons with power W (or an absorbing surface which absorbs a beam of power W).

As the power of sunlight decreases with the distance (and even at Earth it has a maximum of about - 1.8 W/(m^{2}nm) at the wavelength of 500 nm [22]) the sail needs to have a large area and a low weight (withstanding at the same time high temperatures). Current technology allows for the construction of 0.0013 mm thick sails (ten times thinner than kitchen's aluminium foil) with densities of 10 g/m^2 (accounting also for the support structure) [22].

1.4 Work Methodology

In this work we use a spacecraft and a mission architecture similar to the ones used in the Mars Direct and DRM respectively. The results presented here are then derived for a particular mission architecture and spacecraft (since the propulsion system cannot be separated from the mission design, as seen in section 1.2). The mission discussed here has the following guidelines:

Given that public support and budget allocations for space missions is diminishing, a manned mission to a another celestial body might alter the situation. The target proposed is Mars, due to its scientific importance and constant presence in humanity collective imagination. Astronauts must perform a safe trip to the target body and take advantage of the time spent in space and in the planet surface to perform scientific experiments.

The work started with a review of previous missions and mission proposals to Mars and of the Apollo program. We also examine which of the propulsion systems are more suitable for a manned mission. The studied concepts are a chemical engine, a nuclear thermal engine, an electrical engine and a new concept engine, the PEMT (see chapter 2).

In chapter 3 the mission timeline is discussed. As stated, this is an adaptation of the DRM study, with the inclusion of the electrical or PEMT engine on the interplanetary transfer. The primary objective is the minimisation of travel time, with the minimum mass as a secondary objective. Having established how the mission could be performed, a baseline dry mass budget is fixed. This mass is transversal to all alternatives and has the propulsion system as the unknown. For each spacecraft configuration (types and number of engines) the constant parameters are the initial and final orbits. The variable parameters are:

- Departure velocity from the planet;
- Angle of this velocity relative to the planet's velocity;
- Angle of thrust:
  - Relative to the velocity vector;
  - Relative to the heliocentric coordinate system.
- Brake location.

The problem of spacecraft trajectory computation is then considered (chapter 4). This trajectory is simplified assuming that all movement occur at the same plane and the planets are in circular orbits. A patch conic approximation, dividing the mission in three main phases for each leg (Earth to Mars and Mars to Earth), is performed. In the departure and capture phases the Keplerian orbits were used. The interplanetary phase is always computed through numerical integration of the equation of motion.

Finally, the results are analysed and a comparison chart of the different options is presented in chapter 5. The optimum point, for each mission and configuration, is found through a weighted sum of the transfer time and the spacecraft total mass.

Chapter 2

Propulsion Systems For a Manned Mission to Mars

In this chapter the propulsion systems to be studied are presented, along with their main characteristics. The selected engines represent the higher I_{sp}, thrust and thrust-to-weight ratio among the various types of engines available, since the main objective is to minimise the time to reach Mars. We consider engines currently being tested and with flight proven capabilities. We also include engines under development since we want to test their performance in a concrete mission.

2.1 Impulsive Systems

2.1.1 Classical Chemical Engines

Vinci The Vinci engine is being designed for the upper stage of the Ariane 5; it is planned to be operational for flight in 2016.

It uses cryogenic propellants and is re-startable up to five times. Instead of a normal turbo-pump system (with a gas generator to power the pumps that inject the fuel), it is built with an expander cycle (the cooling hydrogen passes through the turbines, powering the pumps, before being injected in the combustion chamber) [30].

RL10B-2 The RL 10 engine has been used since 1963 in the United States. The latest model is the RL10B-2, which is implemented on the Delta IV launch vehicle [31].

The RL 10 is a re-startable engine and was optimised for use in a vacuum environment. One of its particular features is the capability of using methane as the fuel [19]. This is a bonus for Mars exploration supporters, since it is argued that it is possible to produce methane from Mars atmosphere, thus lowering initial spacecraft mass [7].

CECE The Common Extensible Cryogenic Engine (CECE) is currently being developed and tested by Pratt & Whitney Rocketdyne. Although it has already accumulated $5,000\,\mathrm{s}$ of hot-fire time [32], it has not yet been launched.

This engine is considered an evolution of the RL 10. It has improvements at the injector and propellant feed technology, and is aimed at being the support for lunar and in-space mission applications (from 2020 and beyond [32]). The CECE has the capability to re-start up to fifty times and, as the RL 10, has the possibility of using LOX/CH_4 (with a decrease in I_{sp} and thrust) [33].

Table 2.1 shows the main characteristics of the engines considered.

Table 2.1 Classical chemical engines characteristics.

Engine	Propellants	Propellant Ratio	I_{sp} [s]	Thrust [N]	Mass [kg]	F_T/w [N/kg]	Starts (total)
Vinci [30]	LOX/LH_2	5.80	465.0	180,000	550	327	5
RL10B-2 [31]	LOX/LH_2	5.88	465.5	110,000	301	365	15
CECE [33]	LOX/LH_2	5.88	465.0	111,206	256	435	50

After computing F_T/w and analysing the engines description and their characteristics, the selected one is the CECE. Despite its lower thrust, when compared to the Vinci (minus 68,794 N), it is re-startable ten times more, making it more versatile (on our mission at least eight manoeuvres are required, see chapter 3). It also has less than half of the mass of the Vinci.

Although it has a I_{sp} that is lower than the RL10B-2 (a difference of only 0.5 s) it has a higher thrust (greater than 1,206 N) and a lower mass.

Finally it has a higher thrust-to-weight ratio than the others (more than 70 N/kg).

2.1.2 Nuclear Thermal Engines

One of the last nuclear thermal engines to be developed inside the NERVA program was the NERVA II. The goal was to have a higher I_{sp}, and thrust, with a lower weight than the previous ones [34]. It was intended to serve as the propulsion system for manned interplanetary missions, with masses near 1,000 t.

NERVA II produced the required power with a uranium inventory of 360 kg, and had 2 m in diameter. Temperatures of the hydrogen fuel could reach 2,755 K [34]. One of the requirements of the program was an endurance of over 600 min [35].

In table 2.2 we show its main characteristics.

Table 2.2 Nuclear thermal engine characteristics.

Engine	Power [MW]	I_{sp} [s]	Thrust [N]	Mass [kg]
NERVA II [34]	5,000	785	1,036,435.6	11,903.2*
*Mass of the nuclear reactor (total engine mass is 34,019 kg [36])				

2.1.3 Fuel Calculations

Apart from the mass of the propulsion system, it is necessary to calculate how much fuel is needed to execute the required space manoeuvres. When using engines that can be treated as impulsive, like chemical and nuclear thermal ones, one can use the well known Tsiolkovsky rocket equation for ΔV (equation (2.1)). It relates exhaust velocity ($V_{ex} = g_0 I_{sp}$), velocity change (ΔV), propellant and spacecraft dry mass (M_P and M_{Dry} respectively). From it one can obtain the propellant mass required to achieve a certain velocity change, M_P:

$$\Delta V = V_{ex} \ln\left(\frac{M_P + M_{Dry}}{M_{Dry}}\right) \quad \Rightarrow \quad M_P = M_{Dry}\left(\exp\left\{\frac{\Delta V}{g_0 I_{sp}}\right\} - 1\right). \tag{2.1}$$

A complete mission trajectory requires N manoeuvres. Since the fuel mass depends on the initial mass, it is necessary to compute equation (2.1) backwards, i.e. start from the last manoeuvre (N) and work our way back until the first one,

$$
\begin{aligned}
M_P^N &= M^N\left(\exp\left\{\frac{\Delta V_N}{g_0 I_{\mathrm{sp}}}\right\}-1\right), \qquad & M^N &= M_{Dry} \\
M_P^{N-1} &= M^{N-1}\left(\exp\left\{\frac{\Delta V_{N-1}}{g_0 I_{\mathrm{sp}}}\right\}-1\right), \qquad & M^{N-1} &= M_{Dry} + M_P^N \\
&\vdots \\
M_P^T &= M^1\left(\exp\left\{\frac{\Delta V_1}{g_0 I_{\mathrm{sp}}}\right\}-1\right), \qquad & M^1 &= M_{Dry} + \sum_{k=2}^{N} M_P^k.
\end{aligned}
$$

The ΔVs here present are considered to be applied instantaneously at a predetermined location. However, this is not completely correct since an engine does not start and stop instantaneously. There is always a period of time associated with a manoeuvre (when the engine is in operation) and thus a spatial distribution of the burn. This is why we must introduce a loss factor in the equations (ΔV_{loss}).

Although the value of ΔV_{loss} can ultimately be an arbitrary choice, several principles apply:

- According to the Oberth effect a velocity change is more efficient when deep inside a gravity well (i.e. closer to the central body) [37];
- The thrust-to-weight ratio of the engine affects its performance to execute a manoeuvre.

For safety reasons we consider that every ΔV must be incremented by a factor of 10% for a manouevre longer than five minutes (i.e. $\Delta V_{real} = 1.10 \times \Delta V_{theory}$). For a manouevre between one and five minutes we assume a loss of 5%, and for a manouevre requiring less than one minute we impose a 1% loss. The time required by each manoeuvre is related to the engine characteristics by $\Delta t = \frac{\gamma - 1}{\gamma}\frac{I_{\mathrm{sp}} \times g_0}{F_T/M_{initial}}$, where $\gamma = \frac{M_{initial}}{M_{final}}$ [38].

2.2 Non-Impulsive Systems

2.2.1 Modern Electrical Engines

NEXT The NASA's Evolutionary Xenon Thruster (NEXT) is an evolution of the already tested NASA Solar Technology Application Readiness (NSTAR), from the Deep Space 1 mission [39]. NEXT has a larger diameter than the NSTAR, a higher I_{sp} and thrust level, including a higher throttling range [40].

RIT-XT The RIT is a radio frequency ion thruster. It generates ions by high frequency electromagnetic fields [41]. The operational model, the RIT-10, has a thrust of 15 mN. Astrium Gmbh started developing the RIT-XT with the intention to expand its applicability (mainly increasing the thrust) [42].

PPS 1350-G The PPS 1350-G is a plasma thruster with flight proven capability. It was used in the SMART-1 mission, in which it was activated for a total of 5,000 h [43]. In this mission it operated continuously for 260 h and has the capability of reaching 7,300 cycles.

The main characteristics of the electrical engines here discussed are summarised in table 2.3.

Table 2.3 Modern electrical engines characteristics.

Engine	Power [W]	Propellant	I_{sp} [s]	Thrust [N]	Mass [kg]	F_T/w* [N/kg]
NEXT [39]	6,900	Xenon	4,117	0.237	13.5	0.0041
RIT-XT [42]	3,260	Xenon	4,600	0.120	7.0	0.0043
PPS 1350-G [43]	1,500	Xenon	1,660	0.090	5.3	0.0060

*The weight here includes solar panels (so to account for the effect of engine power)

Based on the data of table 2.3 and the engines description, the select engine is the PPS 1350-G. The selection proved to be more difficult than the chemical case, considering the differences in thrust, I_{sp} and power. The PPS is selected due to its higher thrust-to-weight ratio and for having flight proven capabilities.

When compared with the others it can only produce 75% of the RIT thrust, but with 53% of its mass and 46% of the RIT power (38% of the NEXT thrust with 26% and 22% of its mass and power, respectively).

2.2.2 Fuel Calculations

As seen in chapter 1, electrical engines are regarded as non-impulsive ones. For non-impulsive systems the fuel spent and the trajectory are computed at the same time. This led to the combination of the thrust and I_{sp} equations (1.1) and (1.2), repeated here for convenience, for $p_e \approx p_a$:

$$\left.\begin{aligned} F_T &= \dot{m}V_{ex} + A_e(p_e - p_a) \\ I_{sp} &= \tfrac{V_{ex}}{g_0} \end{aligned}\right\} \quad \Rightarrow \quad \dot{m} = \frac{\mathrm{d}M}{\mathrm{d}t} = -\frac{F_T}{I_{sp}g_0}. \tag{2.2}$$

Equation (2.2) is integrated in time to extract the required fuel. The integration method used is the same as for trajectory calculations, discussed in chapter 4.

Note that this equation is valid for chemical and for nuclear thermal engines. However, the Tsiolkovsky equation is a simplification as it assumes an instantaneous velocity change, an approximation that cannot be adopted here.

2.3 New Concept Systems

Within the new concepts that were described in the introduction, we consider the "Pure Electro-Magnetic Thrust" (PEMT). As stated before, the PEMT engine has a nuclear reactor which, instead of expelling a heated working fluid to create thrust (as the case of the NERVA II), uses the solar sail thrust principle (the use of photons to produce thrust).

2.3.1 PEMT Engine

A nuclear reactor releases energy mainly in the form of heat [19]. This thermal energy can be harvested (using a coolant that runs through the reactor core) and used to heat a radiator, which emits electromagnetic radiation (photons). The radiator is in front of a reflecting surface that reflects the radiation. The momentum transferred to the reflecting surface by the hitting photons together with the momentum of the radiator produces the thrust.

To relate the energy needed with the heat produced by the reactor the Stefan-Boltzmann law is used, for a unit surface, $\Phi_{rad} = \varepsilon\sigma T^4$ (where Φ_{rad} is the radiated power in W/m^2, ε the emissivity of the body, T is the temperature of the body in K and σ the Stefan-Boltzmann constant). From the Stefan-Boltzmann law it is also possible to relate the surface area, S (in m^2), of a radiator to its temperature,

$$W = \Phi_{rad}S = \varepsilon\sigma T^4 S. \tag{2.3}$$

The reflecting surface is placed on one side of the radiator so all the radiation is concentrated in a single direction (since the emission of electromagnetic radiation is done in all directions). Integrating the resultant force of this configuration gives $F_{\parallel} \approx \frac{2}{3}\frac{W}{c}$. To achieve the earlier discussed thrust $\left(F = \frac{W}{c}\right)$, a Winston's cone, a non focusing reflecting conical structure (see figure 2.1), must be implemented [3].

To maintain the temperature of the reflecting surface, near the radiator, bellow the material's melting point, in this configuration, we must have $\varepsilon_{back} >> \varepsilon_{front} \rightarrow T_{reflector} = T_{radiator}\left(\frac{\varepsilon_{front}}{\varepsilon_{back}}\right)^4$ [3].

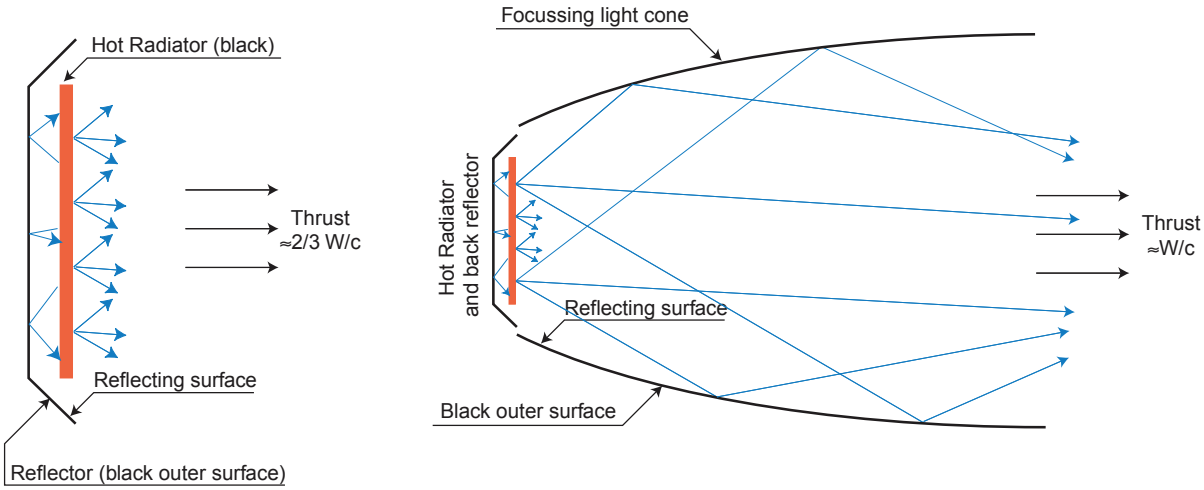

Figure 2.1 Emitting surface and mirrors of Rubbia's concept engine [3].

We have selected a NERVA reactor for our main engine, and resized it making some minor improvements considering the technological advances in the last years. We assume a "NERVA 2000" which can produce 22% more energy with an increase in mass of 26%.

For computing the I_{sp} of a PEMT engine it is suggested in reference [3] to compare nuclear fuel mass with the propellant mass. Considering that the nuclear fuel directly transformed into energy is a fraction of the total nuclear material mass, βM_{Pn}, and it is ejected with the speed of light, c, one can compute the effective exhaust speed as $V_{ex} = \beta c$. This gives $I_{sp} = \frac{V_{ex}}{g_0} = \frac{\beta c}{g_0}$. For the present work we assume that only four percent of the nuclear material mass is transformed into energy (fractional burnup $\beta \approx 0.04$), which is the maximum we can use [23, 24].

As before the engine characteristics are summarised in table 2.4.

Table 2.4 PEMT engine characteristics.

Engine	Power [MW]	I_{sp} [s]	Thrust [N]	Mass [kg]
NERVA 2000	6,100	1,222,812	20	15,000

(Note: If we want to produce the same power using solar panels, we would need 46,544,084 m^2, weighting 39,097 t. See section 3.2.2 for how to calculate these values.)

Although this engine has a I_{sp} far greater than the ones presented so far, this value does not quantify fuel expenditure, i.e. equation (2.2) cannot be applied here and fuel calculations do not include the I_{sp} (see section 2.3.3).

The PEMT engine is still a theoretical concept and, as such, many details are unknown. Several details and difficulties are presented in section 2.3.2 (the reader should note that these are the ones the author came across during the work and others may still exist).

2.3.2 PEMT Details

One of the first questions that arises is how to control the engine power (and hence the thrust). In a nuclear power plant we have energy being continuously produced. However, in space, we have an intermittent use (e.g. a shutdown is desirable when orbiting Mars). Thus, a mechanism must be implemented to stop and to re-start

the nuclear reaction. This type of control can be achieved using control rods [19]. The control rods, when fully inserted, do not allow the nuclear reaction to occur (e.g. when the engine is taken to space they should be in this position, to assure that the engine is not an environmental threat). When they are partially removed, and kept in a predetermined position, the reactor has a certain power output (related to the position of the rods).

Having established how the power output can be controlled, we have to transfer it to the radiator, in the form of heat. This can be achieved through the use of a coolant which will run from the reactor to the radiator (heating up the radiator and cooling the reactor). In order to save volume, mass and pressure, the coolant discussed in reference [3] is Beryllium. It is a light metal with a boiling point of $2,744\,\mathrm{K}$ [44] and a vaporization heat of $32.9\times10^6\,\mathrm{J/kg}$ [3]. However, besides the health precautions required when transferring it to the propulsion system, these values represent a mass flow of about $185\,\mathrm{kg/s}\left(\frac{6.1\times10^9}{32.9\times10^6}\right)$ running through the reactor to the radiator, for our $6.1\times10^9\,\mathrm{W}$ engine. This large value must be maintained without the presence of gravity, being recommended to keep the radiator in rotation so to induce a centrifugal force in the coolant. This solution requires the use of a complex pumping system and is a challenge in terms of designing the radiator and its coolant system.

For the analysis presented above the radiator temperature is assumed to be at $3,300\,\mathrm{K}$ (near the boiling point of the coolant). This high temperature is another challenge since the radiator material must withstand it without melting. In reference [3] carbon nanotubes are suggested. Among the materials that can withstand $3,300\,\mathrm{K}$ without melting (e.g. Tungsten with a melting point of $3,695\,\mathrm{K}$) carbon nanotubes are the lightest ($37\,\mathrm{kg/m^3}$ [45]). The radiator temperature is selected so to ensure a small dimension and a low temperature, following the Stefan-Boltzmann equation (2.3) (see figure 2.2).

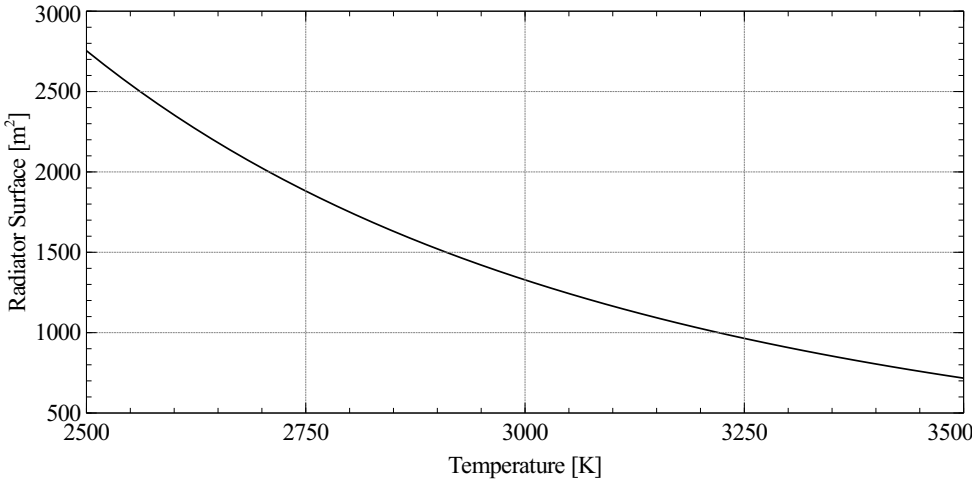

Figure 2.2 Radiator surface area with temperature for $W = 6.1\times10^9\,\mathrm{W}$ and $\varepsilon = 1$.

For the reflector one needs to guarantee that it has a maximum reflecting capability for the wavelength the radiator is emitting, besides being resistant to the high temperatures. To obtain the wavelength (λ) one solves Planck's equation. This depicted in figure 2.3. The maximum is for a wavelength $\lambda_{max} = \frac{2897}{T}\,\mu\mathrm{m}$ [3]. For the Sun's effective temperature $\lambda_{max} = 0.50\,\mu\mathrm{m}$ ($T \approx 5,780\,\mathrm{K}$ [46]). For our radiator at $T = 3,300\,\mathrm{K} \rightarrow \lambda_{max} = 0.88\,\mu\mathrm{m}$ (already outside of the visible spectrum, 0.35 to $0.75\,\mu\mathrm{m}$). Thus, the reflector selected should be capable of reflecting visible and infrared radiation. Even having a radiator with peak emission in the limit of the visible radiation, $0.75\,\mu\mathrm{m} \rightarrow T = 3,863\,\mathrm{K}$, requires reflecting infrared radiation to increase the radiative power. The current technology for solar sails uses composite booms (on the support structure) and Aluminized Mylar sails (or carbon fibre sail substrate) with densities of $10\,\mathrm{g/m^2}$ [22]. The Mylar sail has the advantage of also reflecting infrared radiation.

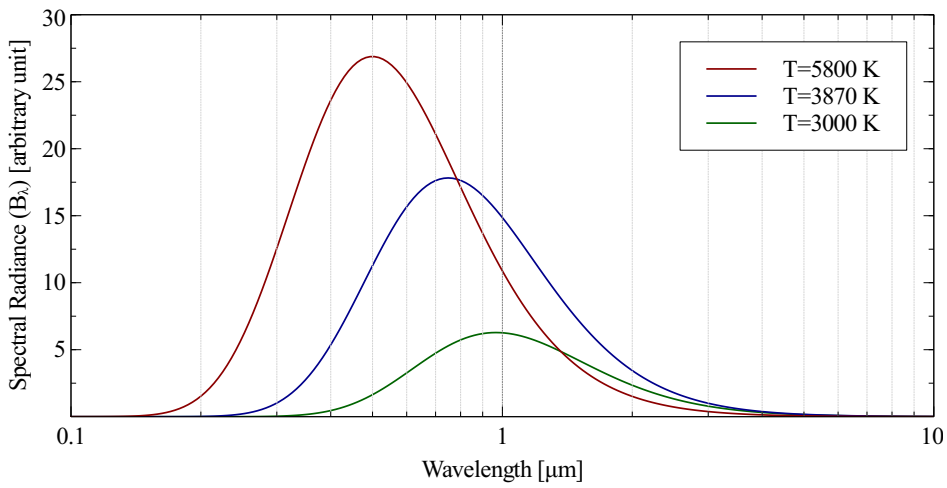

Figure 2.3 Spectral radiance for different temperatures, $B_\lambda(T) = \frac{2hc_0^2}{\lambda^5}\frac{1}{e^{hc_0/(\lambda\sigma T)}-1}$.

2.3.3 Fuel Calculations

The PEMT engine only expels photons, which do not have any rest mass. Due to this particularity the fuel calculations seen before do not apply here. The fuel spent here is nuclear fuel burned in a nuclear reaction. Therefore, one needs to compute how much fuel is burned during the mission to include it in the engine initial mass.

Having the fractional burnup of the reactor ($\beta \approx 0.04$) and the maximum theoretical burnup of a ^{235}U (950 GW.d/t [23]) we derive the specific burnup, sb,

$$sb = 950 \times \beta \quad [\text{GW.d/t}]. \tag{2.4}$$

The total burnup (B) is obtained using the operating time of the engine (t_{on}) and assuming that the engine works with a certain power (W),

$$B = W \times t_{on} \quad [\text{GW.d}]. \tag{2.5}$$

Combining equations (2.4) and (2.5), one obtains the required uranium mass, M_U, as

$$\frac{B}{M_U} = sb \Leftrightarrow M_U = \frac{B}{sb} = \frac{W \times t_{on}}{950\beta}. \tag{2.6}$$

A usual nuclear reactor is loaded with uranium dioxide (UO_2). For calculating its atomic weight one combines the atomic weight of two oxygen atoms ($A_w(O) = 15.9994$ [47]) with one of uranium. However, since the reaction normally occurs with ^{235}U atoms, and these only represent 0.72% of the uranium in natural state, one uses an enriched material. For the purpose of this study we use a highly enriched uranium of 80 wt% ^{235}U (almost considered wepons-grade [48], but feasible [49]). Knowing the relative atomic mass of ^{235}U and ^{238}U ($A_w(^{235}U) = 235.0439299$ & $A_w(^{238}U) = 238.05078826$) [47] it is possible to obtain the atomic weight of the enriched uranium by

$$A_w(U) = \left[\frac{1}{100}\left(\frac{80}{A_w(^{235}U)} + \frac{20}{A_w(^{235}U)}\right)\right]^{-1} \rightarrow A_w(U) = 235.6392, \tag{2.7}$$

which allows to compute the atomic weight of the UO_2 ($A_w(UO_2) = A_w(U) + A_w(O_2) = 235.6392 + 2 \times 15.9994 = 267.6380$).

The mass of uranium dioxide needed to produce a certain power, during a certain period of time, is extracted from the mass of uranium required,

$$M_U = \frac{M_{UO_2} \times 235.6392}{267.6380} \Leftrightarrow M_{UO_2} = \frac{M_U \times 267.6380}{235.6392}. \tag{2.8}$$

Chapter 3

Mission to Mars

Having summarised the available propulsion systems we proceed to implement the mission architecture (in section 3.1) and to define the main characteristics of the spacecraft (in section 3.2). These topics are based on the concepts discussed in chapter 1.

3.1 General Mission Architecture & Mission Timeline

Considering an architecture similar to the DRM proposal, we have a mission with four astronauts, with the goal of minimising both time and mission mass. We use this base architecture for comparison of the different propulsion systems. We consider a mission comprising nine segments:

1. Launch from Earth to a parking orbit and assembly (the launch itself is not considered in the present work as different configurations are required);
2. Escape from Earth's gravity field (includes an orbital raising manoeuvre and the interplanetary injection manoeuvre);
3. Interplanetary transfer from Earth to Mars (EtM);
4. Capture to an orbit around Mars;
5. Mars exploration - until the alignment of the planets needed for the return;
6. Launch from Mars to orbit (this is not developed in this work and it is assumed that the required fuel for ascending from the Mars' surface is the same as the other proposals);
7. Escape from Mars' gravity field (includes an orbital transfer of a transport capsule, carrying the crew, to rendezvous with the spacecraft and the interplanetary injection manoeuvre);
8. Interplanetary transfer from Mars to Earth (MtE);
9. Capture and landing on Earth (while the actual ΔV for landing is not computed, a lowering of the capture orbit is, from where the landing requires a small ΔV).

The first question is whether to send crew and cargo together or separately (as in the other proposals). This decision has a large impact on the entire mission design. The main advantages of sending crew and cargo together are: only one spacecraft is built, which makes the mission simpler; if any problem occurs, the cargo can be managed by the crew; and the systems are designed to last for the time the crew needs them. However, there are some disadvantages to this solution. It is advantageous to send the astronauts in a fast interplanetary trajectory

and it would be a waste of fuel to send the cargo at high speed as well. We would end up with a smaller payload mass, so to keep the total mass in acceptable ranges.

Conversely, if the cargo goes before the crew, we could send with it the required fuel for the manned return trip, lowering substantially the initial mass of the manned spacecraft. A secure landing site would be set beforehand the astronauts leave Earth, if the surface cargo lands on the planet at arrival (as in the other proposals). Nevertheless, the main disadvantage of sending them separately is the requirement that the systems endure longer periods under adverse space conditions, while waiting for the crew to arrive. In case of landing at arrival, they would also need to withstand the Martian atmosphere for a longer period of time.

Considering that the objective of the present mission is to minimise the travel time (as explained in section 1.2.2), we send the cargo and crew separately from each other, without landing the cargo at arrival.

This option has two immediate consequences. Firstly, it implies that at least two launches are needed (one for the cargo and the other for the manned spacecraft). Secondly, it is required to execute a rendezvous around Mars, between the manned spacecraft and the fuel for the return trajectory.

Each segment of the mission is discussed below, and the mission timeline for the Earth to Mars mission phase is displayed in figure 3.1.

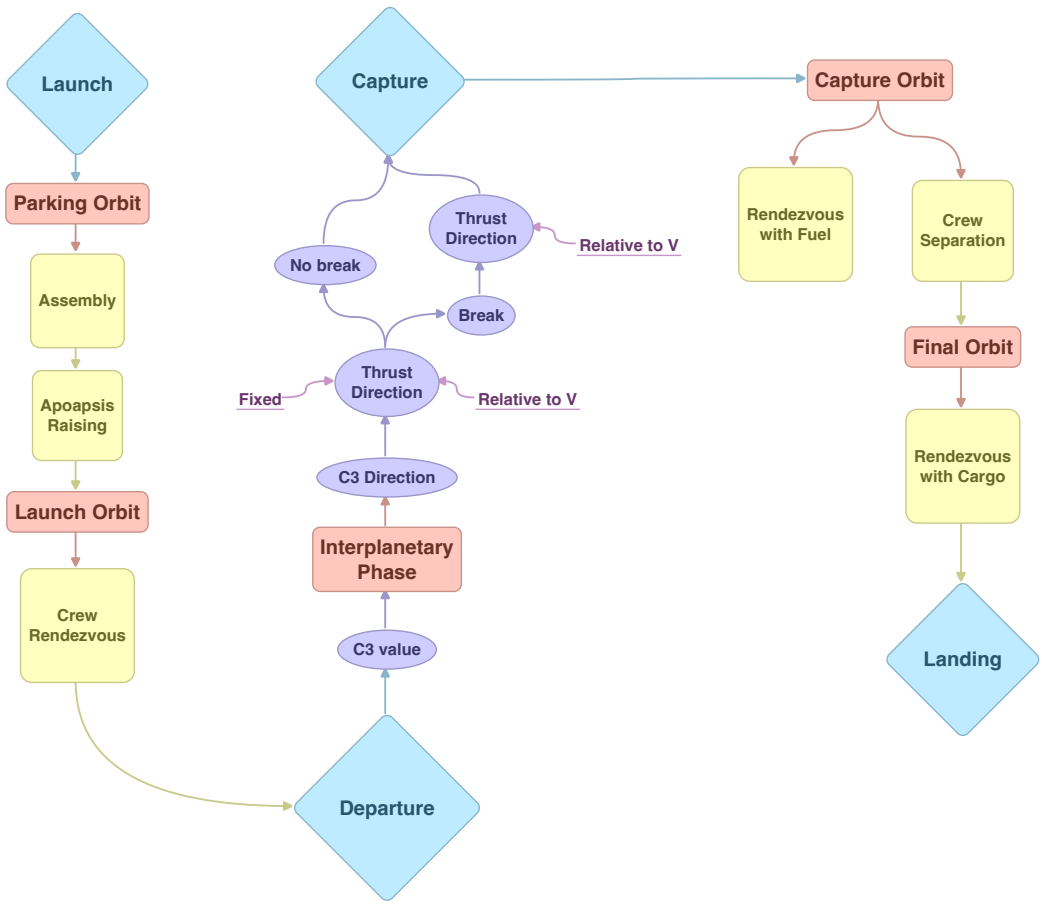

Figure 3.1 Sketch of the mission timeline for the Earth to Mars phase.
Legend: Blue diamond shapes represent single moments.
Red rectangles are mission phases.
Yellow squares represent actions.
Blue-violet oval shapes are variable parameters (and underline terms their options).
C_3 is the square root of the departure velocity of the spacecraft.

3.1.1 Parking Orbit & Departure

In most missions, specially the ones to other celestial bodies, it is usual to use an initial parking orbit. This orbit allows for:

- The initialization of all systems, e.g. deployment of the solar panels (closed during launch);
- To make the necessary tests to the spacecraft systems;
- To wait for the best moment to execute the manoeuvres to leave Earth orbit.

The parking orbit tends to be a low orbit, with low eccentricity, where the launcher has a greater payload capability, maximising the available mass of the spacecraft. In this orbit the interplanetary injection manoeuvre would be more effective (according to the Oberth effect).

For the present mission an orbit with 500 km periapsis altitude and a eccentricity of 0 is selected (following the example of the International Space Station [50]). This altitude is higher than the average parking orbit ([17, 51, 52]). However, an orbital assembly is required for a complex propulsion systems such as Rubbia's concept (the PEMT) or for missions whose initial mass exceeds the launcher capabilities. This implies a longer stay in this orbit and thus an orbit with a low decay rate (which decreases with increasing orbital altitude).

After being fully assembled, and tested, the spacecraft would raise the orbital apoapsis, increasing periapsis speed, before executing the interplanetary injection. This is a common manoeuvre whose primary objective is to lower the ΔV loss (by lowering the time the engine is in operation in each manoeuvre) [9, 51, 52]. The number of intermediary orbits depends on the final ΔV. For simplicity we only considered one orbital raising manoeuvre. The orbit from where the interplanetary injection is performed has an eccentricity of 0.95, an almost hyperbolic orbit, from where the ΔV for the interplanetary transfer is small.

A priori we do not know the time taken for the assembly, and due to the high orbital period of the launch orbit ($T = 11.5\,\mathrm{h}$), the crew would not be inside the habitat module (which together with the propulsion system we call mother ship, described in section 3.2) during this phase of the mission. Only before executing the EtM injection would the crew rendezvous with the mother ship (carried by a smaller launcher in a transport capsule described in section 3.2.3).

3.1.2 Interplanetary Transfer

In the interplanetary phase the main tested scenarios are the coast trajectory (for impulsive systems) and the powered trajectory (for non-impulsive and new concept systems). Three parameters must be examined in each scenario:

- Direction of the spacecraft velocity at departure;
- Direction of the thrust;
- Whether acceleration is continuous or whether braking is performed before arriving to the target planet.

On a Hohmann transfer orbit the optimal direction of the velocity at departure would be parallel to the planet's velocity, so to have a greater final velocity (see section 4.3). However, for a shorter transfer, the modulus of the velocity as well as its direction are important. One has to search for the optimum direction of this velocity aiming to minimise travel time and mass.

For a similar reason the thrust direction is an important parameter. Having the thrust parallel to the velocity would increase its absolute value without affecting the direction. This is not at first the best option when the trajectory is not a straight line. If the thrust is not parallel to the velocity, we can change the velocity direction,

possibly reaching an outer point faster on a curvilinear trajectory. This option implies a sacrifice on the change of the absolute value of the velocity. To test this situation a search for the optimum direction of the thrust is performed. Clearly this test only applies to the powered trajectory.

A possible situation that can arise in a powered travel, is that one may reach the destination with a velocity that is too large for a classical single impulse brake. A solution is to start braking before arriving, i.e. after a predetermined position invert the thrust direction. The brake may also minimise the capture fuel requirements since non-impulsive engines have a higher I_{sp}. This parameter is tested for different distances to the target planet and with the thrust in different directions.

3.1.3 Capture on Mars

The capture manoeuvre on Mars could be performed with a classical single impulse brake (with chemical or nuclear thermal engines), continuous thrust brake and/or aerobraking. The aerobraking is still a matter of research and, until now, only performed in small spacecraft (smaller than a manned spacecraft) [53]. Another disadvantage of aerobraking, valid also for the continuous thrust brake, is the time taken to perform. Both types of manoeuvres need long periods of execution time (as seen in the SMART-1 mission [25] and in references [3, 9]), which goes against the objective of minimising travel time. This is also the reason not to use the continuous thrust option for the departure.

To fulfil our objective of minimising travel time we use the classical single impulse brake. A periapsis altitude of 300 km for the capture orbit was selected, based on previous missions [51, 54, 55] and for being well above Mars' atmosphere (126.2 km to ≈ 200 km high [56]). To minimise the fuel spent on the capture manoeuvre one uses a highly elliptical orbit, ensuring that the spacecraft is captured (eccentricity of 0.9).

Afterwards, the mother ship (habitat module and propulsion system) would remain at this orbit until the return. This is done so to save fuel (by not lowering the spacecraft orbit, and then raising it again for the departure). On this capture orbit the fuel for the return would be waiting for a subsequent rendezvous with the mother ship.

Whilst the mother ship remains behind, the crew (inside the transport capsule) would intercept the cargo before landing on Mars, at a lower circular orbit (200 km high). On this lower orbit the crew can use the atmosphere to brake and land. It would leave in this final orbit the engine used on the circularisation since it is not needed on the planet.

3.1.4 Return Trajectory

After completion of the ground mission, the crew enters in a return capsule (possibly carrying return samples) and leaves the planet's surface, rendezvousing with the engine left on circular orbit. An orbital decay is assumed, due to the lower periapsis altitude, and the engine left in orbit has now a lower periapsis altitude (180 km).

Raising the orbit, it would rendezvous with the mother ship prior to the MtE injection manoeuvre.

On the return interplanetary phase the same parameters seen above (section 3.1.2) need to be tested.

The capture on Earth is similar to the one on Mars. The same periapsis altitude is used, despite the higher boundary of Earth's atmosphere. This aims to save fuel and to increase safety, i.e. a manoeuvre at the same height on Earth and Mars implies a greater fuel expenditure on Earth, but having a lower periapsis altitude increases the risk of crashing on the planet.

Subsequently, the crew enters the return capsule, detaches from the mother ship, leaving it at the capture orbit, lowers the periapsis and circularises the orbit before landing on Earth.

The sketch representing the Mars to Earth mission timeline is displayed in figure 3.2.

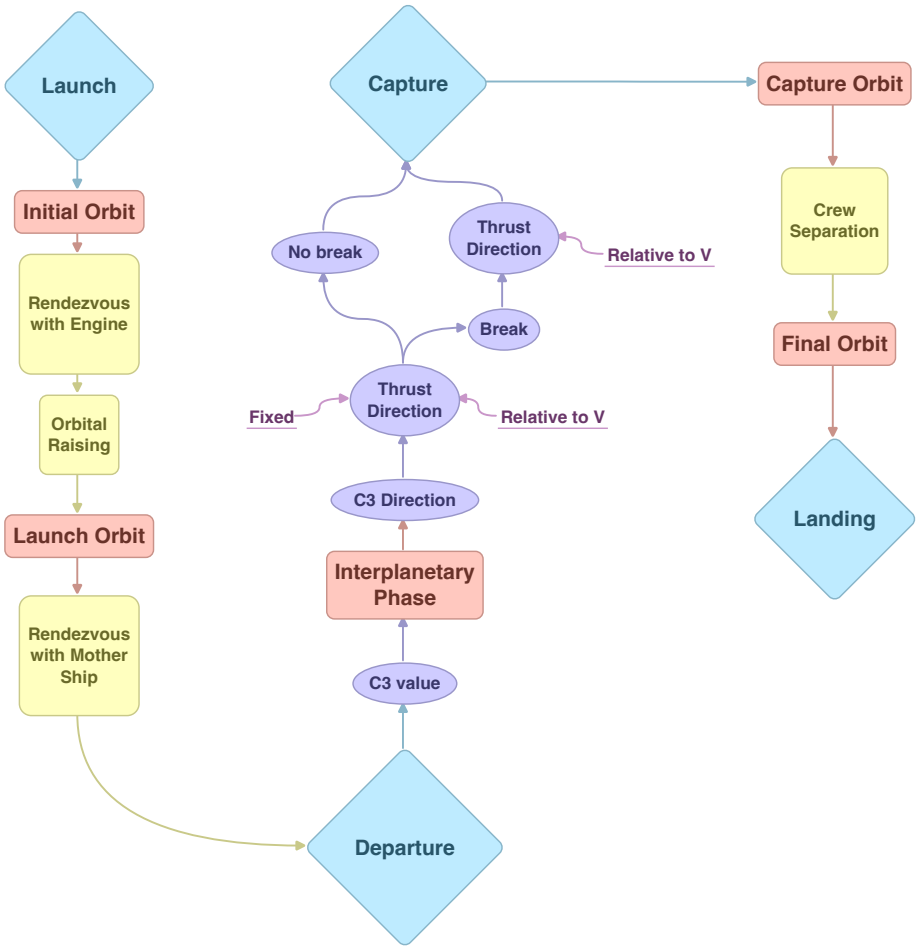

Figure 3.2 Sketch of the mission timeline for the Mars to Earth phase.
Legend: Blue diamond shapes represent single moments.
Red rectangles are mission phases.
Yellow squares represent actions.
Blue-violet oval shapes are variable parameters (and underline terms their options).
C_3 is the square root of the departure velocity of the spacecraft.

3.1.5 Cargo Mission

Being simpler the cargo mission has fewer options. The first step is the launch to an Earth parking orbit. Here a long assembly is not expected and the parking orbit can have a lower periapsis and eccentricity. After checking that everything is functioning properly it would execute the EtM injection (again a classical single impulse option is used).

For the interplanetary phase a slower trajectory is intended, with savings on departure and capture. The option of using a powered transfer is also tested, to lower even further the departure and capture fuel requirements.

Upon arrival at Mars it would execute the capture to a highly elliptical orbit (as the manned spacecraft). The cargo does not perform the MtE trajectory, being left on Mars for other possible missions to the planet. For this reason all the spacecraft, apart from the fuel for the manned return trajectory, would be lowered to a circular orbit. It would then remain at this orbit powered down, until the crew arrives.

3.1.6 Mission Data

In table 3.1 a summary of the orbital characteristics for the manned mission, justified in the previous sections, is presented.

Table 3.1 Orbital characteristics for the manned mission.

Manned Spacecraft	Departure		Capture	
Earth to Mars	Initial Orbit	Launch Orbit	Capture Orbit	Final Orbit
Periapsis Altitude [m]	500×10^3	500×10^3	300×10^3	200×10^3
Eccentricity	0	0.95	0.9	0
Mars to Earth	Initial Orbit	Launch Orbit	Capture Orbit	Final Orbit
Periapsis Altitude [m]	180×10^3	300×10^3	300×10^3	180×10^3
Eccentricity	0	0.9	0.9	0

The cargo mission orbital characteristics are shown in table 3.2.

Table 3.2 Orbital characteristics for the unmanned mission.

Cargo Spacecraft	Departure		Capture	
Earth to Mars	Initial Orbit	Launch Orbit	Capture Orbit	Final Orbit
Periapsis Altitude [m]	200×10^3	200×10^3	300×10^3	200×10^3
Eccentricity	0	0.95	0.9	0

A mission trade tree is displayed in figure 3.3. Here we can see which propulsion system is used in each mission segment. When a coast transfer is selected no propulsion system is used during the interplanetary phase.

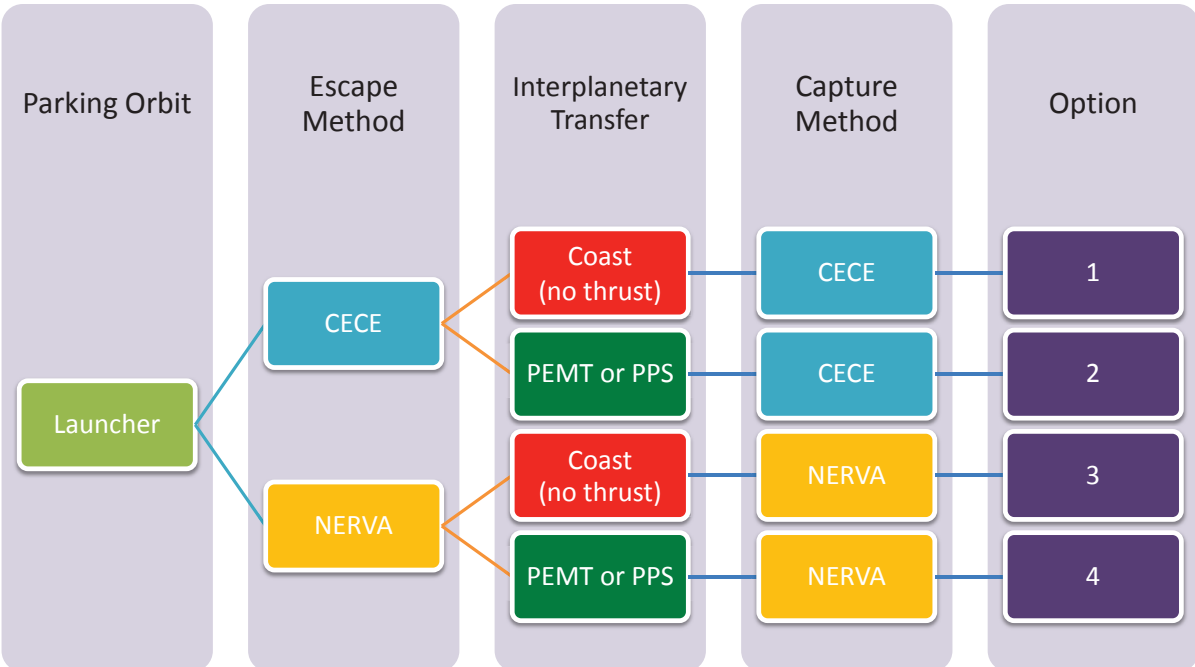

Figure 3.3 The different mission options tested for the manned spacecraft.
The CECE is the classical chemical engine, the NERVA is the nuclear thermal engine, the PPS is the electrical engine and the PEMT is Rubbia's concept.

For the cargo we want a minimum fuel option since time is not a priority. The only options considered are the coast transfer or a powered electrical transfer, with a chemical propulsion departure and capture.

3.2 Preliminary Spacecraft Design

Some considerations about the spacecraft must be made. These must be broad enough to allow for changes in the design while giving a good idea about the mass of the spacecraft. This is an important parameter of the project since it is closely related to the trajectory performed with non-impulse propulsion, and to the complexity of the mission itself.

The manned spacecraft encompasses a human habitat module (which caries the crew during the interplanetary transfers), the propulsion system, with engines and respective components, and a transport capsule. The first two comprise what we call the mother ship. The unmanned spacecraft has a cargo module, the corresponding propulsion system and a Mars ascent vehicle (MAV).

3.2.1 Human Habitat & Cargo Modules

The human habitat module of the spacecraft and the cargo module are an extrapolation from Mars Direct and DLR proposals ([7, 10]), using the guidelines presented in reference [57]. The mass of these modules is within the range of the previous proposals data and uses a higher margin than the one in Mars Direct (see table 3.3).

Table 3.3 Mass of the modules used in the mission.

(a) Human habitat module.

Components	Tonnes
Electric power	1.00
Habitat structure	17.00
Communications	0.20
Data handling	0.05
Control	0.45
EVA suits (4)	0.40
Scientific Payload	0.50
Consumables	7.11
Sub-total	26.71
Spares and Margin (18%)	4.81
Total	**31.52**

(b) Cargo module.

Components	Tonnes
Batteries	0.12
Electrical power central	3.50
Communications	0.10
Data handling	0.05
Control	0.45
EVA suits (4)	0.40
Scientific Payload	1.00
Consumables	6.92
Biconic brake	2.45
Surface habitat	17.70
Rover	3.00
Sub-total	35.69
Spares and Margin (18%)	6.42
Total	**42.11**

The human habitat module (table 3.3a) has the following components:

- Electric power - This is a group of components which supply all the energy to the module and include solar panels and batteries;
- Habitat structure - The structure that houses the crew during transit to and from Mars, including the life support system and interior furniture;
- Communications & Data handling - All the hardware which enables the communication with Earth and connects all the systems inside the module;
- Control - Referes to the Attitude and Orbit Determination and Control System (AODCS), without considering the main propulsion system;
- Extra-Vehicular Activity (EVA) suits - Crew suits for launch and landing (and if a space walk is performed);
- Scientific Payload - The tools necessary to perform scientific experiments in transit;

- Consumables - All the food needed for the transfer to and from Mars (a two year trip is considered).

The cargo module (table 3.3b) carries the surface habitat together with most of the payload for the surface exploration, apart from the fuel for the human return. The cargo module thus differs from the human habitat on these components:

- Batteries and Electrical power central - This two components give all the energy the module requires when in flight and when stationed on the planet's surface;
- Biconic brake - The system which allows the module to land on Mars' surface, i.e. is a series of components that protects and brakes the module when it enters Mars' atmosphere;
- Surface Habitat - The structure that will house the crew during the surface stay (similar to the structure for space);
- Rover - As the name states it is a land vehicle for the astronauts;
- EVA suits - The suits needed for the crew to make Mars walks;

3.2.2 Spacecraft Propulsion System Components

The propulsion system is composed by several parts, the number depending on the type of propulsion. While chemical and nuclear thermal systems have two primary parts (the main engine and the fuel tanks), the electrical and PEMT systems have three. The electrical has a main engine, fuel tanks and solar panels, and the PEMT has a main engine, radiator and reflector cone. As the main engine features have already been discussed in chapter 2, we discuss now the remaining parts.

Fuel Tanks

Fuel tanks have an associated dry mass that must be included on the spacecraft. However, following the example of the Apollo mission these tanks are discarded as soon as they are empty (see section 1.2.3). We have a mass of tanks for the departure, M_T^D, for the interplanetary transfer (when needed), M_T^I, for the capture, M_T^C, and finally for the remaining transfers, M_T^{HT}. All of these masses affect fuel needs and, therefore, the time of each mission phase. We require fuel tanks with minimum mass to fuel ratio.

The first step is to compute the fuel volume for a manoeuvre. For it we need the fuel mass computed in sections 2.1.3 and 2.2.2 and to know LOX/LH_2 or Xenon densities and engine ratios (R). The expressions relating these quantities, derived from reference [58], are:

$$v_P = \begin{cases} v_{LOX} + v_{LH_2} = \dfrac{R \times m_P}{(1+R)\rho_{LOX}} + \dfrac{1 \times m_P}{(1+R)\rho_{LH_2}} = \dfrac{m_P(\rho_{LOX} + R \times \rho_{LH_2})}{\rho_{LH_2} \times \rho_{LOX}(1+R)} \\ \\ v_{Xenon} = \dfrac{m_P}{\rho_{Xenon}} \end{cases} \tag{3.1}$$

$$\rho_{LOX} = 1141\,\mathrm{kg/m^3} \qquad \rho_{LH_2} = 67.8\,\mathrm{kg/m^3} \qquad \rho_{Xenon} = 3057\,\mathrm{kg/m^3}.$$

We can have large volumes of fuel for a single manoeuvre. If those are contained in a single tank it can induce some problems, e.g. change in centre of gravity during a manoeuvre. The fuel capacity of the tank is then a factor that needs to be taken in consideration. For the present mission we use a similar fuel tank distribution as the one currently being used by the Fregat upper stage, which has six tanks in a torispherical dome configuration [59, 60]. This prevents using tanks with oversized dimensions and allows for a good distribution of the fuel mass.

Many types of fuel tanks are available and have been used in many different missions, with different dimensions, fuel capacities and masses. We plot the capacity and density of each tank (from reference [61]), and a fitting function (figure 3.4).

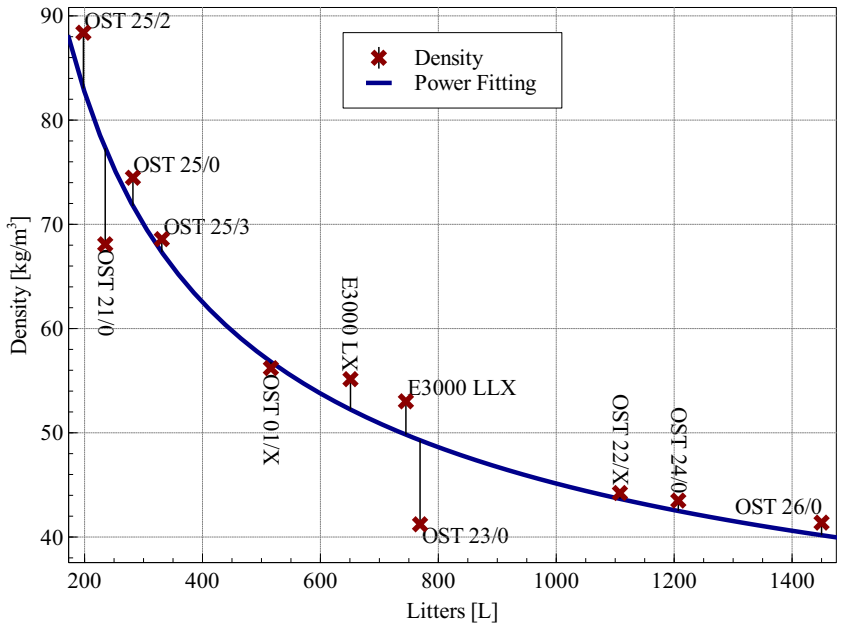

Figure 3.4 Fuel tank density, and capacity, for several fuel tanks (from reference [61]) and a fitting function.

The fitting function was computed in MATLAB® using a power approximation, whose parameters are presented in the table 3.4. As a test for the fitting function we estimate the density of the Space Shuttle tank (mass $78,100$ pounds $\approx 35,426$ kg, volume $526,126$ gallons $\approx 1,991,604$ L and density $\approx 17.79\,\mathrm{kg/m^3}$)[62] with an error of 1.7% (yielding $\approx 18.1\,\mathrm{kg/m^3}$).

Table 3.4 Fitting function parameters (R^2 and Adjusted R^2 are fitting quality parameters) [63].

Model	a	b	c	R^2	Adjusted R^2	Maximum of the Residuals
$a.L_T^b + c$	1,106.38	-0.53	17.62	0.9457	0.9336	9.22

With this function we compute the fuel tank density (ρ_T) and combined fuel tank mass (M_T) by:

$$L_P = \frac{v_P}{0.001} \rightarrow L_T = \frac{L_P}{n_T} \begin{cases} \rho_T = a \times L_T^b + c \\ \\ v_T = \frac{v_P}{n_T} \end{cases} \quad M_T^i = \rho_T \times v_T \quad \Rightarrow \quad M_T = M_T^i \times n_T, \tag{3.2}$$

where n_T is the number of tanks, $n_T = 6$, and M_T^i the mass of each tank.

Solar Panels

Among the several kinds of power sources (presented in section 1.3.3) the solar photovoltaic is used. This system converts solar radiation to electrical energy using solar panels. The solar panels described here supply the necessary power only for the propulsion system. The size of the solar array depends on:

- Power requirements (W), given by the selected engine;

- Position of the spacecraft in relation to the Sun, which affects the energy received by the solar cells, i.e. solar irradiance (S_0);
- Deviation from the optimum angle of incidence (α), which is the perpendicular to the surface of the solar panel;
- Energy storage efficiency ($\epsilon_{storage}$);
- The type of the solar cell used, i.e. the efficiency of the cells at the beginning of life (ϵ_{cells}), its degradation (D) and finally the areal density (ρ_A^{sp}).

Many types of solar panels are available in the market and, after some research, the Emcore ZTJ Photovoltaic Cell is selected. The choice is made given its high efficiency (ϵ_{cells} = 29.5%), for being the latest kind of solar cells (3rd Generation Triple-Junction cell) with the lowest mass (ρ_A^{sp} = 0.84 kg/m^2) and already space qualified (with proven flights) [64]. The degradation rate of the cells is 0.4 %/year [64]. The equations for the solar panels area and mass, derived from reference [58], are:

$$A^{sp} = \frac{W}{S_0 \times cos(\alpha) \times \epsilon_{cells} \times \epsilon_{storage} \times (1-D)^t}, \tag{3.3}$$

$$M^{sp} = A_{panels} \times \rho_A^{sp}. \tag{3.4}$$

For safety reasons the computations of size and mass are performed for the worst case scenario. For the present mission this is when the engines are at full power (power of the engine shown in table 2.3) in orbit of Mars (S_0 = 590 W/m^2 at the mean distance from the Sun [65]). It also means a life time, t_{life}, equal to the longer mission time, an EtM and MtE Hohmann transfer (t_{life} = 3 years). Some values are selected for the deviation angle and storage efficiency from reference [58] (α = 30° and $\epsilon_{storage}$ = 88%). The area and mass necessary for a single electrical engine operating during the entire mission are presented in table 3.5.

Table 3.5 Values of surface area and solar array mass for a single electrical engine.

Engine	Solar Panel Surface [m^2]	Mass of Solar Array [kg]
PPS 1350-G	11.45	9.61

Radiator & Reflector Cone

Some of the characteristics of the radiator and reflector cone were already discussed in sections 2.3.1 and 2.3.2, namely: the materials use for each one are carbon nanotubes (ρ_{rad} = 37 kg/m^3 [45]) and aluminized mylar (ρ_{ref} = 10 g/m^2 [22]) respectively; and the radiator temperature is T = 3,300 K.

The dimensions of both components depend on the thrust one wishes to extract from the engine. For this work a thickness of 0.5 m is assumed for the radiator, to account for the coolant system (discussed in section 2.3.2), which is well within the current technology since structural sheets with thickness smaller than 1 mm are already available [45]. From the Stefan-Boltzmann equation (2.3) and equation (1.4) we have

$$S = \frac{c \times F_T}{\varepsilon \sigma T^4}, \tag{3.5}$$

which, combined with the materials density, determines the mass of the radiator.

3.2.3 Transport Capsules

The only two components left to account for are the transport capsules. This data is shown in table 3.6. The transport capsule carries the crew from Earth to the mother ship and then to Mars (upon arrival). It uses the aeroshell to land on Mars. On the other hand, the MAV is the vehicle used by the astronauts to leave Mars and rendezvous with the mother ship. Again it would also be used for landing on Earth.

When leaving Earth the transport capsule would be taken to space (and then to rendezvous with the mother ship) by a launcher, when leaving Mars the MAV has to perform this task. Thus, we do not need to include a fuel component on the transport capsule. The fuel mass of the MAV shown in table 3.6 is taken from Mars Direct [7].

Table 3.6 Transport capsule and MAV masses (in tonnes).

Earth to Mars		Mars to Earth	
Transport Capsule	4.00	MAV	5.80
Aeroshell	1.80	MAV Fuel	12.20
Total	5.80		18.00

3.2.4 Mass Budget

Combining the data, the mass budget for the manned mission is shown in table 3.7. Table 3.8 shows the mass budget for the unmanned mission.

Table 3.7 Mass budget for the manned spacecraft.

Element	Mass	Comment
Crew	$M^{Crew} = 0.4\,\text{tonnes}$	A crew of four elements.
Spacecraft Structural Mass		
Habitat Module	$M^{Hab} = 31.52\,\text{tonnes}$	Section 3.2.1.
Transport Capsule & Aeroshell	$M^{TC} = 5.8\,\text{tonnes}$	
Propulsion System		
Departure and Capture Engine	M_{En}^{DC}	Sections 2.1.1 and 2.1.2.
Interplanetary Engine	M_{En}^{I}	Sections 2.2.1 and 2.3.1.
Solar Panels	M^{SP}	Section 3.2.2.
Radiator & Reflector	M^{RR}	Section 3.2.2.
Propellants	$M_P^T = M_P^D + M_P^I + M_P^C + M_P^{HT}$	Sections 2.1.3, 2.2.2 and 2.3.3.
Tanks	$M_T^T = M_T^D + M_T^I + M_T^C + M_T^{HT}$	Section 3.2.2.
Dry Mass	$M_{Dry} = 37.71 + M_{En}^{DC} + M_{En}^{I} + M^{SP} + M^{RR}$	In the dry mass the tanks are not included since they would be discarded after each manoeuvre.
Total Mass	$M_{Total} = M_{Dry} + M_P^T + M_T^T$	

In both tables we can see that while the crew, the modules (habitat and cargo) and the transport capsules are constants (obtained from extrapolations of previous proposals), the others are problem variables, depending on the mission options. The engine mass, solar panels and radiator & reflector depend on the system selected and the number of engines. The propellants and tanks also depend on the time of execution of the manoeuvres (related to the trajectory performed).

Table 3.8 Mass budget for the unmanned spacecraft.

Element	Mass	Comment
Spacecraft Structural Mass		
Cargo Module	M^{Cargo} = 42.11 tonnes	Section 3.2.1.
MAV & Fuel	M^{MAV} = 18 tonnes	
Propulsion System		
Departure and Capture Engine	M_{En}^{DC}	Section 2.1.1.
Interplanetary Engine	M_{En}^{I}	Section 2.2.1.
Solar Panels	M^{SP}	Section 3.2.2.
Propellants	$M_P^T = M_P^D + M_P^C + M_P^{HT}$	Section 2.1.3.
Tanks	$M_T^T = M_T^D + M_T^C + M_T^{HT}$	Section 3.2.2.
Propellant Payload	M^{PP}	
Dry Mass	$M_{Dry} = 60.11 + M_{En}^{DC} + M_{En}^{I} + M^{SP} + M_{En}^{PP}$	In the dry mass the tanks are not included since they would be discarded after each manoeuvre.
Total Mass	$M_{Total} = M_{Dry} + M_P^T + M_T^T$	

In the unmanned spacecraft (table 3.8) the fuel payload entry represents the propellants and tanks needed for the manned return trajectory. Due to this entry, the cargo mission can only be computed after the manned mission calculations.

Chapter 4

Trajectory Problem & Solution

In this chapter we derive the equation of motion and its solution. We then apply it on the departure, interplanetary travel and arrival. The departure and arrival were computed with impulsive trajectories, while the interplanetary was considered to be a non-impulsive one (sometimes with null thrust).

For the approximation of the impulsive trajectories all manoeuvres are considered to be made in a time instance. For non-impulsive trajectories we have a continuous acceleration problem. However, the objective is always to calculate a trajectory between two planets and obtain the time of flight and corresponding ΔVs (to obtain fuel requirements with implications on the total mass of the spacecraft).

4.1 Equations of Motion

Firstly we determined the equation of motion starting with Newton's 2nd law. The spacecraft position ($\vec{\boldsymbol{r}}$), velocity ($\dot{\vec{\boldsymbol{r}}}$), acceleration ($\ddot{\vec{\boldsymbol{r}}}$) and force ($\vec{\boldsymbol{F}}$) are written as follows:

$$\vec{\boldsymbol{r}} = x\vec{\boldsymbol{i}} + y\vec{\boldsymbol{j}} + z\vec{\boldsymbol{k}} \qquad \dot{\vec{\boldsymbol{r}}} = \dot{x}\vec{\boldsymbol{i}} + \dot{y}\vec{\boldsymbol{j}} + \dot{z}\vec{\boldsymbol{k}} \qquad \ddot{\vec{\boldsymbol{r}}} = \ddot{x}\vec{\boldsymbol{i}} + \ddot{y}\vec{\boldsymbol{j}} + \ddot{z}\vec{\boldsymbol{k}}$$
$$\vec{\boldsymbol{F}} = F_x\vec{\boldsymbol{i}} + F_y\vec{\boldsymbol{j}} + F_z\vec{\boldsymbol{k}}.$$

In general the spacecraft is subjected to two forces:

Gravity It acts along a line that joins the centres of mass of the spacecraft and the central body and it has the direction of the latter ($\vec{\boldsymbol{u}}_{\boldsymbol{r}}$). It is a conservative force proportional to the gravitational parameter $\mu = GM$ (where G is Newton's constant and M the relevant gravitational mass). $\rightarrow \vec{\boldsymbol{F}}_{\boldsymbol{g}} = -\frac{\mu m}{r^2}\vec{\boldsymbol{u}}_{\boldsymbol{r}}$;

Thrust It is the force given by the engines of the spacecraft. It is a non-conservative force and its direction is defined by the vector $\vec{\boldsymbol{u}}_{\boldsymbol{F_T}}$. $\rightarrow \vec{\boldsymbol{F}}_{\boldsymbol{T}} = F_T\vec{\boldsymbol{u}}_{\boldsymbol{F_T}}$.

Combining these definitions we have (with $r = \sqrt{x^2 + y^2 + z^2}$)

$$\vec{\boldsymbol{F}} = m\ddot{\vec{\boldsymbol{r}}} \qquad \text{and} \qquad \vec{\boldsymbol{u}}_{\boldsymbol{r}} = \frac{\vec{\boldsymbol{r}}}{r} \qquad \Rightarrow \qquad \ddot{\vec{\boldsymbol{r}}} = -\frac{\mu}{r^3}\vec{\boldsymbol{r}} + \frac{F_T}{m}\vec{\boldsymbol{u}}_{\boldsymbol{F_T}}. \tag{4.1}$$

Equation (4.1) can be divided in three Cartesian components involving nine unknowns (position, velocity and acceleration).

Impulsive Trajectories When only gravity is present, equation (4.1) can be simplified to

$$\ddot{\vec{\boldsymbol{r}}} + \frac{\mu}{r^3}\vec{\boldsymbol{r}} = 0. \tag{4.2}$$

The solution for this equation is the well known trajectory equation of the Keplerian orbits [66].

Non-Impulsive Trajectory When a spacecraft is subjected to a continuous thrust, equation (4.1) cannot be simplified. For that reason one cannot apply the Keplerian solution to the trajectory and a numerical integration is performed.

4.1.1 Thrust Direction

The thrust direction is a parameter of the problem (as seen in section 3.1.2).

When using the impulsive approximation we assume that the thrust is in the velocity direction. However, when using a continuous thrust and performing trajectory optimisation, it is usual to include a control parameter for the thrust direction [67].

On this work we do not intend to optimise the trajectory but to compare the propulsion systems. We use two options for the thrust direction:

1. The thrust has a constant angle with the velocity vector (figure 4.1a);
2. The thrust has a constant angle relative to the Sun (figure 4.1b).

The first option depends on the orientation of the velocity $\left(\vec{\boldsymbol{u}}_{\dot{\vec{\boldsymbol{r}}}} = \frac{\dot{\vec{\boldsymbol{r}}}}{\|\dot{\vec{\boldsymbol{r}}}\|}\right)$, and can be mathematically written as

$$\vec{\boldsymbol{u}}_{\boldsymbol{F_T}} = \left(R^i(\theta_{F_T}) \times \frac{\dot{\vec{\boldsymbol{r}}}}{\|\dot{\vec{\boldsymbol{r}}}\|}\right) \quad \Rightarrow \quad \vec{\boldsymbol{F}}_{\boldsymbol{T}} = F_T \times \left(R^i(\theta_{F_T}) \times \frac{\dot{\vec{\boldsymbol{r}}}}{\|\dot{\vec{\boldsymbol{r}}}\|}\right), \tag{4.3}$$

where $R^i(\theta_{F_T}) = \begin{bmatrix} \cos(\theta_{F_T}) & -\sin(\theta_{F_T}) \\ \sin(\theta_{F_T}) & \cos(\theta_{F_T}) \end{bmatrix}$ is a rotation matrix and $\|\dot{\vec{\boldsymbol{r}}}\| = \sqrt{\dot{x}^2 + \dot{y}^2 + \dot{z}^2}$ is the norm of the velocity vector.

On the second option the thrust depends on an unitary vector of the Cartesian coordinate system shown in figure 4.1b, maintaining the angle in all interplanetary trajectory, and is written as

$$\vec{\boldsymbol{u}}_{\boldsymbol{F_T}} = \left(R^i(\theta_{F_T}) \times \begin{bmatrix} 0 \\ 1 \end{bmatrix}\right) \quad \Rightarrow \quad \vec{\boldsymbol{F}}_{\boldsymbol{T}} = F_T \times \left(R^i(\theta_{F_T}) \times \begin{bmatrix} 0 \\ 1 \end{bmatrix}\right). \tag{4.4}$$

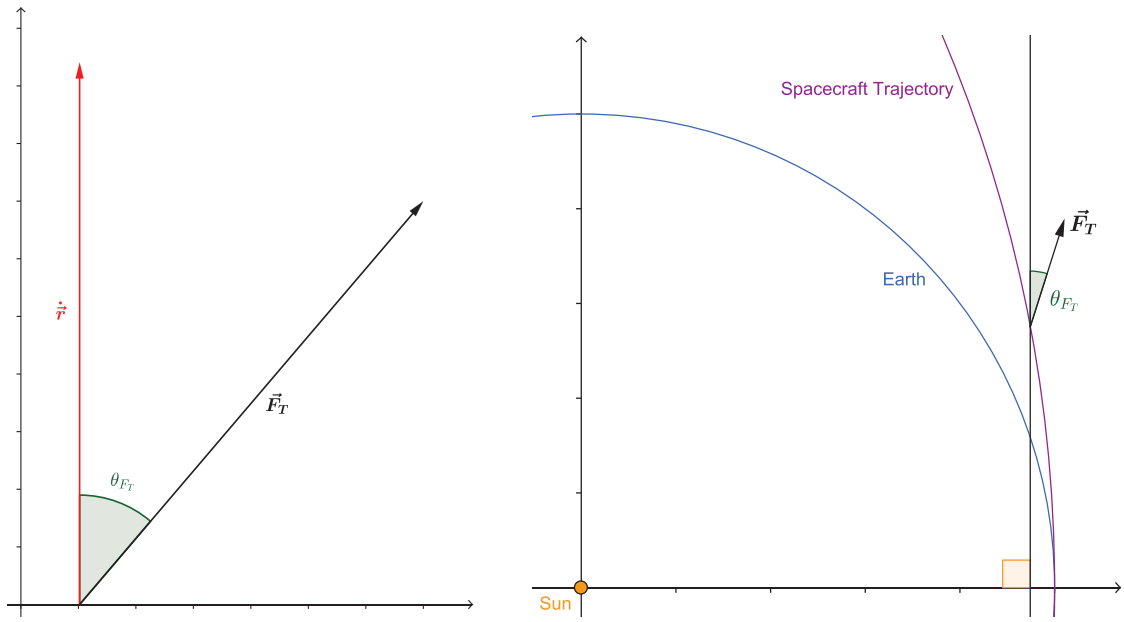

(a) $\vec{\boldsymbol{F}}_{\boldsymbol{T}}$ relative to the spacecraft velocity. **(b)** $\vec{\boldsymbol{F}}_{\boldsymbol{T}}$ relative to the Heliocentric Coordinate System.

Figure 4.1 Orientation of the thrust in the interplanetary phase (positive angles are counterclockwise).

4.1.2 Trajectory Assumptions

The first simplification concerns the motion of the planets. It is assumed that both planets move in coplanar circular orbits. By assuming a circular motion, the departure date, and hence the location of it, does not affect the trajectory since the velocity of both planet and distance between them are constant. The only requirement on the planets position is the phase angle between them, so to reach the target planet. This allows for a standard procedure for the departure location between all the different trajectories. Having both orbits at the same plane simplifies the problem to two dimensions, reducing the number of unknowns to six.

By separating the trajectory in three phases (departure, interplanetary phase and arrival), the second simplification is the so called "patched conics". This is a simplification for the three body problem, i.e. in each phase we considered that the spacecraft movement is only affected by the central body (the planet or the Sun) neglecting the forces exerted by other celestial bodies. This is a valid approximation when one compares the size of the sphere of influence (SOI) of each planet (where the gravity of the planet is the dominant force) to the whole trajectory between both planets (where the gravity of the Sun is the dominant force), and the time spent on the interface between the different phases. In the end the conics are matched, i.e. the velocity at the end of a phase must be the same at the beginning of the other.

4.1.3 Numerical Method

In the present work the solution of equation (4.1) is obtained numerically and, as such, it is necessary to reduce the three second order differential equations to six first order differential equations. For the non-impulsive systems we can also solve the fuel usage problem at the same time, using the equation described in section 2.2.2. Therefore, we introduced the auxiliary variables ($\boldsymbol{\Upsilon}$) and their derivatives ($\dot{\boldsymbol{\Upsilon}}$):

$$\begin{array}{ccccccc} \Upsilon_1 = x & \Upsilon_2 = y & \Upsilon_3 = z & & \dot{\Upsilon}_1 = \Upsilon_4 & \dot{\Upsilon}_2 = \Upsilon_5 & \dot{\Upsilon}_3 = \Upsilon_6 \\ \Upsilon_4 = \dot{x} & \Upsilon_5 = \dot{y} & \Upsilon_6 = \dot{z} & & \dot{\Upsilon}_4 = \ddot{x} & \dot{\Upsilon}_5 = \ddot{y} & \dot{\Upsilon}_6 = \ddot{z} \\ & \Upsilon_7 = m & & & & \dot{\Upsilon}_7 = \dot{m}. & \end{array}$$

These form a system of first order differential equations, $\dot{\boldsymbol{\Upsilon}} = \boldsymbol{f}(t, \boldsymbol{\Upsilon})$, with $\boldsymbol{f}(t, \boldsymbol{\Upsilon})$ as

$$\boldsymbol{f} = \begin{Bmatrix} \Upsilon_1 \\ \Upsilon_2 \\ \Upsilon_3 \\ -\frac{\mu}{r^3}\Upsilon_1 + \frac{F_T}{m}\frac{\Upsilon_4}{\|\dot{\boldsymbol{r}}\|} \\ -\frac{\mu}{r^3}\Upsilon_2 + \frac{F_T}{m}\frac{\Upsilon_5}{\|\dot{\boldsymbol{r}}\|} \\ -\frac{\mu}{r^3}\Upsilon_3 + \frac{F_T}{m}\frac{\Upsilon_6}{\|\dot{\boldsymbol{r}}\|} \\ -\frac{F_T}{I_{\mathrm{sp}} g_0} \end{Bmatrix}.$$

The numerical method we use to solve the system is the Explicit Runge-Kutta method expressed as

$$\boldsymbol{\Upsilon}_{i+1} = \boldsymbol{\Upsilon}_i + H f(t_i, \boldsymbol{\Upsilon}_i, H), \tag{4.5}$$

where $f(t_i, \boldsymbol{\Upsilon}_i, H)$ is an increment function evaluated at several mid points (in the time interval t_i to $t_i + H$) [68]. An automatic variable step size solution is also used, to increase the accuracy of the algorithm, i.e. a step size smaller for rapid changes in the solution and larger for slow changes. This is called an embedded method and is obtained by combining two adjacent-order Runge-Kutta methods. The RKp is the Runge-Kutta method of order

p and it uses the pth order Taylor series. The commonly used in astronomy is the Runge-Kutta-Fehlberg 7th order formula with 8th order error estimate (RKF7(8)) [68].

Using the notation of Curtis (reference [38]) we have for the nodes $\{\boldsymbol{a}\}$, coupling coefficients $[\boldsymbol{b}]$ and weights $\{\boldsymbol{c}\}$ the following equations for $\boldsymbol{\Upsilon}_{i+1}$:

$$\begin{aligned}
\tilde{t}_m &= t_i + a_m H \quad m = 1, 2, \cdots, s \\
\tilde{\boldsymbol{\Upsilon}}_m &= \boldsymbol{\Upsilon}_i + H \sum_{n=1}^{m-1} b_{mn} \tilde{\boldsymbol{f}}_n \quad m = 1, 2, \cdots, s \\
\text{7th order } \boldsymbol{\Upsilon}_{i+1} &= \boldsymbol{\Upsilon}_i + H \sum_{m=1}^{s} c_m \tilde{\boldsymbol{f}}_n \left(\tilde{t}_m, \tilde{\boldsymbol{\Upsilon}}_m\right) \quad s = \text{number of stages} \qquad (4.6) \\
\text{8th order } \boldsymbol{\Upsilon}^*_{i+1} &= \boldsymbol{\Upsilon}_i + H \sum_{m=1}^{s} c^*_m \tilde{\boldsymbol{f}}_n \left(\tilde{t}_m, \tilde{\boldsymbol{\Upsilon}}_m\right). \qquad (4.7)
\end{aligned}$$

For computing the step size we determine $\boldsymbol{\Upsilon}^*_{i+1}$ and $\boldsymbol{\Upsilon}_{i+1}$. We compute the difference between both solutions determining the maximum scalar value (for all the N first order equations). This yields an estimate of the local error $\rightarrow \boldsymbol{e} = \boldsymbol{\Upsilon}_{i+1} - \boldsymbol{\Upsilon}^*_{i+1} \rightarrow e = \max\left(|e_1|, \cdots, |e_N|\right)$.

With this we update H after each time step, increasing it if it is smaller than a predefined tolerance (tol) or decreasing it if it is higher, following the ideas presented in reference [68]:

$$\begin{aligned}
&H^* = H_{old}\left(\tfrac{tol}{e}\right)^{\frac{1}{p+1}} \\
&\beta = 0.25^{\frac{1}{p+1}} \qquad \Rightarrow \quad H_{new} = \min\left(\beta H^*, \beta_{max} H_{old}\right). \\
&\begin{cases} \beta_{max} = 1.5 & \text{for a step-acception} \\ \beta_{max} = 1 & \text{for a step-rejection} \end{cases}
\end{aligned} \qquad (4.8)$$

The result of an iteration of the RKF7(8) is only acceptable if the error is lower than tol. The integration is done until a predetermined condition is achieved. The coefficients a, b and c for the RKF7(8) are in appendix A.1, and the MATLAB® code for the numerical integration is in appendix A.3.

4.2 Departure

For the departure phase we use chemical or nuclear thermal engines (for the reasons explained in section 3.1.3), where the impulsive approximation is valid, thus allowing the use of equation (4.2).

For the spacecraft to escape the departure planet and start the interplanetary trajectory it must have a certain velocity at the frontier of the SOI, V^D_∞, when the distance to the planet is considered to be infinite. Considering the spacecraft is in a launch orbit around the planet we must give a ΔV^D to enter the escape hyperbola (figure 4.2).

The algorithm we use to compute the ΔV^D is the following:

1. Specify:
   - r_p - Periapsis radius of the launch orbit;
   - e^l - Eccentricity of the launch orbit;
   - μ - Gravitational parameter of the departure planet ($\mu_\oplus$ or $\mu_♂$ in our problem);
   - V^D_∞ - Hyperbolic excess velocity ($= \sqrt{C_3}$).

2. Calculate the orbital parameters of the launch orbit:
   - h^l - Angular momentum $\rightarrow h^l = \sqrt{\mu \times r_p \times (e^l + 1)}$;
   - a^l - Semimajor axis $\rightarrow a^l = \dfrac{(h^l)^2}{\mu} \dfrac{1}{1-(e^l)^2}$;
   - V_p^l - Periapsis velocity $\rightarrow V_p^l = \sqrt{\dfrac{\mu\left(2a^l - r_p\right)}{a^l \times r_p}}$;
3. Calculate the orbital parameters of the hyperbolic escape orbit (knowing that r_p of both orbits is the same):
   - e^D - Eccentricity $\rightarrow e^D = \dfrac{r_p \times (V_\infty^D)^2 + \mu}{\mu}$;
   - h^D - Angular momentum $\rightarrow h^D = \sqrt{\mu \times r_p \times (e^D + 1)}$;
   - a^D - Semimajor axis $\rightarrow a^D = \dfrac{(h^D)^2}{\mu} \dfrac{1}{(e^D)^2 - 1}$;
   - V_p^D - Periapsis velocity $\rightarrow V_p^D = \sqrt{\dfrac{\mu\left(2a^D + r_p\right)}{a^D \times r_p}}$;
4. Obtain the ΔV^D to supply to the spacecraft

$$\Delta V^D = V_p^D - V_p^l = \sqrt{(V_\infty^D)^2 + \frac{2\mu}{r_p}} - \sqrt{\frac{\mu \times (1+e^l)}{r_p}}. \tag{4.9}$$

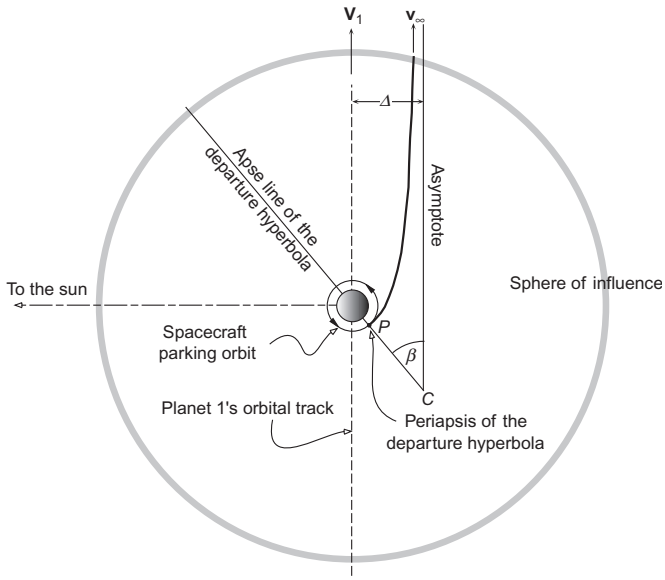

Figure 4.2 Orbits described by the spacecraft during the departure phase, when inside the SOI (for the case that V_∞^D is aligned with the planet's velocity, V_1, and the spacecraft is in a circular parking orbit) [38].

4.3 Interplanetary Phase

The interplanetary phase is computed with a direct application of the numerical scheme expressed by equation (4.6).

Here we specify the spacecraft initial position ($\vec{\boldsymbol{r}} = [x \quad y]$), velocity ($\dot{\vec{\boldsymbol{r}}} = [\dot{x} \quad \dot{y}]$) and mass.

The velocity of the spacecraft at the beginning ($\vec{V_D}^{(v)}$) is computed as a vector addition of the planet's orbital velocity ($\vec{V_1}$) and the velocity of the spacecraft at the end of the departure phase (V_∞^D). Using the velocity at the end of the interplanetary journey ($\vec{V_A}^{(v)}$), and performing a vector subtraction with the planet's velocity ($\vec{V_2}$), we compute V_∞^C for the capture phase. An example of this procedure is seen in figure 4.3 and in section 4.3.1.

Two conditions are use as stopping criteria of the RKF7(8), due to the automatic step size control:

1. If the distance of the spacecraft to the target planet is smaller than 0.3% of the planet's SOI dimension;
2. If the distance of the spacecraft to the Sun is greater than that of the planet, for an Earth to Mars transfer, smaller in case of a Mars to Earth transfer.

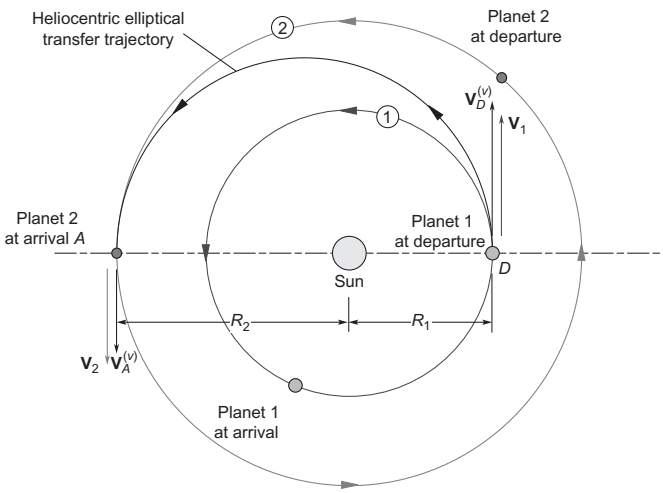

Figure 4.3 Example of an interplanetary Hohmann transfer orbit [38].

4.3.1 Velocity at the Start and at the End

The spacecraft velocity at the end of the departure phase, V_∞^D, can be oriented in any direction, depending on the location of the periapsis [38]. This location is selected based on the requirements of the interplanetary phase. In this work the direction of the velocity is determined with respect to the planet's velocity (see figure 4.4). The vector addition to obtain $V_D^{(v)}$ is thus

$$\vec{V_D}^{(v)} = \vec{V_\infty}^{D} + \vec{V_1} = V_\infty^D \times \left(R^i(\theta_V) \times \begin{bmatrix} 0 \\ 1 \end{bmatrix} \right) + \begin{bmatrix} 0 \\ V_1 \end{bmatrix}, \tag{4.10}$$

where $R^i(\theta_V)$ is the rotation matrix and θ_V the angle between V_∞^D and the planet's mean orbital velocity (from reference [69]). V_1 in our work is always a vertical vector at the spacecraft departure location.

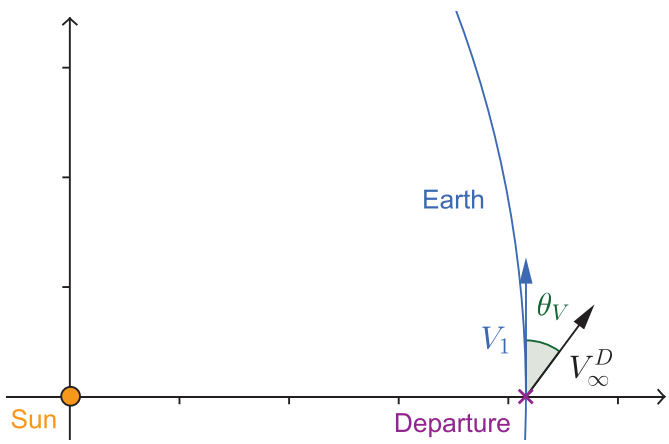

Figure 4.4 Planet and spacecraft velocities at departure (positive angles are counterclockwise).

While $\vec{V_1}$ on our work is a vertical vector with modulus equal to the planet's mean orbital velocity, it is necessary to determine $\vec{V_2}$, to obtain V_∞^C. On figure 4.5 we see that

$$\vec{V_2} = \begin{bmatrix} V_2 \times \sin(\alpha) \times a \\ V_2 \times \cos(\alpha) \times b \end{bmatrix},$$

where $\alpha = \left\| \arctan\left(\frac{y_f}{x_f}\right) \right\|$ and a & b are constants alternating between -1 and 1 depending on the quadrant (for the image example $a = -1$ and $b = -1$ since both components must be negative). The x_f and y_f comes from the numerical integration as well as the spacecraft final velocity ($\vec{V_A}^{(v)}$).

The velocity for the capture phase is given by

$$V_\infty^C = \vec{V_A}^{(v)} - \vec{V_2} = \vec{V_A}^{(v)} - \begin{bmatrix} V_2 \times \sin(\alpha) \times a \\ V_2 \times \cos(\alpha) \times b \end{bmatrix}. \tag{4.11}$$

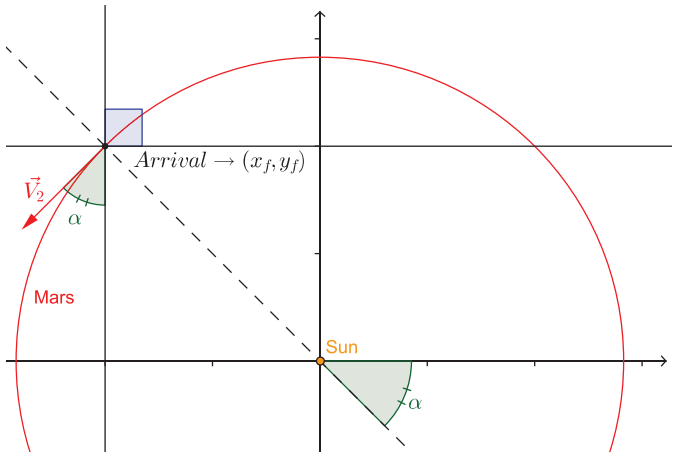

Figure 4.5 Geometric construction of arrival planet's velocity, which depends on the arrival location x_f and y_f.

For the return the same algorithm is followed, with the difference of subtracting V_∞^D at the departure. since we aim to travel from an outer planet to a inner one.

4.3.2 Heliocentric Angles

After reaching the target planet we compute the initial phase angle between the planets (ϕ_0) using the heliocentric angles (figure 4.6) and the following algorithm:

1. Calculate the initial and final heliocentric angles of the spacecraft ($\theta_{SC}^i = \arctan\left(\frac{y_i}{x_i}\right)$ and $\theta_{SC}^f = \arctan\left(\frac{y_f}{x_f}\right)$), correcting the quadrant when needed;
2. Using the angular velocity of each planet (n_P) and the time of flight (TOF), determine the final heliocentric angle of the departure planet ($\theta_{P_1}^f = \theta_S^i + n_{P_1} \times TOF$) and the initial heliocentric angle of the arrival planet ($\theta_{P_2}^i = \theta_S^f - n_{P_2} \times TOF$);
3. Compute the initial phase angle as $\phi_0 = \theta_{P_2}^i - \theta_{P_1}^i$.

If $\phi_0 > 0$ the arrival planet must be ahead of the departure one and vice versa, if $\phi_0 < 0$. The value of the angular velocity of each planet is determined dividing 2π by the sidereal orbital period obtained in reference [69].

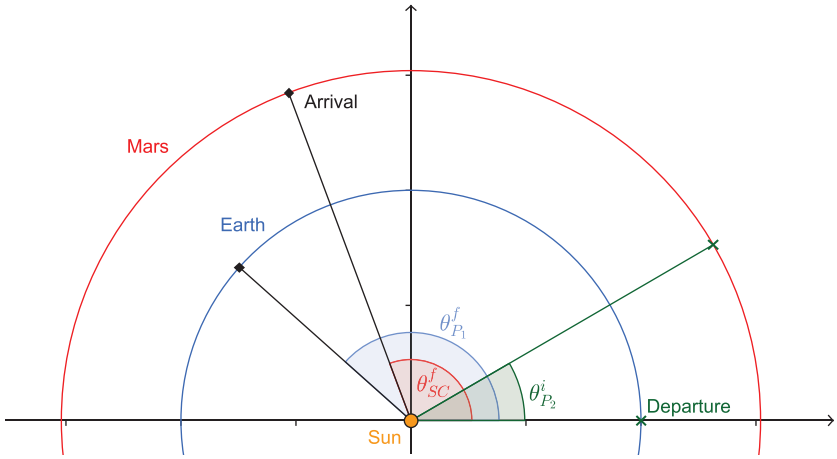

Figure 4.6 Heliocentric angles at the departure and arrival on an Earth to Mars transfer (positive angles are counterclockwise).

4.3.3 Waiting Time

An important quantity is the waiting time on Mars (t_w), i.e. the time we need to wait on Mars for Earth to have the correct phase angle so the spacecraft can rendezvous with it on the return trip. The waiting time can only be determined after having the TOF for the EtM and MtE transfers. It is determined using the following equations (where $N = 0, 1, 2, ...$ to give a positive time):

$$\begin{aligned}
\phi_0^{EtM} &= \theta^f_{♂} - \theta^f_{\oplus} \text{ in the Earth to Mars trajectory} \\
\phi_0^{MtE} &= \theta^i_{♂} - \theta^i_{\oplus} \text{ in the Mars to Earth trajectory} \\
\Phi &= \phi_0^{MtE} - \phi_0^{EtM} \\
t_w &= \frac{\Phi - 2\pi N}{n_M - n_E}.
\end{aligned} \tag{4.12}$$

4.4 Capture

For the capture phase we use a chemical or nuclear thermal engines and therefore equation (4.2), as in the departure.

The calculations for the capture hyperbola are similar to those described in section 4.2, with the difference that the ΔV^C is the velocity change given to the spacecraft to leave the hyperbola and remain in orbit at the arrival planet (figure 4.7).

As seen in the previous section, V^C_∞ at the SOI frontier is given by the interplanetary transfer. To obtain ΔV^C the following algorithm is used:

1. Specify:
   - r_p - Periapsis radius of final orbit;
   - e^f - Eccentricity of final orbit;
   - μ - Gravitational parameter of the arrival planet ($\mu_\oplus$ or $\mu_♂$ in our problem);
   - V^C_∞ - Hyperbolic excess velocity.
2. Compute the orbital parameters of the final orbit and of the hyperbolic orbit as in section 4.2;

3. Obtain the ΔV^C to supply to the spacecraft:

$$\Delta V^C = V_p^C - V_p^f = \sqrt{(V_\infty^C)^2 + \frac{2\mu}{r_p}} - \sqrt{\frac{\mu \times (1 + e^f)}{r_p}}. \tag{4.13}$$

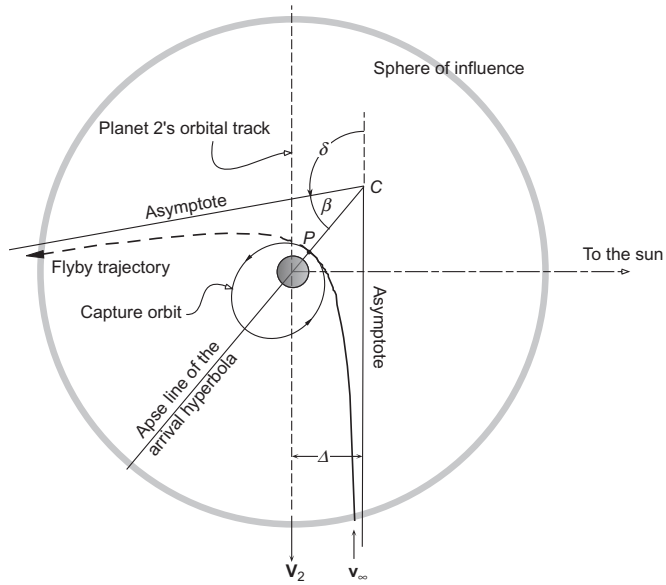

Figure 4.7 Orbits described by the spacecraft during the capture phase, when inside the SOI (for the case that V_∞^C is aligned with the planet's velocity V_2) [38].

4.5 Orbital Transfers Around the Planet

For all other remaining transfers we use a two impulse manoeuvre (if we need to change the periapsis radius, e.g. rendezvous of the transfer capsule with the mother ship) or a simple one impulse manoeuvre on the periapsis (if we want to maintain the periapsis radius, e.g. the orbital raising before departure from Earth).

For a one impulse manoeuvre we have only one periapsis radius, and two eccentricities (of the initial and final orbit). We compute the periapsis velocity of both orbits as in section 4.2. In this case we do not have a transfer orbit since we change immediately at the periapsis between the initial orbit (numbered one) and final orbit (numbered two). The ΔV provided to the spacecraft is

$$\Delta V_1 = \left\| V_p^2 - V_p^1 \right\|. \tag{4.14}$$

For a two impulse manoeuvre we have to define the initial and final periapsis radius. As above we compute the orbital parameters of the initial and final orbit using the eccentricity of both orbits. We assign the periapsis radius of the transfer orbit to be the lower periapsis, and the apoapsis of the transfer the higher apoapsis, and compute the eccentricity of the transfer orbit $\left(e^t = \frac{r_a - r_p}{r_a + r_p}\right)$ and remaining orbital parameters (again as in section 4.2). We calculate the ΔVs necessary for the two impulses manoeuvre by

$$\begin{aligned} \Delta V_1 &= V_p^t - V_p^1 \\ \Delta V_2 &= V_a^2 - V_a^t, \end{aligned} \tag{4.15}$$

from a lower orbit to a higher orbit (orbit 3 in figure 4.8) and

$$\Delta V_1 = V_a^t - V_a^1$$
$$\Delta V_1 = V_p^2 - V_p^t, \tag{4.16}$$

from a higher orbit to a lower orbit (orbit 3' in figure 4.8).

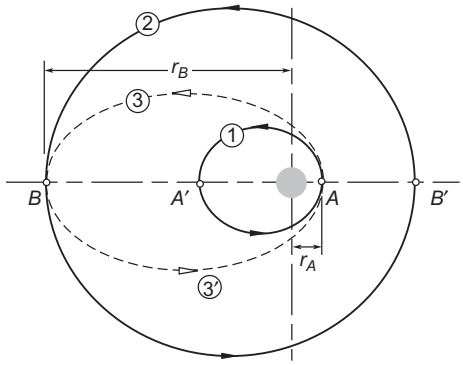

Figure 4.8 Transfers between two elliptical coplanar orbits (adapted from reference [38]).

4.6 Algorithm Validations

Having defined how to computed all orbits and developed the algorithms in MATLAB® we performed a series of tests on the numerical integration and on the algorithm itself.

4.6.1 Numerical Integration Tests

To test the errors when performing the numerical integration we compare it with an analytical solution. The test case here is the ellipse and the hyperbola Cartesian equations centered at (x_0, y_0):

$$\frac{(x - x_0)^2}{a^2} + \frac{(y - y_0)^2}{b^2} = 1 \tag{4.17}$$
$$\frac{(x - x_0)^2}{a^2} - \frac{(y - y_0)^2}{b^2} = 1. \tag{4.18}$$

Ellipse We determine the Hohmann transfer between Earth and Mars (which is a half ellipse). Applying ΔV_1 we compute the outgoing transfer and with ΔV_2 the return. Replacing every (x, y) pair in equation (4.17) by the coordinates given by the numerical integration, we look for the maximum difference to the right hand side of equation (4.17). For this case the foci is the Sun, making the centre $(x_0 = -(ae), y_0 = 0)$ in our Heliocentric Cartesian coordinate system - figure 4.9.

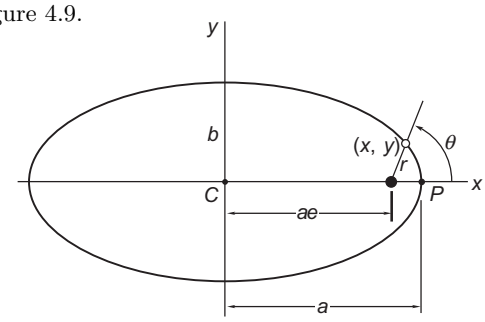

Figure 4.9 Drawing of an elliptical orbit [38].

The maximum difference is of the order of 10^{-6} and can be seen at appendix A.2, figure A.1.

Hyperbola We compute the arrival hyperbola characteristics (periapsis radius, eccentricity, semimajor axis and conjugate axis $b = a\sqrt{e^2-1}$). We determine the (x, y) position on the hyperbola whose distance is equal to the planet's SOI, and corresponding velocity, by:

$$r = a^C \frac{(e^C)^2 - 1}{1 + e^C \cos(\theta)} \overset{r=SOI}{\rightarrow} \theta = -\arccos\left[\left(\frac{a^C\left((e^C)^2-1\right)}{SOI} - 1\right) \times \frac{1}{e^C}\right] \Rightarrow$$

$$\Rightarrow \quad (x; y) = \left(-a^C \frac{e^C + \cos(\theta)}{1 + e^C \cos(\theta)} + \left(a^C + r_p\right); \quad b\frac{\sqrt{(e^C)^2-1}\sin(\theta)}{1 + e^C \cos(\theta)}\right) \quad \text{and} \quad V = \left(\frac{\mu(2a^C + r)}{a^C \times r}\right)^{1/2}. \tag{4.19}$$

Using the numerical integration, we obtain every pair (x, y) of the hyperbola to replace in equation (4.18). In this case the foci of the hyperbola is the planet's centre and thus $(x_0 = a + r_p, y_0 = 0)$ - figure 4.10.

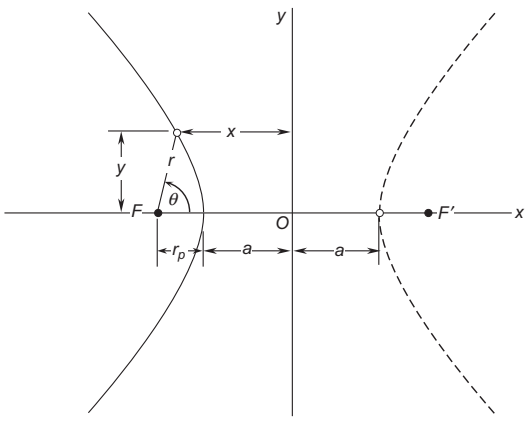

Figure 4.10 Drawing of an hyperbolic orbit [38].

The error for the hyperbola is found to be greater than the ellipse, reaching a difference of 0.003 to the exact value of 1 of equation 4.18 (see appendix A.2, figure A.2).

4.6.2 Test Cases

In order to test the implemented algorithm two experiments were conducted. The first test consists in the developed program solving two examples from reference [38] where the initial and final position, manoeuvre time and fuel spent are given. Secondly, we perform the Hohmann manoeuvre and extract the error in travel time, ΔV at arrival (since we imposed the initial ΔV) and on the departure and arrival manoeuvres. We also test the waiting time using the same Hohmann transfer for the return.

Examples With the input of the initial position, velocity and mass (together with thrust and I_{sp}) we compute the resulting data after a predetermined time. The data provided in reference [38] together with the error obtained is shown in tables 4.1 and 4.2. We can see that the errors are very small, meaning that the program returns good values even for non null thrust (which is the case in section 4.6.1).

Table 4.1 First example data and obtained errors ($F_T = 10,000\,\text{N}$, $I_{sp} = 300\,\text{s}$ and burn time = 261 s).

	Initial Data	Final Theoretical Data	Maximum Error Obtained [%]
Position [m]	$[6,858 \times 10^3,\ 0,\ 0]$	$[6,551.56 \times 10^3,\ 2,185.85 \times 10^3,\ 0]$	0.0107
Velocity [m/s]	$[0,\ 7.71 \times 10^3,\ 0]$	$[-2.4223 \times 10^3,\ 9.07202 \times 10^3,\ 0]$	0.0110
Mass [kg]	2000	1112.495	0.00791

Table 4.2 Second example data and obtained errors (F_T = 2.5 N, I_{sp} = 10,000 s and burn time = 21.038 days).

	Initial Data	Final Theoretical Data	Maximum Error Obtained [%]
Position [m]	$[6,678 \times 10^3,\ 0,\ 0]$	$[-19,935 \times 10^3,\ -37,176 \times 10^3,\ 0]$	0.1892
Velocity [m/s]	$[0,\ 7.73 \times 10^3,\ 0]$	$[2.6755 \times 10^3,\ -1.516 \times 10^3,\ 0]$	0.0950
Mass [kg]	1000	953.6645	9.52×10^{-7}

Hohmann Transfer Here we use the analytical Hohmann trajectory whose theoretical data is presented in table 4.3, on which we can also see the errors obtained for this data using the numerical integration. By performing this analysis we can also test the departure, capture and chemical fuel algorithm (table 4.4). The departure is from a 300 km high circular orbit. The final orbit at arrival has an eccentricity of 0.3833 and a periapsis radius of 5,447 km. All parameters return errors lower than 1 %, apart from the waiting time (1.2%).

Table 4.3 Hohmann transfer theoretical data and obtained errors.

	Theoretical	Error [%]
C_3 [m^2/s^2]	8,661,249	0.1678
V_∞ [m/s]	2,648	0.0565
TOF [days]	258.82	0.2515
Waiting Time [days]	453.8	1.1570

Table 4.4 Departure and arrival data (from reference [38]) and obtained errors.

	Theoretical Initial Orbit	Error [%]	Theoretical Final Orbit	Error [%]
ΔV[m/s]	3,590	0.012	1,470	0.0282
$\frac{\Delta m}{m}$	0.705	0.0297	-	-

Chapter 5

Results & Discussion

In this chapter we present and discuss the obtained results, the values of the relevant parameters and the procedure to compute the several missions. A discussion on the need to have an angle variation in the thrust and initial velocity is also presented.

5.1 Mission Computational Procedure

For manned Earth to Mars missions the calculations procedure is:

1. Compute the ΔV of the orbital raising manoeuvre for Earth departure, described in section 3.1.1, using equation (4.14);
2. For coast interplanetary missions (options 1 and 3 of figure 3.3) compute:
   (a) The departure ΔV using equation (4.9);
   (b) The interplanetary transfer (with null thrust), discussed in section 3.1.2, using the numerical method and equations (4.10) and (4.11) for the initial and final velocity, respectively;
   (c) The arrival ΔV using equation (4.13);
3. For powered interplanetary missions (options 2 and 4 of figure 3.3) we have to reverse the manoeuvres order and compute the arrival first, the interplanetary transfer second (now with an applied thrust) and then the departure;
4. Compute the ΔV of the crew circularisation manoeuvre executed around Mars at arrival (only performed by the crew inside the transport capsule, and not by the entire spacecraft, to rendezvous with the cargo at the lower circular orbit) as discussed in section 3.1.3 using equations (4.16);
5. Compute the fuel expenditure of the manoeuvres above (using equation (2.1) for impulsive manoeuvres, equation (2.2) for electrical propulsion and equation (2.8) for Rubbia's concept engine) in the inverse order (crew circularisation, arrival, interplanetary transfer, departure and orbital raising) since the fuel used in a manoeuvre must be included in the ones before.

For manned Mars to Earth missions the calculations procedure is:

1. Compute the ΔV of the crew orbital transfer manoeuvre, around Mars, from the lower circular orbit to the highly elliptical launch orbit, as described in section 3.1.4, using equations (4.15);

2. For coast interplanetary missions and for powered interplanetary missions we use the same procedure described above in the Earth to Mars mission;
3. Compute the ΔV of the crew orbital transfer manoeuvre executed around Earth at arrival (as discussed in section 3.1.4) using equations (4.16);
4. Compute the fuel expenditure of the manoeuvres (using the same equations as before) in the inverse order (crew orbital transfer on Earth, arrival, interplanetary transfer, departure and crew orbital transfer on Mars)

We have to iterate this procedure several times, since we compute the fuel expenditure and the powered interplanetary missions in an inverse order. We stop the iterations when we have a variation on the interplanetary time of flight (TOF) of less than one day and a variation on the spacecraft total mass of less than 0.1% of the spacecraft dry mass.

The calculations procedure for the Earth to Mars cargo mission (described in section 3.1.5), only performed after the manned mission, is:

1. Compute the ΔV of the orbital raising manoeuvre for Earth departure using equation (4.14);
2. For the coast and powered interplanetary missions compute as the Earth to Mars manned mission;
3. Compute the ΔV of the orbital transfer manoeuvre executed around Mars at arrival using equations (4.16);
4. Compute the fuel expenditure of the manoeuvres (using equation (2.1) for impulsive manoeuvres and equation (2.2) for electrical propulsion) in the inverse order (orbital transfer, arrival, interplanetary transfer, departure and orbital raising).

The orbital transfer manoeuvre on Mars is performed by the cargo spacecraft without the fuel for the manned return mission, which is left in the highly elliptical capture orbit, as described in sections 3.1.3 and 3.1.5.

5.2 Mission Parameters Values

To compute the various mission scenarios we consider the following parameters (discussed in chapter 3):

1. Propulsion System - table 5.1:
   - Engine Type - chemical (CECE), nuclear thermal (NERVA), electrical (PPS 1350-G) and/or Rubbia's concept (PEMT);
   - Number of Engines and Mass of the System - apart from fuel tanks and propellants.
2. Characteristic Energy (C_3) - table 5.2:
   - Absolute value - initialised with the Hohmann transfer value, progressively increasing it;
   - Vector direction (θ_V).
3. Thrust Direction (θ_{F_T}), relative to the spacecraft velocity or to the Sun - table 5.2;
4. Brake - table 5.2:
   - Location - starting at the middle of the transfer, progressively braking closer to the target planet;
   - Thrust direction - a search for the optimum direction for the thrust when braking.

Given the masses, thrusts and characteristics of the engines selected we use the combinations shown in table 5.1.

Table 5.1 Propulsion systems mass and combinations used.

Engine	Method of Use	Unitary Propulsion Dry Mass [kg]	Engine Combinations Used
CECE	Impulsive	255.8	2
NERVA	Impulsive	34,019.0	1
PPS 1350-G	Non-Impulsive	14.9	10, 15, 25, 35, 45, 55, 75, 100, 150
PEMT	Non-Impulsive	31,926.8	1, 2, 3, 4, 5, 6, 8, 10

The combination of two CECE engines provides a higher thrust than the other chemical engines, with a still smaller mass than the Vinci (see table 2.1). Conversely, given the large mass and high thrust of the NERVA, we do not use more than one engine in the base configuration.

Nevertheless, it is important to keep all manoeuvres around the planets with execution times less than 15 min, i.e. in order to reduce the ΔV_{loss} it is usual not to have an impulsive engine working for more than 15 min ([9, 51, 52, 55, 56]). The time a manoeuvre takes to execute is related to the thrust of the engine (see section 2.1.3).

In the MATLAB® program it is specified that on a manoeuvre whose execution time is greater than those 15 min the number of engines must be increased, which are discarded afterwards. We have a high range of C_3, which corresponds to a large number of manoeuvres (some whose ΔV would be unrealistic), we then impose a limit of a hundred engines to prevent the program entering into an endless loop. The option of increasing the number of engines would probably not be used in a real mission. Instead, an increase in the number of manoeuvres to raise the apoapsis would be the preferred solution. Nonetheless, the option of adding engines is selected due to programming simplicity and flexibility to implement. This implies that the mass of the mission is a sign of the complexity of the mission.

The number of PPS 1350-G engines selected is due to its low thrust and mass. Using ten engines we get 14.9 kg mass and a thrust of 0.9 N. When we reach 35 engines we have a mass similar to the two CECE (522 kg), but only 0.0014% of the thrust. Even though, it has an I_{sp} with more 1,195 s, saving much more fuel than those two CECE engines. For these reasons we start with ten engines, instead of with just one.

The PEMT engine although having a high mass, has also a high I_{sp}. The combinations used are therefore smaller, with a maximum of ten engines, but at the same time giving the possibility to test the system evolution (by using seven different possibilities).

Table 5.2 Parameters range searched.

Parameter	Range	Comment
C_3	$\left[\Delta V^{HT} \times (1+0.02)^i\right]^2$	i = 0 to 200 with increments of 1
Angles (θ_V, θ_{F_T})	0, -5, -10, -15, -20, -25, -30, -35, -40, -45, -50, -60, -70, -80	For EtM this implies all vectors are turned outwards. In the MtE vectors are turned inwards.
Brake Location	EtM $\rightarrow r^i + \dfrac{r_♂ - r^i}{2}$	i = 1, 2, 3, 4, 5, 6, 7.
	MtE $\rightarrow r^i - \dfrac{r^i - r_\oplus}{2}$	$r^1 = r_\oplus$ on EtM and $r^1 = r_♂$ on MtE

The C_3 range comes from the primary objective, i.e. since we aim to minimise travel time we desire transfers with C_3 values greater than the Hohmann transfer. However, to increase the C_3 value slowly, so that usual values can be found, and to test some extreme cases, an exponential rate is the selected solution.

The selected angles have a similar justification. At first we aim for a small variation of angle so to change the velocity direction slowly, while after 45° the variation can be larger. The option is also influenced by the number of iterations needed by the increase in the number of angles, since we have to run the mission computational procedures, described in section 5.1, for every C_3, angle and spacecraft configuration.

In references [70, 71] the brake usually starts at, or after, the middle of the trajectory. We start at the middle and divide the remaining distance in two, until we are close enough that the next location would be inside the planet's SOI (where capture occurs). Each brake location is tested for each C_3, angle and spacecraft configuration.

5.3 Effect of Angle Variation of Velocity and Thrust & Optimum Point

The effect of varying the initial velocity angle is perceived at first on the Mars to Earth transfer with impulsive systems. Without varying the angle, when the value of $\sqrt{C_3}$ is greater than the planet's velocity, the spacecraft travels opposite to the planets movement (figure 5.1).

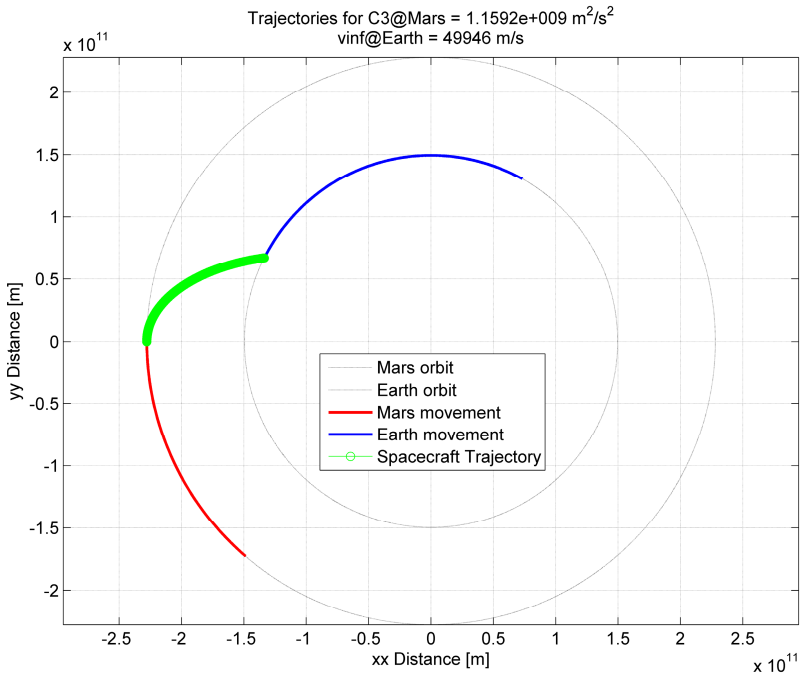

Figure 5.1 Mars to Earth interplanetary phase for the classical chemical option with $\theta_V = 0$ (the planet movement is counterclockwise).

This has a strong effect on the results since the mass of the mission is increasing together with the TOF, when the spacecraft travels backwards (seen after the minimum point in figure 5.2).

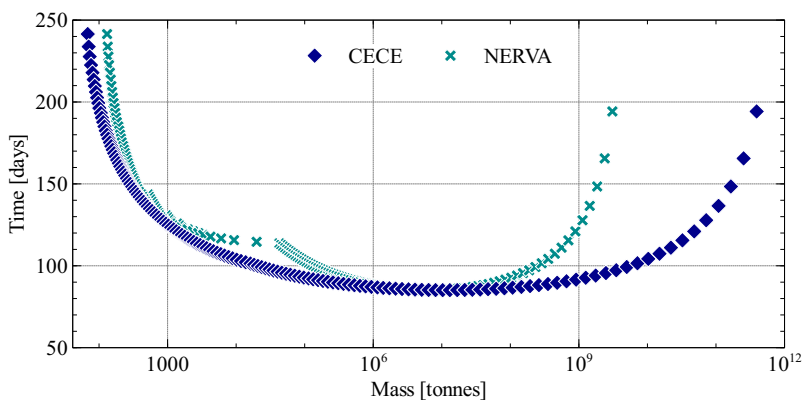

Figure 5.2 Mars to Earth transfers with chemical and nuclear thermal systems.

At first this was not expected, after all the Hohmann transfer is performed with V_∞^D and V_1 aligned, and this effect only occurs with C_3 far greater than what is normally used. We then test the effect of varying the angles on

both Earth to Mars and Mars to Earth transfers, for example using the PPS 1350-G engine. As seen in figure 5.3, we start having differences of one thousand tonnes or more.

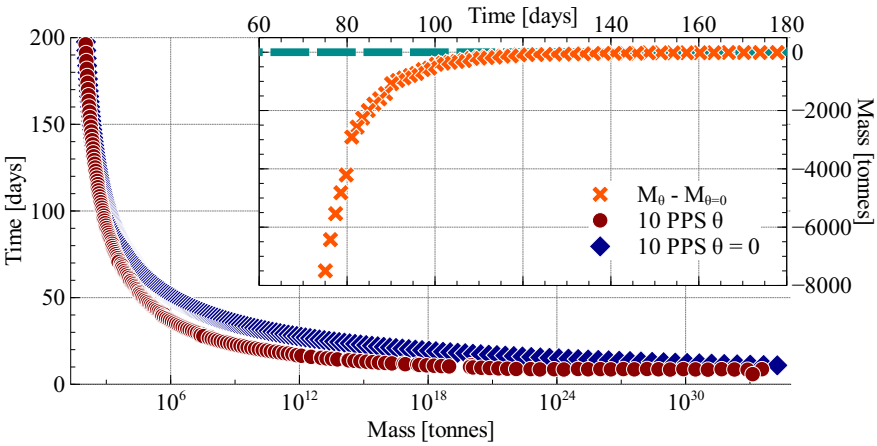

Figure 5.3 Earth to Mars transfers using ten PPS 1350-G engines in the interplanetary phase. In the upper corner is the mass difference between both solutions (where only trajectories whose TOF difference between them were less than two days are presented).

To perceive these effects we plot the results obtained for every θ_V and θ_{F_T}, using the same C_3 (figure 5.4). In figure 5.4a we can clearly see how a variation on the direction of the initial velocity (maintaining the same absolute value) can result in differences of 100 t or more. The variation of θ_{F_T} does not produce a strong effect on the mass and the main change is on the TOF (figure 5.4b).

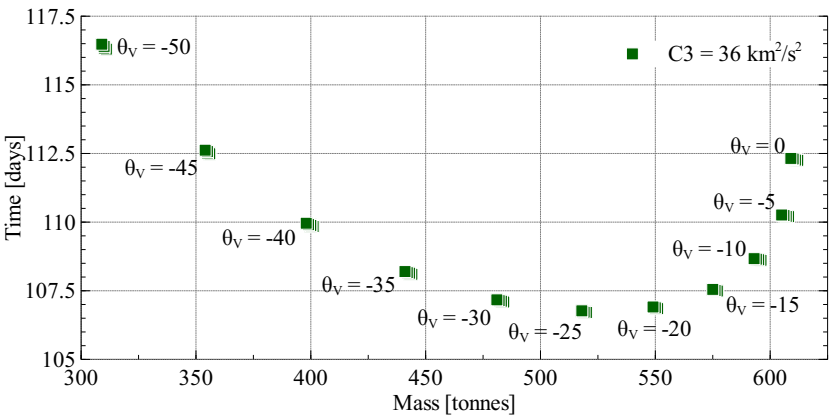

(a) Effect of θ_V.

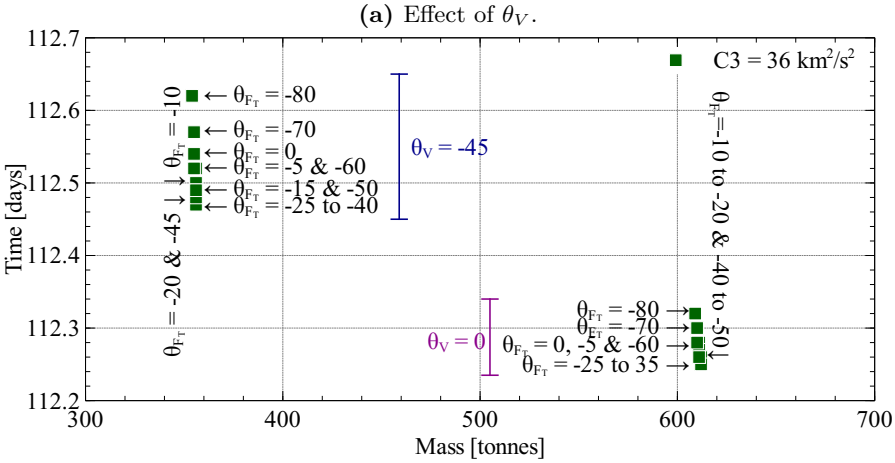

(b) Zoom on the $\theta_V = -45$ and 0 to see the effect of θ_{F_T}.

Figure 5.4 Earth to Mars transfer using ten PPS 1350-G engines and a value of $C_3 = 36\,\mathrm{km}^2/\mathrm{s}^2$.

A closer scrutiny of the results reveals that the cause for the mass variation is the value of the velocity at arrival (figure 5.5). Through the change of the initial angle we induce a variation on the interplanetary TOF, and most importantly, a different spacecraft velocity vector at arrival to the target planet ($\vec{V_A}^{(v)}$) and thus V_∞^C. This affects the arrival manoeuvre (in terms of the required propellent), and hence influences every manoeuvre before. Seeing the impulsive fuel calculations uses equation (2.1), we have an exponential effect (as seen in figure 5.3).

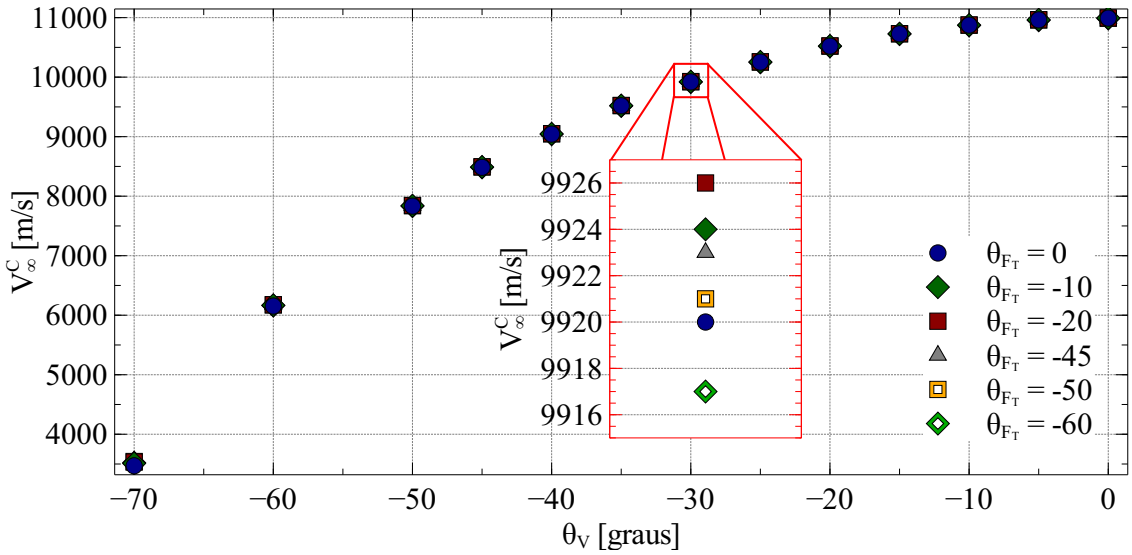

Figure 5.5 Variation of V_∞^C with θ_V and θ_{F_T}, for a $C_3 = 36\,\mathrm{km}^2/\mathrm{s}^2$.

We then consider the variation of θ_V and θ_{F_T} in all calculations (using the range presented in table 5.2). By having different angles we have several results for a single C_3 and we have to select which θ_V and θ_{F_T} are better, and thus used to compute the entire trajectory. Our option is to save the interplanetary results with less travel time and with less mass, and to use a simple algorithm to compute the results which are employed in the remaining calculations (departure and arrival). This has to be done in an automatic fashion so not to overwhelm the program with data and, at the same time, to run it faster.

We use as the starting point the first result whose trajectory reached the target planet (result X), after having convergence of mass and time (due to the iterations discussed in section 5.1):

$$\begin{aligned}
\theta_{V_{opt}} &= \theta_V^X \\
\theta_{F_{T\,opt}} &= \theta_{F_T}^0 \\
t_{opt} &= t^X \\
M_{opt} &= M^X,
\end{aligned}$$

where $\theta_{V_{opt}}$ and $\theta_{F_{T\,opt}}$ are the optimum angles for the velocity and thrust direction, respectively, t_{opt} the optimum time of flight for the corresponding transfer and M_{opt} the corresponding spacecraft total mass. Testing the remaining angles of the velocity and thrust for the same absolute value of velocity at departure and spacecraft configuration, we update the optimum values ($\theta_{V_{opt}}$, $\theta_{F_{T\,opt}}$, t_{opt} and M_{opt}) if we find a transfer (i) whose

$$(t^i < t_{opt} \vee t^i < t^X) \wedge M^i < M_{opt}.$$

This algorithm arises from the results of figures 5.4 and 5.5. To test it we simulate the mission using 35 PPS engines for the same C_3 range, for the minimum time points, minimum mass points and the resulting optimum points. The results are displayed in figure 5.6.

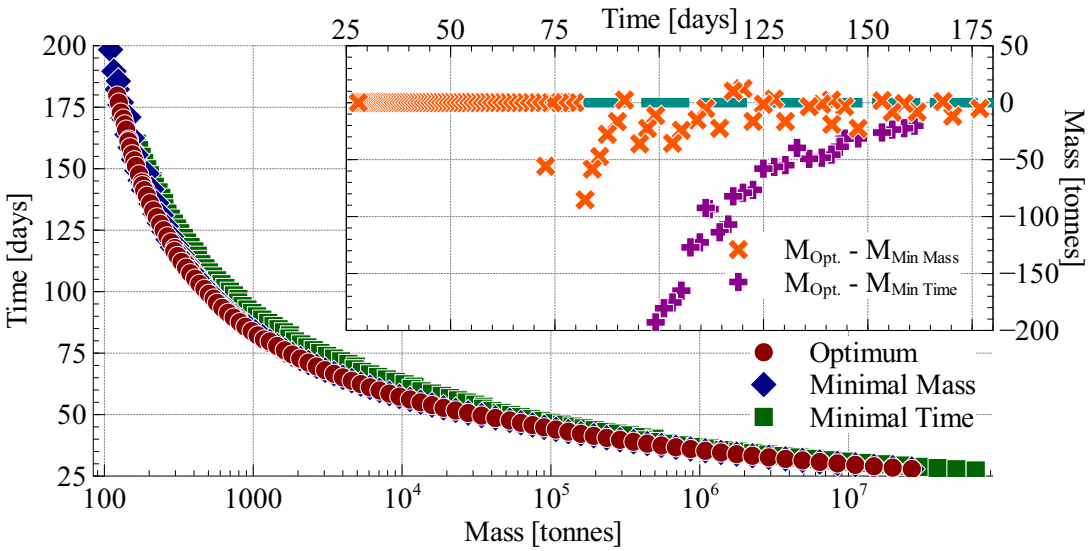

Figure 5.6 Earth to Mars transfers using 35 PPS 1350-G engines and considering minimal interplanetary travel time, minimum interplanetary mass and optimum points for the same C_3 range. The upper graph is the mass difference between the solutions (where only trajectories whose TOF difference between them is less than two days are presented).

We can see that the minimum mass requires a greater C_3 value to reach the same TOF of the optimum (verified by the upper left points in figure 5.6). For times of flight lower than ≈ 70 days the optimum corresponds to the minimum mass. On the remaining transfers the optimum has lower masses than the minimum mass points (apart from a few points whose maximum mass difference equals 12.3 t). This is explained by the difference in C_3 and V_∞^C between both cases, i.e. although the C_3 is always greater for the minimum mass case, and V_∞^C for the optimum case, the difference in C_3 far outweigh differences in V_∞^C, making the minimum mass heavier for the same TOF.

Meanwhile, the minimum time uses smaller C_3 values than the optimum for the same TOF. However, since it travels faster it has a V_∞^C always higher, whose effect now outweigh the increase in C_3 in the optimum case. This increments the mass required to execute the arrival manoeuvre, and thus all masses before that.

We then compare the effect of having the thrust direction relative to the orientation of the spacecraft velocity (θ_{F_T}) or fixed relative to the Sun ($\theta_{F_{T\,Fix}}$), as explained in section 4.1.1. In figure 5.7 we can see that the thrust relative to the Sun has a maximum mass gain of 400 t, for results with TOF less than ≈ 65 days. However, for this range of TOF, not only is the C_3 value greater than what is commonly used, but the minimum spacecraft mass is 3,637 t. This mass is well above the recommended limit discussed below. For the remaining results the difference between both solutions is less than ≈ 25 t, favourable to the thrust relative to the spacecraft velocity (i.e. the mass of this solution is lower than that of $\theta_{F_{T\,Fix}}$). For this reason, henceforth, we consider only the thrust direction relative to the orientation of the spacecraft velocity.

As stated in reference [7], and discussed in section 1.2.1, a spacecraft with more than 1,000 t is to be avoided. However, since we aim to test new propulsion systems and how fast one can travel to Mars and back, we did not impose this condition. This results in a high range of possible solutions, with masses reaching orders of 10^{12} t or more (as seen in figure 5.3). Thus, only missions with masses lower than 2,500 t are considered.

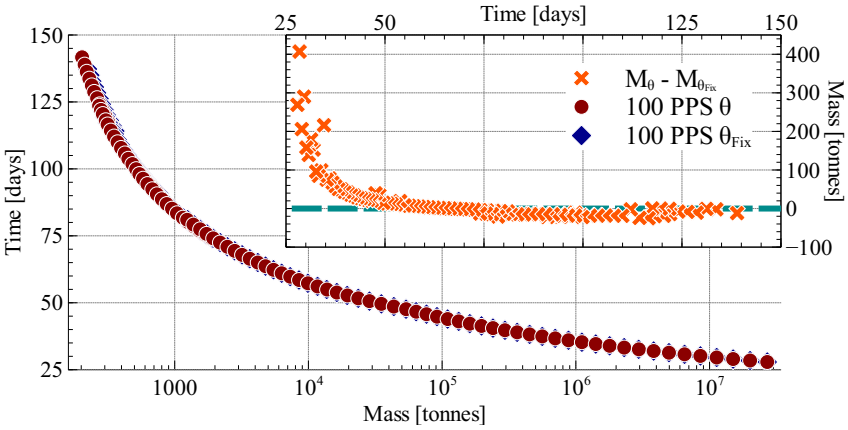

Figure 5.7 Earth to Mars transfers using one hundred PPS 1350-G engines in the interplanetary phase, with thrust relative to the spacecraft velocity and relative to the Sun.
The upper graph is the mass difference between both solutions (where only trajectories whose TOF difference between them is less than two days are presented).

To select an optimum point of all the computed trajectories, for each configuration, and since we aim to minimise time and mass, we use a weighted sum of those two,

$$N_{opt} = \min\left[\left(\frac{M^i}{\max\left(M^i\right)} \times 0.25 + \frac{t^i}{\max\left(t^i\right)} \times 0.75\right) \times \max\left(t^i\right)\right], \tag{5.1}$$

where i runs between one and the maximum number of points computed. Being the time the primary objective it has a weight of 75%, while mass only acounts for 25% of the equation. N_{opt} is thus the iteration number with the optimum characteristics.

5.4 Impulsive Systems - Chemical versus Nuclear Thermal

The first missions to be tested are the classical chemical and the nuclear thermal systems (options one and three of figure 3.3). These missions serve as the comparison case. On figure 5.8, we have the region of masses lower than 2,500 t for the Earth to Mars transfer with these systems.

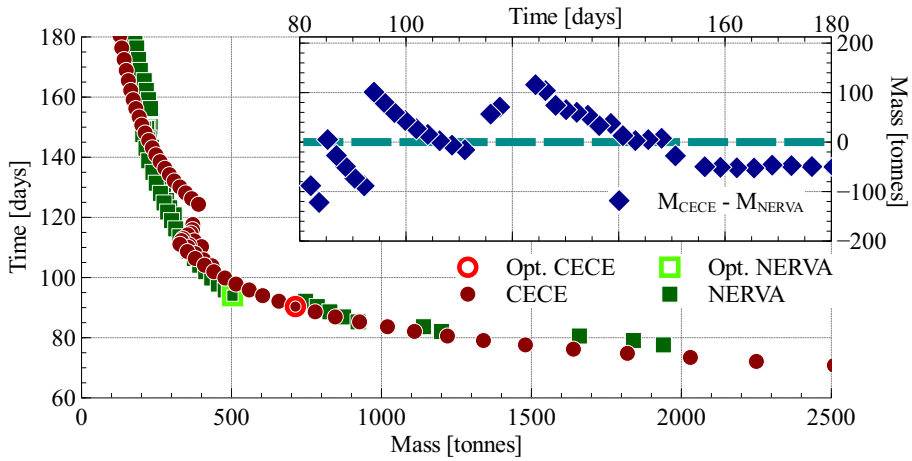

Figure 5.8 Earth to Mars transfers with chemical and nuclear thermal systems.
In the upper corner is the mass difference between both systems (where only trajectories whose TOF difference between them is less than two days are presented).

Firstly, an important fact to note is the leaps seen in the NERVA system, e.g. on the green squares we see a leap between more than 80 days and less than 80 days. The leap is explained by the imposition on the program to keep all manoeuvres with less than 15 min by increasing the number of engines (see section 5.2). This effect

also exists in the CECE mission. However, it is not visible since adding 255.8 kg does not have the same effect as adding 34,019 kg.

In figure 5.8 it can also be seen the effect of adjusting θ_V and the impact it has on the trajectory. For example, with a TOF of ≈ 110 days we see an overlapping in transfers. Although they have different C_3, they yield almost equal times of flight and masses through changes in θ_V.

Comparing both solutions, CECE and NERVA, we observe that NERVA is a better solution only for times of flight of ≈ 115 to ≈ 150 days or ≈ 95 to ≈ 105 days. Nevertheless, the difference between both solutions is never greater than 200 t (for this range of TOF). On the return, however, the difference in mass is always favourable to the classical chemical solution (figure 5.9).

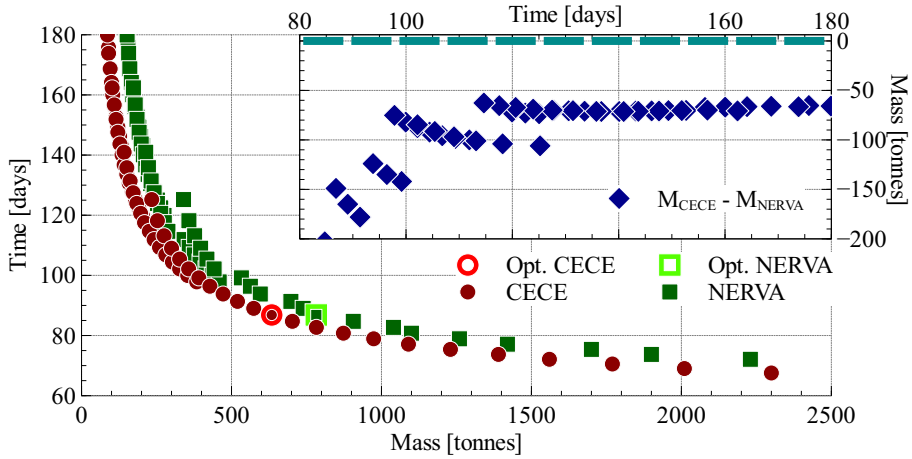

Figure 5.9 Mars to Earth transfers with chemical and nuclear thermal systems.
In the upper corner is the mass difference between both systems (where only trajectories whose TOF difference between them is less than two days are presented).

Using all the trajectories computed for EtM and MtE, we calculate the waiting time, the total mission time and the total mission mass for each one (figure 5.10). In this figure we see that even if we travel faster to Mars and back we have approximately the same mission time since the waiting time is increasing. There is however a leap in waiting time for return times of flight of ≈ 125 days. Although the same feature of increasing waiting time with decreasing TOF is found, the position of Earth and Mars is such that we wait up to 400 days less to undergo the return trip.

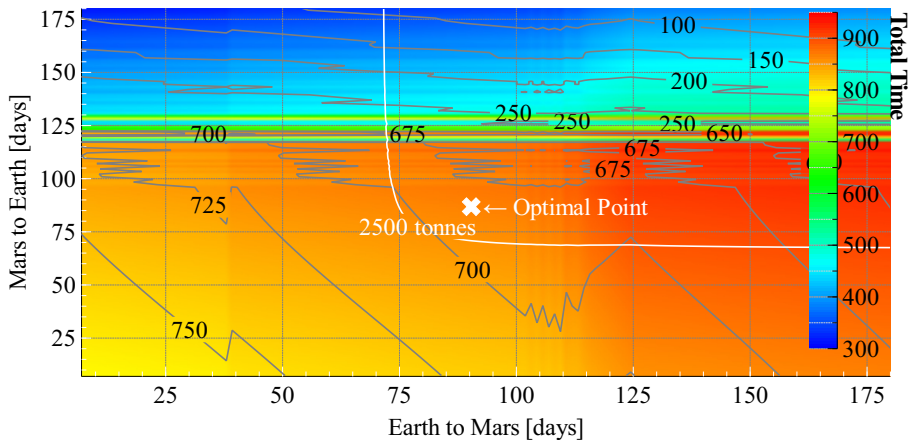

Figure 5.10 Total time (background colours), waiting time (grey numbered lines), total mission mass division (2,500 t white line) and optimum selected point of the CECE propulsion system.

Nonetheless, the waiting time is not only related with the travel time, but also with θ_V, i.e. we discover that even with an equal travel time, with a different θ_V the target planet would need to be in a different rendezvous

location, affecting the waiting time for the return. This is evident when the waiting time for the NERVA propulsion system is plotted. Even though both CECE and NERVA have about the same total time throughout the different times of flight, we notice a concentration of small mission times with small times of flight. Zooming on that section (figure 5.11) reveals that is possible to reach Mars fast enough and have a waiting time of four or less days before returning. Nevertheless, this occurs only when reaching the target fast enough so that the departure planet is behind us (in terms of heliocentric angles), and for masses far greater than the 2,500 t limit.

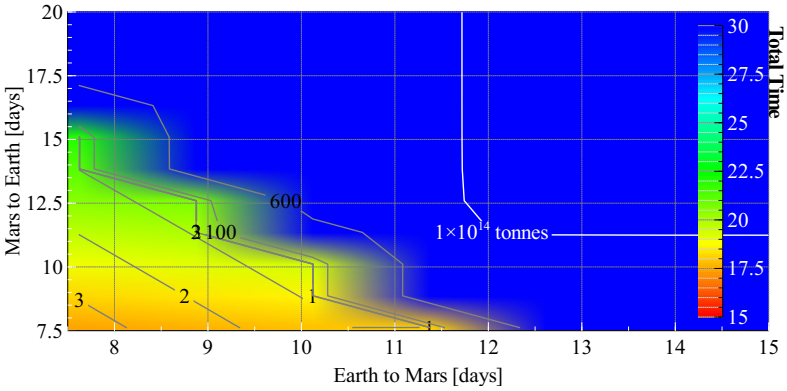

Figure 5.11 Total time (background colours), waiting time (grey numbered lines) and total mission mass division (1×10^{14} t white line) for the NERVA propulsion system.

We compute then the cargo mission for each system using the respective optimum points, obtaining the data represented in tables 5.3a and 5.3b for CECE and NERVA, respectively. To analyse tables 5.3 it is important to remember that the dry mass of the cargo mission includes a propellent payload (which is 598,634.98 t and 721,326.93 t for CECE and NERVA, respectively). The cargo mission with lowest mass, in both cases, is the classical chemical departure and arrival with a coast transfer.

Table 5.3 Chemical and nuclear thermal global mission data.
Note: The first entry of the waiting time is the time the crew must wait before launching to Mars, the second is the waiting time to return to Earth.

(a) CECE Propulsion System

	Delta-V [m/s]	Dry Mass [kg]	Mass [kg]	Time [days]	Waiting Time [days]
Cargo	2,947.94	659,257.13	2,077,881.91	258.17	573.44
Earth to Mars	8,420.30	38,231.65	713,111.41	90.35	689.66
Mars to Earth	10,584.66		636,866.63	86.83	
Human Total		38,231.65	1,311,746.40	866.83	
Mission Total		697,488.79	2,790,993.33	1,698.44	

(b) NERVA Propulsion System

	Delta-V [m/s]	Dry Mass [kg]	Mass [kg]	Time [days]	Waiting Time [days]
Cargo	2,947.94	781,949.08	2,450,123.50	258.17	572.56
Earth to Mars	8,093.33	71,739.00	503,269.13	93.98	686.90
Mars to Earth	10,584.66		793,065.93	86.83	
Human Total		71,739.00	1,224,596.06	867.71	
Mission Total		853,688.08	2,953,392.63	1,698.44	

The first issue to comment is that more than 90% of the mass of the missions is fuel (hereinafter fuel referes to proppelants and the tanks to transport it). This is a common feature of all impulsive systems, given their low I_{sp}.

Analysing both missions we noticed that although the human mission total time has a difference of only one

day, the NERVA system has 87 t less than the CECE. This is mainly due to the EtM transfer, where the difference between both solutions is approximately 200 t. The variance is mitigated by the MtE transfer since the CECE system is always a better solution, evident in figure 5.9. When adding up the cargo mission, this difference changes sign, meaning that the CECE total mission mass has less 163 t than the NERVA. This is mainly related to the propellent payload the cargo carries (122 t more for the NERVA).

For this reason we regard the chemical propulsion system as a better choice and, henceforth, is the only system we consider for departure and capture. The CECE is also a better solution due to its simplicity and for being more environmentally friendly than the NERVA (given all nuclear political problems associated) [35, 72].

Comparing our mission choice and the Mars Direct we were able to save 43 days on the total time of the human mission (in particular more than 90 days in each transfer), while keeping the manned spacecraft well below the 1,000 t limit advocated in Mars Direct. As expected, we could not keep the cargo mission below this limit since the fuel for the manned return trajectory is carried by it, instead of producing it on Mars.

5.5 Non-Impulsive Systems - Electrical and PEMT

For non-impulsive systems there are many more solutions than for the impulsive ones. We present then each in a different section.

5.5.1 Electrical Engine

The PPS 1350-G has a very low thrust and mass and a very high I_{sp}. By having it continuously working during the entire interplanetary phase, for the same C_3 as a Hohmann transfer, we obtain a gain, in terms of TOF, of 43 days using just ten engines.

Computing all transfers and analysing the results we can ascertain that the 35 engine configuration is the one with lowest mass for the same TOF. For times of flight higher than ≈ 140 days the difference is always lower than 15 t. This difference increases when we decrease the TOF. There are, however, some isolated points where the difference is favourable to other configurations, but this difference never exceeds more than 35 t (apart from one point with 150 engines with 58 t). This behaviour can be seen in figure 5.12. In it the 10, 15, 25 and 45 engines configurations, whose masses are always greater than the 35 configuration, are not showed for clarity.

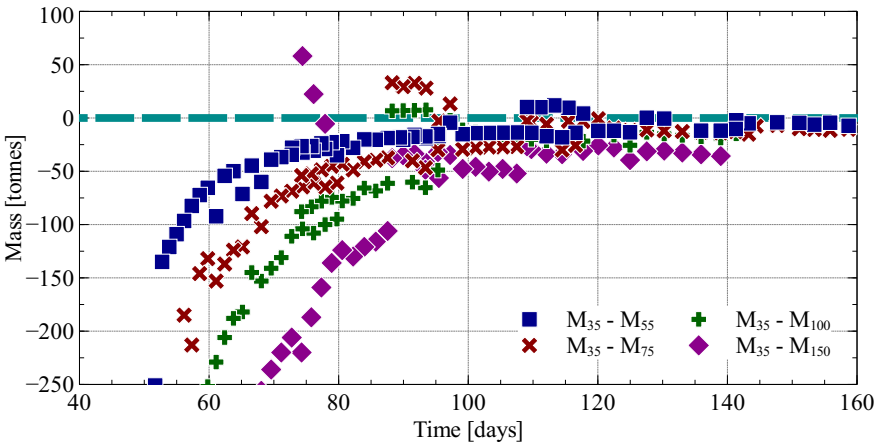

Figure 5.12 Plot of the difference in mass between the configurations in the Earth to Mars transfer (where only trajectories whose TOF difference between them is less than two days are presented).

On the return we observe the same behaviour, the 35 engine configuration always with lower mass apart from

a few points with maximum difference of 30 t (for this reason it is not displayed here). Again the difference is more pronounced on times of flight lower than ≈ 140 days. The points outside an almost exponential growth are closely related to the difference in θ_V and θ_{F_T}.

Following the same procedure used for the impulsive systems we compute the waiting time, the total mission time and the total mission mass. Plotting the data for the manned mission of the 35 engines configuration we obtain figure 5.13. The optimum point for the EtM and MtE, as well as for the cargo mission, is presented in table 5.4. The minimal mass for the cargo mission, in this case, is achieved using 75 PPS engines in the interplanetary phase.

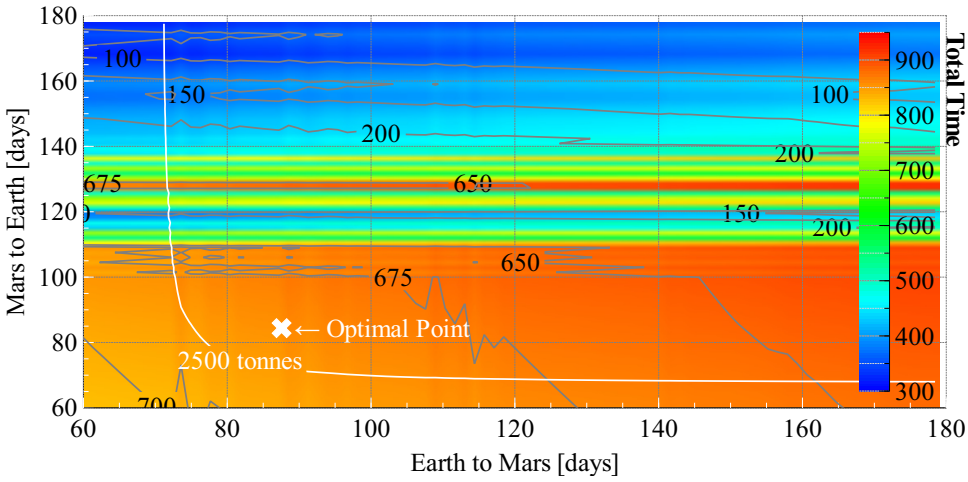

Figure 5.13 Total time (background colours), waiting time (grey numbered lines), total mission mass division (2,500 t white line) and optimum selected point of the 35 PPS 1350-G propulsion system.

Table 5.4 Electrical global mission data.
Note: The first entry of the waiting time is the time the crew must wait before launching to Mars, the second is the waiting time to return to Earth.

	Delta-V [m/s]	Dry Mass [kg]	Mass [kg]	Time [days]	Waiting Time [days]
Cargo	2,890.13	770,273.07	2,409,992.33	255.68	581.94
Earth to Mars	9,482.62	38,753.64	811,122.90	87.56	685.00
Mars to Earth	10,796.35		747,286.01	84.40	
Human Total		38,753.64	1,519,655.26	856.96	
Mission Total		809,026.71	3,221,115.23	1,694.59	

As expected, the total time exhibits the same behaviour seen for the impulsive systems (the faster the travel is, the longer the waiting time on Mars before returning is). As the impulsive systems, more than 90% of the mission mass is fuel (proppelants and tanks). However, for example in the EtM transfer we have a fuel mass of 772,369 kg of which only 0.22% is for the interplanetay phase. This means that the CECE, in this mission, uses more 764,163 kg in four manoeuvres (apoapsis raising, departure, capture and orbit circularization) than 35 PPS engines working for 87 days.

Adding all the contributions and comparing with the chemical option, with coast interplanetary transfer, we find that the crew has to spend almost 10 days less in the entire mission with an addition of 200 t. Although at first, this seems to be a large difference, it is important to note that it represents fuel additions to the spacecraft. Another important aspect is that we still keep the manned spacecraft mass below the 1,000 t limit of Mars Direct.

Braking

Executing the brake before arriving to the target planet with the PPS 1350-G we find that for most trajectories either the TOF is higher or the spacecraft is heavier, when the TOF is approximately the same. This suggests that when a system has such a low thrust there is no need to lower the spacecraft arrival velocity.

5.5.2 PEMT Engine

The PEMT engine is expected to have a better performance in terms of TOF. Despite its greater mass, in comparison with the CECE or the PPS 1350-G, it can work continuously with a thrust of 20 N (with an equivalent exhaust velocity equal to the speed of light). With a C_3 equal to the Hohmann transfer we had a gain of 82 days.

Plotting all transfers for the different configurations yields figure 5.14. For clarity, the two, four, five and six engines configurations are not showed since the mass is always higher. In this figure it is clearly shown that the one engine configuration has the smallest mass for all trajectories. It is also possible to see the effect of the angle variation by the overlap of results (e.g for a TOF ≈ 80 days).

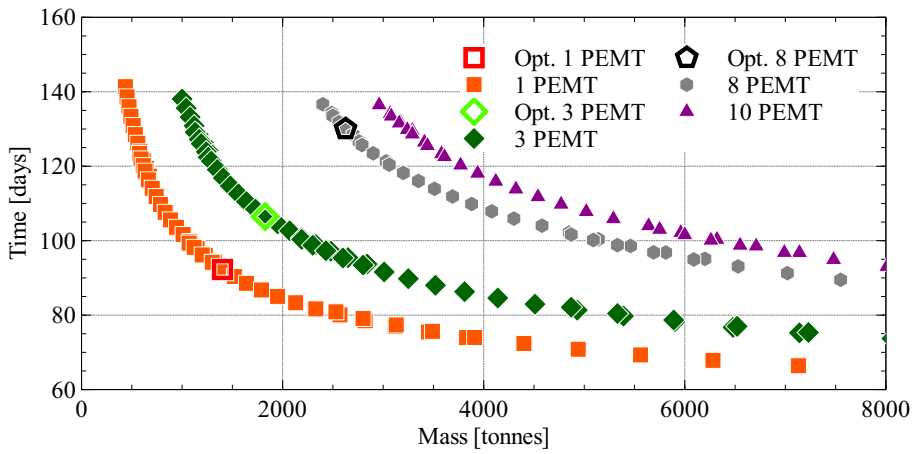

Figure 5.14 Earth to Mars transfers with PEMT system, including optimum points for the configurations with mass lower than 2,500 t.

On the return the behaviour is similar and it is not represented here. Instead, we show in figure 5.15 the total time, the waiting time and the optimum point location of the one PEMT configuration.

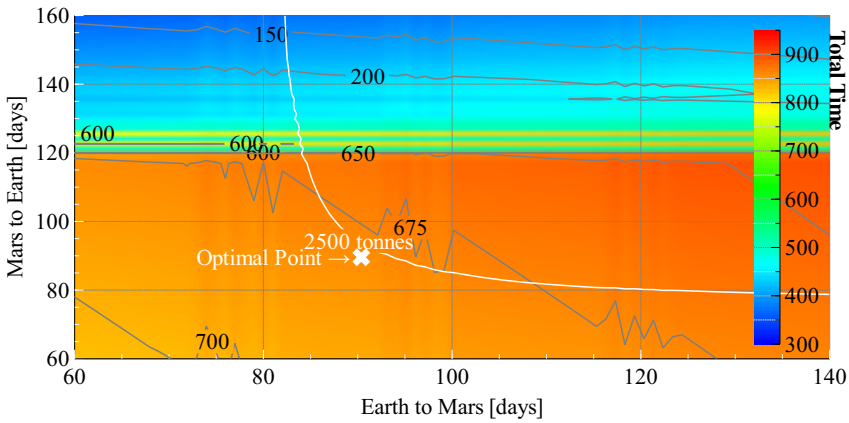

Figure 5.15 Total time (background colours), waiting time (grey numbered lines), total mission mass division (2,500 t white line) and optimum selected point of the one PEMT propulsion system.

As the electrical (PPS) and chemical (CECE) systems, the PEMT total time remains approximately the same until a return TOF of 120 days, since the waiting time increases when the TOF decreases. For return trips longer than 120 days the total time is reduced drastically, due to the planetary alignment, and this remains approximately the same for all Earth to Mars times of flight (again due to the variation of the waiting time). However, in opposition to the PPS and CECE, the combination of optimum points of Earth to Mars and Mars to Earth results in a human mission total mass greater than $2,500$ t. Nevertheless, this does not violate the decision of using missions with masses lower than $2,500$ t since the return fuel for the human mission is carried by the cargo. The EtM, MtE and cargo missions data are presented in table 5.5.

Table 5.5 PEMT global mission data.
Note: The first entry of the waiting time is the time the crew must wait before launching to Mars, the second is the waiting time to return to Earth.

	Delta-V [m/s]	Dry Mass [kg]	Mass [kg]	Time [days]	Waiting Time [days]
Cargo	2,947.94	1,155,800.86	3,584,830.70	258.17	580.35
Earth to Mars	9,114.40	70,158.42	1,515,396.48	90.38	679.14
Mars to Earth	10,173.64		1,165,337.13	89.57	
Human Total		70,158.42	2,610,575.19	859.08	
Mission Total		1,225,959.28	5,100,227.18	1,697.60	

Although the total mass of the human mission is 111 t above the mass limit, each transfer is well below. However, the cargo mission, like the CECE and PPS, by having to carry the return fuel has a higher mass and, in this case, it exceeds our $2,500$ t limit.

After careful analysis it was found that since energy is generated through a nuclear reactor, which only burns 4% of the total nuclear material, the spacecraft is far heavier at arrival, requiring much more propellent than other systems to execute the capture manoeuvre. Obviously this has an exponential effect on previous manoeuvres. For example, in the EtM transfer we require 16 t of nuclear material for the interplanetary phase which is ten times more than the PPS (although it is still only $\approx 1\%$ of the total fuel mass). Afterwards, in the PPS mission, we reach Mars with a V_∞^C of $9,927$ m/s and having already consumed all propellent and discarded the tanks (leaving it just with the dry mass and fuel for the remaining transfers). With the PEMT we have a $V_\infty^C = 9,636$ m/s, but it still has $15,897$ kg of nuclear material (apart from the dry mass and fuel for the remaining transfers).

The cargo mission with lower mass for carrying the return fuel for the PEMT mission ($1,095$ t), is achieved using just classical chemical engines with a coast transfer.

Adding up all the dry mass, the total mass and time we found that a human mission can have 7 days less than the impulsive system mission, but is heavier by $1,299$ t. This means that if we compare it with the PPS mission, we have two more days and $1,090$ t in excess. These mass differences clearly increase if we consider the cargo mission as well. The time difference decreases when comparing with the CECE mission.

Braking

When braking with the PEMT we have considerable changes in mass, while the TOF did not have a significant increase, contrary to the PPS. In figure 5.16 we show the tested trajectories. For a TOF lower than 120 days, the full range of braking points were not tested since they always showed less mass difference than the middle point brake (as the ≈ 90 days TOF transfer demonstrates).

As one could expect, when braking occurs before arriving, the TOF increases. However, the maximum difference between the TOF of a trajectory with no brake and one with a brake is never greater than 5 days (and

it clearly occurs when we brake at half distance). Despite that increase in TOF we have savings of mass reaching 130 t, which increases with increasing C_3.

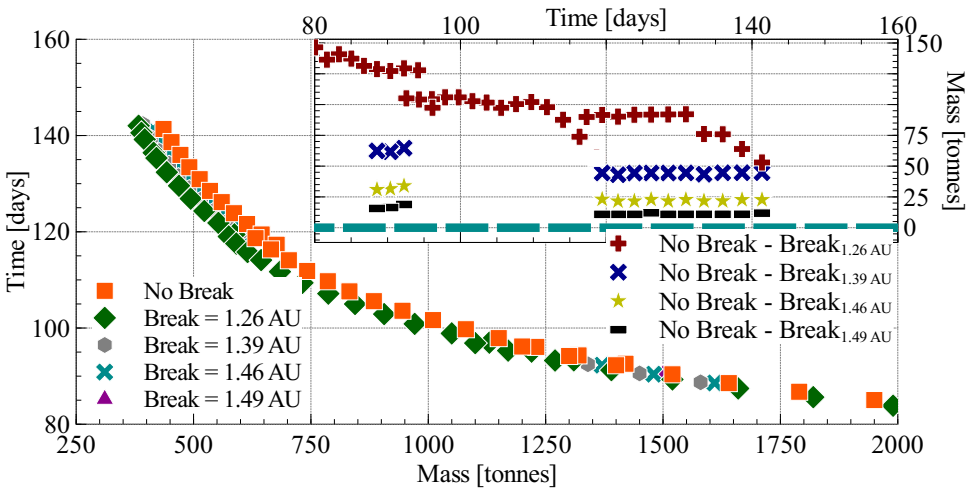

Figure 5.16 Earth to Mars transfers with PEMT system braking after a predetermine point. In the upper corner is the mass difference between the various solutions (transfers are compare with the same C_3).

On return we were able to decrease the TOF and the mass. When travelling is towards an inner planet, the spacecraft velocity decreases, which means that on a return trajectory braking (i.e. change of thrust direction) means we are in fact accelerating the spacecraft. That is the reason for the decrease in TOF. The mass savings here can be greater and can reach 200 t.

Having lower masses for approximately the same TOF, a new optimum point for the PEMT system can be used, as represented in table 5.6. We see that we can lower the total mass of the human mission to below the 2,500 t limit. We have then more 1,092 t with less five days than the impulsive mission (more 884 t and four days than the electrical mission).

Table 5.6 PEMT global mission data (inverting the thrust direction after the middle distance between Earth and Mars).
Note: The first entry of the waiting time is the time the crew must wait before launching to Mars, the second is the waiting time to return to Earth.

	Delta-V [m/s]	Dry Mass [kg]	Mass [kg]	Time [days]	Waiting Time [days]
Cargo	2,890.13	1,077,516.31	3,341,905.62	256.45	580.42
Earth to Mars	9,114.40	70,158.42	1,388,146.57	91.25	679.10
Mars to Earth	10,173.64		1,085,561.18	90.96	
Human Total		70,158.42	2,403,549.32	861.32	
Mission Total		1,147,674.73	4,730,052.18	1,698.18	

The cargo mission is still well above the 2,500 t limit, although carrying a propellent payload of just 1,015 t (less 80 t than before). Here the minimum mass is achieved using chemical at departure and arrival, and 100 PPS engines on the interplanetary phase.

5.6 Impulsive versus Non-Impulsive Systems

The results from the classical chemical solution, 35 PPS engine configuration and one PEMT, for the Earth to Mars transfer, are shown in figure 5.17.

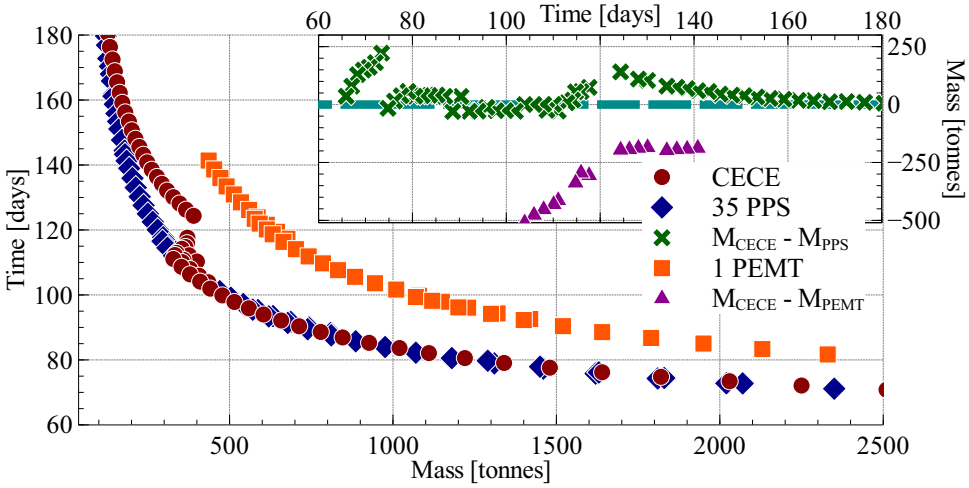

Figure 5.17 Earth to Mars transfers with all selected propulsion systems.
In the upper corner is the mass difference between both systems (where only trajectories whose TOF difference between them is less than two days are presented).

The PPS propulsion system, apart from a few points where the maximum difference is never greater than 30 t, is a better solution than a simple chemical departure and arrival with a coast interplanetary transfer (for equal times of flight). This behaviour is not seen on the optimum solutions because the optimum point for each system results in different TOF (a difference well above the 2 days margin). Nevertheless, it was already expected that it yields better solutions since we are adding up to an already largely optimised system (the CECE) a low mass and high I_{sp} system (even though with low thrust).

By contrast, the PEMT has always a higher mass than all the other scenarios, for these times of flight. The principal reason is the need to carry so much nuclear material to use just 4% of it.

When smaller times of flight are achieved, the tendency inverts and the PEMT results in a far better solution, with mass differences above 113, 153, 267 t (figure 5.18). This behaviour suggests that for trajectories to celestial bodies farther from Earth than Mars, where a higher ΔV is needed, the PEMT engine could represent a better solution.

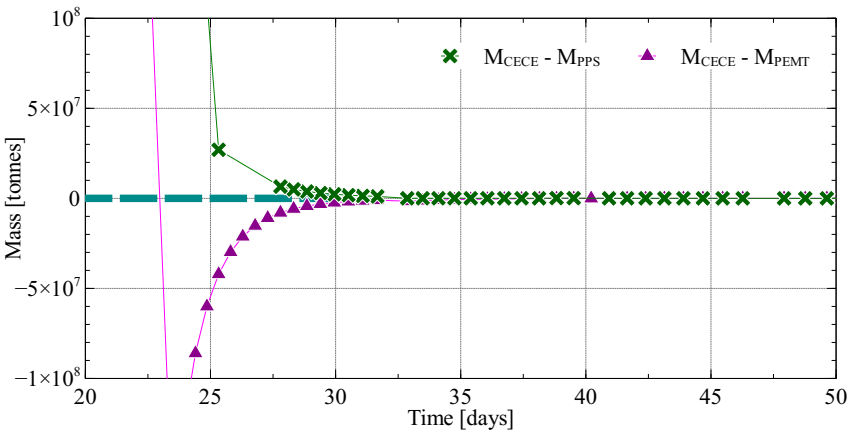

Figure 5.18 The difference between the systems for the Earth to Mars transfer (where only trajectories whose TOF difference between them is less than two days are presented).

For a better understanding of the differences between the optimum solutions for each system, we show in table 5.7 and in figure 5.19 the core of our findings.

Firstly, we see that the maximum fuel expenditure is during departure and capture (especially at departure). Secondly, an increase of TOF implies a decrease of the waiting time and vice versa.

The PPS configuration has a human mission time lower than the others, with a small increase in mass (in comparison to the chemical solution). This difference is due to the extra fuel needed at departure manoeuvres (more ≈ 100 t for the EtM transfer and ≈ 90 t for the MtE transfer) and the capture on the MtE transfer (≈ 9 t more). In the capture manoeuvre, on the EtM transfer, we have a saving of less than ≈ 12 t.

Conversely, the PEMT has a smaller gain in the mission time compared to the CECE, with a high increase in mass (more than 626 t on the EtM departure and capture, ≈ 395 t on the MtE departure and capture), for the reasons discussed above.

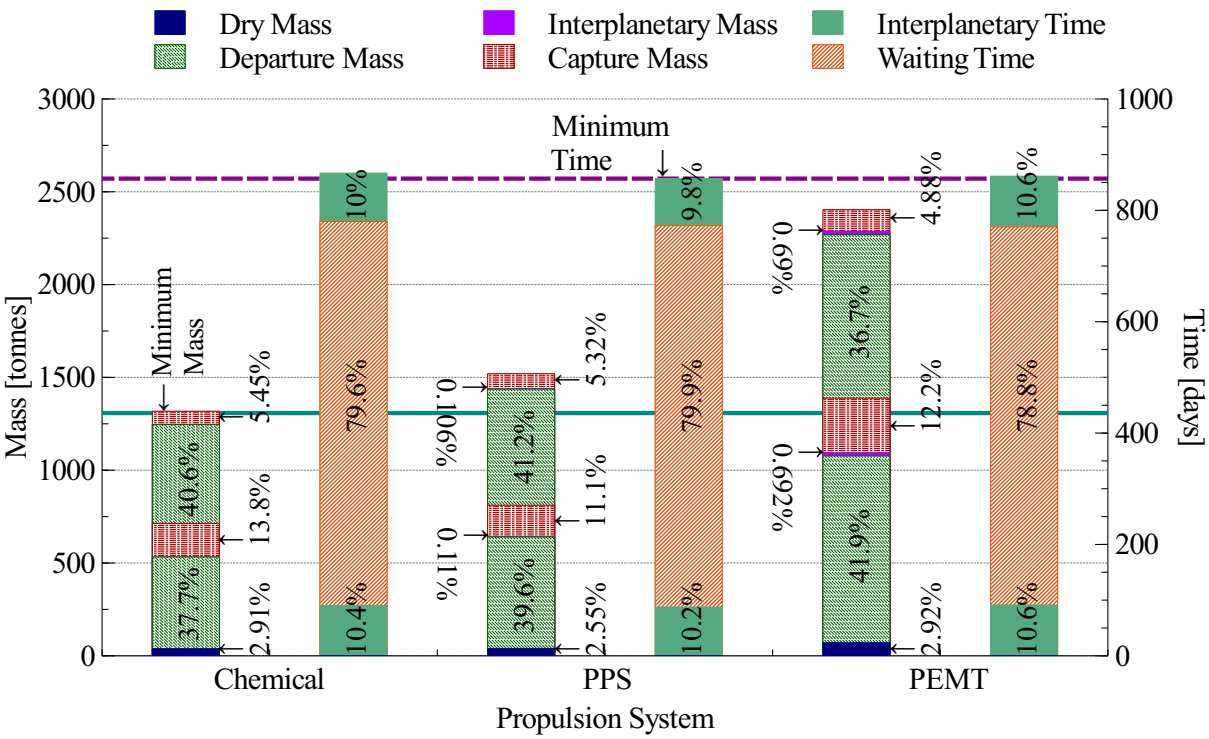

Figure 5.19 Plot of the mass and time for the optimum solutions of each propulsion system (with percentages of the total mass and total time for each human mission).

Table 5.7 Summary of results for the time and the mass of each propulsion system (W. T. means waiting time).
Note: The first entry of the waiting time is the time that the crew must wait before launching to Mars, the second is the waiting time to return to Earth.

System	Time [days]							Mass [t]				
	Cargo	W. T.	Human EtM	W. T.	Human MtE	*Human Total*	*Mission Total*	Cargo	Human EtM	Human MtE	*Human Total*	*Mission Total*
CECE	258.17	573.44	90.35	689.66	86.83	866.83	1,698.4	2,077.9	713.11	636.87	1,311.8	2,791.0
PPS 1350-G	255.68	581.94	87.56	685.00	84.40	856.96	1,694.6	2,401.0	811.12	747.29	1,519.7	3,221.1
PEMT	258.17	580.35	90.38	679.14	89.57	861.32	1,698.2	3,584.8	1,515.4	1,165.3	2,403.6	4,730.1

Chapter 6

Conclusions and Outlook

In this work a comparison of the performance of different propulsion systems for a manned mission to Mars is carried out. These propulsion systems (discussed in chapter 2) are paradigmatic of each form of propulsion:

- The CECE - for the classical chemical propulsion;
- The NERVA - for the nuclear thermal propulsion;
- The PPS 1350-G - for the modern electrical propulsion;
- The PEMT - as the new concept propulsion.

The mission architecture was discussed in chapter 3 having as primary objective the minimisation of the mission time, and the minimisation of the mass as secondary. The mission comprised an assembly on low Earth orbit, a classical single impulse departure (with a prior apoapsis raising manoeuvre), an interplanetary coast transfer or powered transfer (depending on the propulsion system), a classical single impulse capture and finally a circularisation of the orbit (only by the crew) and landing.

The spacecraft mass budget uses some values of the previous mission proposals for the constants (e.g. the human habitat and cargo modules), keeping the propulsion system mass (including engines, fuel and propellant) as the variable.

The trajectory to be performed by the spacecraft has been computed using the classical Keplerian orbits, for the departure and capture, and carried out through a numerical integration of the equation of motion,for the interplanetary phase. The Runge-Kutta-Fehlberg 7th order formula with 8th order error estimate was used, with automatic step adaptation. This numerical method proved to be quite accurate (section 4.6).

Our analysis has shown that the classical chemical propulsion is the best solution within the impulsive systems. In most cases, for the same TOF, it has the smallest mass. When the TOF is slightly higher than the nuclear thermal system, a small increase in mass could overcome this situation.

When we add to the chemical departure and capture an electrical system one is able to reach the target destination faster with smaller masses, for most cases and when comparing with the same TOF. This better performance is achieved since one lowers TOF without increasing C_3.

The same cannot be said for the PEMT system. The principal reason for this behaviour is the fact it uses only a low fraction of the total nuclear material fuel to produce energy. If this fraction is increase, through technological improvements, the performance of the PEMT system can be greatly improved. Nevertheless, as it stands, the PEMT concept shows a better result for higher C_3 values, suggesting that it is more suitable for farther destinations than Mars.

The results presented here lasted several computer hours, approximately three and a half months with four computers working simultaneously.

The mission to Mars could be optimised considering a three dimensional trajectory. This optimisation would help to obtain a more accurate trajectory, but also the best thrust direction in every segment of the interplanetary phase. An algorithm for departure where the number of apoapsis raising manoeuvres is changed, instead of the option of increasing the number of engines, can be also beneficial.

In what concerns the PEMT engine, we believe that it is more suitable for other objectives than Mars.

For the PPS 1350-G engine our analysis indicates that an interesting combination might involve more than ten engines. However, the interaction between them should be studied as in reference [40].

As a final statement, we believe that despite its complexity a manned mission to Mars is possible. Indeed, following Zubrin ideas, we were able to see that a manned exploration to the red planet is theoretically possible with the current propulsion technology.

References

[1] National Institute of Standards and Technology. Fundamental Physical Constants from NIST, 2011. URL http://physics.nist.gov/cuu/Constants/index.html. Access on the 12th of March 2012.

[2] Barry N. Taylor and Ambler Thompson. The International System of Units (SI), 2008. URL http://physics.nist.gov/Pubs/SP330/sp330.pdf.

[3] Carlo Rubbia. Nuclear space propulsion with a pure electromagnetic thrust. In *European Organization For Nuclear Research*, Geneva, 2002. CERN. URL http://cdsweb.cern.ch/record/541446.

[4] National Aeronautics and Space Administration. Mars Exploration Rovers: Spirit/Opportunity, 2011. URL http://solarsystem.nasa.gov/missions/profile.cfm?Sort=Target&Target=Mars&MCode=MER&Display=ReadMore. Access on the 10th of October 2012.

[5] European Space Agency. ESA - Mars Express, 2012. URL http://www.esa.int/SPECIALS/Mars_Express/index.html. Access on the 10th of October 2012.

[6] iMARS Working Group. Preliminary Planning for an International Mars Sample Return Mission. Technical report, 2008. URL http://mepag.jpl.nasa.gov/reports/iMARS_FinalReport.pdf.

[7] Robert Zubrin and Richard Wagner. *The Case for Mars: the plan to settle the red planet and why we must.* The Free Press, New York, 1996. ISBN 0684827573. URL http://lccn.loc.gov/96026560.

[8] Stephen J. Hoffman and David I. Kaplan. Human Exploration of Mars: The Reference Mission of the NASA Mars Exploration Study Team. Technical report, National Aeronautics and Space Administration, Houston, 1997.

[9] Stephen Kemble. *Interplanetary Mission Analysis and Design.* Praxis Publishing, Berlin, 2006. ISBN 3540299130. URL http://lccn.loc.gov/2005935455.

[10] D.S.F. Portree. Humans to Mars: Fifty years of mission planning, 1950-2000. Technical report, NASA History Division, Washington DC, 2001. URL http://en.scientificcommons.org/27166911.

[11] National Aeronautics and Space Administration. Report of the 90-day Study on Human Exploration of the Moon and Mars. Technical report, National Aeronautics and Space Administration, 1989. URL http://isulibrary.isunet.edu/opac/index.php?lvl=notice_display&id=3151http://history.nasa.gov/90_day_study.pdf. Access on the 30th of September 2012.

[12] European Space Agency. ESA - Space for health - Musculo-skeletal system: Bone and Muscle loss, 2008. URL http://www.esa.int/esaMI/Space_for_health/SEMACYUOM8F_0.html. Access on the 30th of June 2012.

[13] Francis A. Cucinotta and Marco Durante. Risk of Radiation Carcinogenesis. In *Space Radiation*, chapter Chapter 4, pages 119 – 170. 2009. URL http://spaceradiation.usra.edu/references/Ch4RadCarcinogen.pdf.

[14] Bret G Drake. From the Moon to Mars, 2007. URL http://www.lpi.usra.edu/meetings/leag2007/presentations/20071001.drake.pdf.

[15] Mars Architecture Steering Group. Human Exploration of Mars - Design Reference Architecture 5.0. Technical Report 10, NASA Headquarters, October 2009. URL http://www.nasa.gov/pdf/373665main_NASA-SP-2009-566.pdf.

[16] Hoppy Price, Alisa Hawkins, and Torrey Radcliffe. Austere Human Missions to Mars. In *AIAA Space 2009 Conference*, Pasadena, California, 2009. URL http://trs-new.jpl.nasa.gov/dspace/bitstream/2014/41431/1/09-3642.pdf.

[17] W. David Woods. *How Apollo Flew to the Moon*. Springer, New York, extended edition, 2011. ISBN 9781441971784. URL http://lccn.loc.gov/2011921113.

[18] National Aeronautics and Space Administration. Launch Vehicle/Spacecraft Key Facts, 2012. URL http://history.nasa.gov. Access on the 29th of April 2012.

[19] Martin J. L. Turner. *Rocket And Spacecraft Propulsion: Principles, Practice And New Development*. Springer Berlin Heidelberg, New York, 3rd edition, 2008. ISBN 9783540692027. URL http://lccn.loc.gov/2008933223.

[20] Paul A. Czysz and Claudio Bruno. *Future Spacecraft Propulsion Systems: Enabling Technologies For Space Exploration*. Springer, Berlin, 2nd edition, 2009. ISBN 9783540888130. URL http://lccn.loc.gov/2008939148.

[21] George P. Sutton and Oscar Biblarz. *Rocket Propulsion Elements*. John Wiley & Sons, New York, 7th edition, 2001. ISBN 0471326429. URL http://lccn.loc.gov/00027334.

[22] Giovanni Vulpetti, Les Johnson, and Gregory L. Matloff. *Solar Sails: A Novel Approach to Interplanetary Travel*. Copernicus Books, New York, 2008. ISBN 9780387344041. URL http://lccn.loc.gov/2008929597.

[23] John R. Lamarsh and Anthony J. Baratta. *Introduction to Nuclear Engineering*. Prentice Hall, Upper Saddle River, 3rd ed. edition, 2001. ISBN 0201824981. URL http://lccn.loc.gov/2001016394.

[24] Dan Gabriel Cacuci. *Handbook of Nuclear Engineering*. Springer, London, 2010. ISBN 9780387981307. URL http://lccn.loc.gov/2010927884.

[25] European Space Agency. ESA - SMART-1, 2007. URL http://www.esa.int/SPECIALS/SMART-1/index.html. Access on the 11th of June 2012.

[26] M. Tajmar and O. Bertolami. Hypothetical gravity control and possible influence on space propulsion. *JOURNAL OF PROPULSION AND POWER*, 21(4):692–696, 2005. URL http://arxiv.org/abs/physics/0412176.

[27] O. Bertolami and F.G. Pedro. Gravity control propulsion: Towards a general relativistic approach. *Journal of the British Interplanetary Society*, 60:285–288, 2007. URL http://arxiv.org/abs/physics/0610116.

[28] Vince Stricherz. Newfangled space-propulsion technology could help clean up Earth orbit, 2012. URL http://phys.org/news/2012-04-newfangled-space-propulsion-technology-earth-orbit.html. Access on the 12th of April 2012.

[29] MicroThrust. MicroThrust, 2011. URL www.microthrust.eu. Access on the 25th of April 2012.

[30] EADS Astrium. Vinci Rocket Engine - Thrust Chamber, 2012. URL http://cs.astrium.eads.net/sp/launcher-propulsion/rocket-engines/vinci-rocket-engine.html. Access on the 12th of March 2012.

[31] Pratt & Whitney Rocketdyne. RL10B-2, 2009. Obtained on the 12 of March 2012.

[32] Pratt & Whitney Rocketdyne. CECE, 2009. Obtained on the 12 of March 2012.

[33] Pratt & Whitney Rocketdyne. Common Extensible Cryogenic Engine (CECE), 2009. URL http://www.pw.utc.com/products/pwr/propulsion_solutions/cece.asp. Access on the 12th of March 2012.

[34] D. L. Black, L. H. Cooper, P. W. Dickson, J. S. Stefanko, and C. Kim. Preliminary study of the NERVA II reactor design. Technical report, National Aeronautics and Space Administration, 1964. URL http://hdl.handle.net/2060/19750070200.

[35] Milton Klein and R. W. Schroeder. Nerva Program Requirements Document, 1970.

[36] The Encyclopedia of Science. NERVA (Nuclear Engine for Rocket Vehicle Application), 2012. URL http://www.daviddarling.info/encyclopedia/N/NERVA.html. Access on the 29th of March 2012.

[37] Hermann Oberth. Ways to Spaceflight. Technical report, National Aeronautics and Space Administration, 1972. URL http://ntrs.nasa.gov/archive/nasa/casi.ntrs.nasa.gov/19720008133_1972008133.pdf.

[38] Howard D. Curtis. *Orbital Mechanics For Engineering Students*. Butterworth-Heinemann, Amsterdam, 2nd edition, 2010. ISBN 9780123747785. URL http://lccn.loc.gov/2010286309.

[39] Jerold W. Emhoff and Iain D. Boyd. Modeling of Total Thruster Performance for NASA‘s Evolutionary Xenon Thruster Ion Optics. *JOURNAL OF PROPULSION AND POWER*, 22(4):741–748, 2006.

[40] National Aeronautics and Space Administration. NASA‘s Evolutionary Xenon Thruster, 2008.

[41] Hans J Leiter, Rainer Killinger, Helmut Bassner, Johann Müller, and Ralf Kukies. Development of the Radio Frequeny Ion Thruster RIT XT - A Status Report. Technical report, Astrium GmbH, Munich, 2001.

[42] EADS Astrium. EADS Astrium Ion Propulsion Systems, 2012. URL http://cs.astrium.eads.net/sp/spacecraft-propulsion/ion-propulsion/index.html. Access on the 12th of March 2012.

[43] Snecma. PPS 1350-G Stationary Plasma Thruster, 2011. Obtained on the 12 of March 2012.

[44] Los Alamos National Laboratory. Periodic Table of Elements: Los Alamos National Laboratory, 2011. URL http://periodic.lanl.gov/4.shtml. Access on the 24th of June 2012.

[45] Kenji Hata. From highly efficient impurity-free CNT synthesis to DWNT forests, CNTsolids and supercapacitors. *Society of Photo-Optical Instrumentation Engineers*, 2007. URL http://www.nanocarbon.jp/english/research/image/review.pdf.

[46] Barrie William Jones. *Life in the Solar System and Beyond*. Springer, Chichester, U.K., 2004. ISBN 1852331011. URL http://lccn.loc.gov/2003067313.

[47] National Institute of Standards and Technology. Atomic Weights and Isotopic Compositions for All Elements, 2011. URL http://physics.nist.gov/cgi-bin/Compositions/stand_alone.pl. Access on the 24th of June 2012.

[48] C. W. Forsberg, C. M. Hopper, J. L. Richter, and H. C. Vantine. Definition of Weapons-Usable Uranium-233. Technical Report March, Oak Ridge National Laboratory, Oak Ridge, Tennessee, 1998. URL http://www.ornl.gov/sci/radiation_transport_criticality/HopperPubs/DefWeaponsUsableU-233ORNLTM13517.pdf.

[49] R. D. Mosteller. Detailed Reanalysis of a Benchmark Critical Experiment: Water-Reflected Enriched-Uranium Sphere. In Los Alamos National Laboratory, editor, *Annual Meeting of the American Nuclear Society*, Los Alamos, NM, 1994. URL http://www.osti.gov/bridge/servlets/purl/10120434-rruwqp/native/10120434.pdf.

[50] SpaceRef Interactive Inc. Space Shuttle and International Space Station User's Guide, 2012. URL http://www.spaceref.com/iss/. Access on the 15th of August 2012.

[51] Jet Propulsion Laboratory. Mars Reconnaissance Orbiter, 2010. URL http://mars.jpl.nasa.gov/mro/. Access on the 20th of April 2012.

[52] Jet Propulsion Laboratory. Mars Science Laboratory, 2011. URL http://mars.jpl.nasa.gov/msl/. Access on the 20th of April 2012.

[53] Jill L. H. Prince, Richard W. Powell, and Dan Murri. Autonomous Aerobraking: A Design, Development, And Feasibility Study. Technical report, NASA Langley Research Center, Hampton, 2011. URL http://ntrs.nasa.gov/archive/nasa/casi.ntrs.nasa.gov/20110014523_2011015083.pdf.

[54] European Space Agency. ESA Science & Technology: Mars Express, 2012. URL http://sci.esa.int/science-e/www/area/index.cfm?fareaid=9. Access on the 20th of April 2012.

[55] Jet Propulsion Laboratory. Mars Odyssey, 2011. URL http://mars.jpl.nasa.gov/odyssey/. Access on the 20th of April 2012.

[56] Jet Propulsion Laboratory. Mars Science Laboratory - Curiosity Rover, 2011. URL http://mars.jpl.nasa.gov/msl/. Access on the 20th of April 2012.

[57] Peter Fortescue, John Stark, and Graham Swinerd. *Spacecraft Systems Engineering*. Wiley, Hoboken, N.J, 4th ed. edition, 2011. URL http://lccn.loc.gov/2011015486.

[58] Charles D. Brown. *Elements of Spacecraft Design*. American Institute of Aeronautics and Astronautics, Inc., Reston, VA, 2002. ISBN 1563475243. URL http://lccn.loc.gov/2002010232.

[59] LaSpace. Fregat, 2002. URL http://www.laspace.ru/rus/fregat_construction.php. Access on the 12th of April 2012.

[60] Eric W. Weisstein. Torispherical Dome, 2012. URL http://mathworld.wolfram.com/TorisphericalDome.html. Access on the 12th of April 2012.

[61] ASTRIUM Space Transportation. Propellant Tanks for Spacecraft, 2010. URL www.space-propulsion.com.

[62] National Aeronautics and Space Administration. The External Tank, 2006. URL http://www.nasa.gov/returntoflight/system/system_ET.html. Access on the 12th of April 2012.

[63] The MathWorks Inc. Linear Regression, 2012. URL http://www.mathworks.com/help/techdoc/data_analysis/f1-5937.html.

[64] Emcore Corporation. ZTJ Photovoltaic Cell Datasheet, 2011. URL http://www.emcore.com/assets/photovoltaics/ZTJ_datasheet.pdf.

[65] Robert M. Haberle, Christopher P. Mckay, James B. Pollack, Owen E. Gwynne, David H. Atkinson, Joseph Appelbaum, Geoffrey A. Landis, Richard W. Zurek, and Dennis J. Flood. Atmospheric Effects On The Utility Of Solar Power On Mars. *Resources of Near-Earth Space*, pages 845–885, 1993. URL http://www.uapress.arizona.edu/onlinebks/ResourcesNearEarthSpace/resources30.pdf.

[66] Roger R. Bate, Donald D. Mueller, and Jerry E. White. *Fundamentals of Astrodynamics*. Dover Publications, New York, 1971. URL http://lccn.loc.gov/73157430.

[67] Cl Ranieri and Ca Ocampo. Indirect Optimization of Three-Dimensional Finite-Burning Interplanetary Transfers Including Spiral Dynamics. *Journal of guidance, control, and dynamics*, 32(2):445–455, March 2009. ISSN 0731-5090. doi: 10.2514/1.38170. URL http://doi.aiaa.org/10.2514/1.38170http://cat.inist.fr/?aModele=afficheN&cpsidt=21654189.

[68] Ernst Hairer, Gerhard Wanner, and Syvert P. Nø rsett. *Solving Ordinary Differential Equations I: Non-stiff Problems*. Springer, London, 2nd edition, 2009. ISBN 9783642051630. URL http://lccn.loc.gov/2009939073.

[69] David R. Williams. Planetary Fact Sheets, 2005. URL http://nssdc.gsfc.nasa.gov/planetary/planetfact.html. Access on the 12th of April 2012.

[70] Bruce A. Conway, editor. *Spacecraft Trajectory Optimization*. Cambridge University Press, New York, 2010. ISBN 9780521518505. URL http://lccn.loc.gov/2010025018.

[71] Luca Derosa and Claudio Maccone. Propulsion tradeoffs for a mission to Alpha Centauri. *Acta Astronautica*, 60(8-9):711–718, April 2007. ISSN 00945765. doi: 10.1016/j.actaastro.2006.10.003. URL http://linkinghub.elsevier.com/retrieve/pii/S0094576506003894.

[72] The Planetary Society. Nuclear Space Initiative: A Planetary Society White Paper, 2005. URL http://www.planetary.org/action/opinions/nuclear_propulsion_0505.html.

Appendix A

Trajectory Problem Annexes

A.1 Runge-Kutta-Fehlberg Coefficients

The coefficients for the RKF7(8) are:

$$a = \begin{Bmatrix} 0 & 2/27 & 1/9 & 1/6 & 5/12 & 1/2 & 5/6 & 1/6 & 2/3 & 1/3 & 1 & 0 & 1 \end{Bmatrix}$$

$$b = \begin{bmatrix} 0 & 0 & 0 & 0 & 0 & 0 & 0 & 0 & 0 & 0 & 0 & 0 \\ 2/27 & 0 & 0 & 0 & 0 & 0 & 0 & 0 & 0 & 0 & 0 & 0 \\ 1/36 & 1/12 & 0 & 0 & 0 & 0 & 0 & 0 & 0 & 0 & 0 & 0 \\ 1/24 & 0 & 1/8 & 0 & 0 & 0 & 0 & 0 & 0 & 0 & 0 & 0 \\ 5/12 & 0 & -25/16 & 25/16 & 0 & 0 & 0 & 0 & 0 & 0 & 0 & 0 \\ 1/20 & 0 & 0 & 1/4 & 1/5 & 0 & 0 & 0 & 0 & 0 & 0 & 0 \\ -25/108 & 0 & 0 & 125/108 & -65/27 & 125/54 & 0 & 0 & 0 & 0 & 0 & 0 \\ 31/300 & 0 & 0 & 0 & 61/225 & -2/9 & 13/900 & 0 & 0 & 0 & 0 & 0 \\ 2 & 0 & 0 & -53/6 & 704/45 & -107/9 & 67/90 & 3 & 0 & 0 & 0 & 0 \\ -91/108 & 0 & 0 & 23/108 & -976/135 & 311/54 & -19/60 & 17/6 & -1/12 & 0 & 0 & 0 \\ 2383/4100 & 0 & 0 & -341/164 & 4496/1025 & -301/82 & 2133/4100 & 45/82 & 45/164 & 18/41 & 0 & 0 \\ 3/205 & 0 & 0 & 0 & 0 & -6/41 & -3/205 & -3/41 & 3/41 & 6/41 & 0 & 0 \\ -1777/4100 & 0 & 0 & -341/164 & 4496/1025 & -289/82 & 2193/4100 & 51/82 & 33/164 & 19/41 & 0 & 1 \end{bmatrix}$$

$$c^* = \begin{Bmatrix} 0 & 0 & 0 & 0 & 0 & 34/105 & 9/35 & 9/35 & 9/280 & 9/280 & 0 & 41/840 & 41/840 \end{Bmatrix}$$

$$c = \begin{Bmatrix} 41/840 & 0 & 0 & 0 & 0 & 34/105 & 9/35 & 9/35 & 9/280 & 9/280 & 41/840 & 0 & 0 \end{Bmatrix}$$

A.2 Validation

In this section graphics of the problem validation are presented.

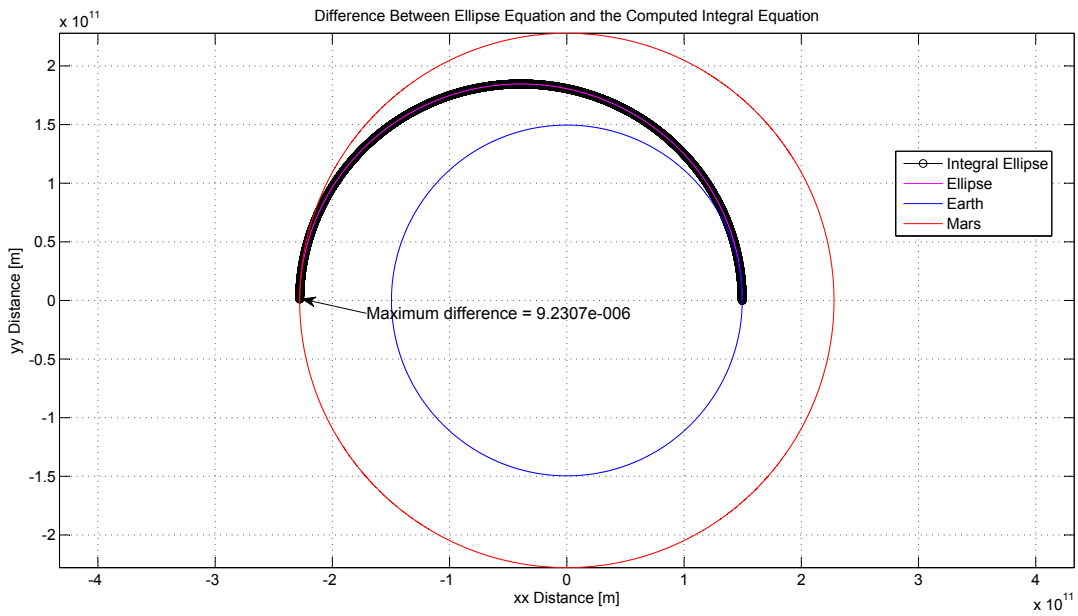

(a) Earth to Mars Hohmann Elliptical Transfer.

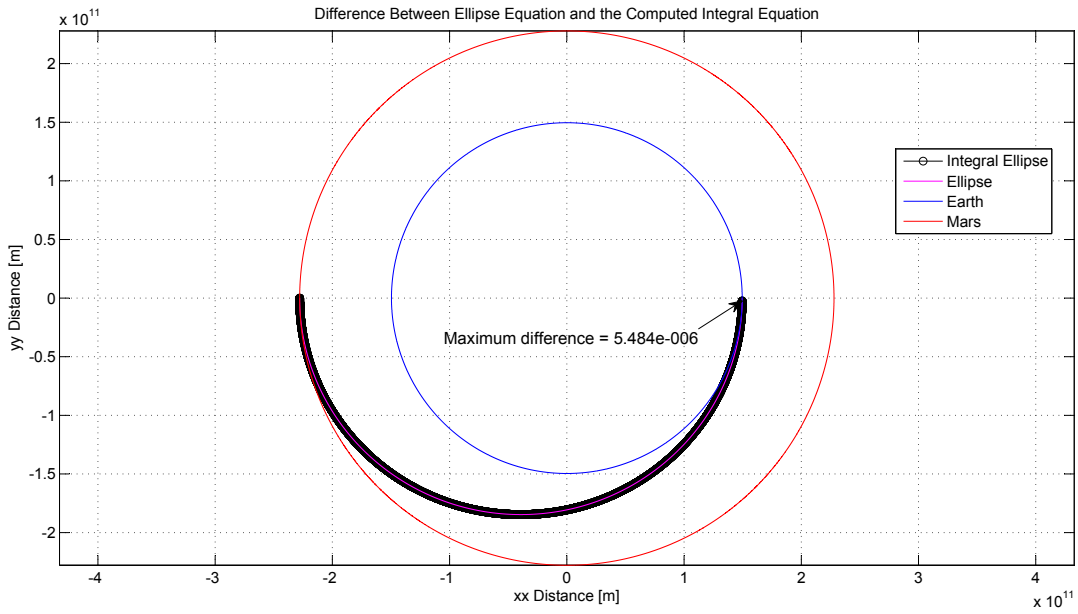

(b) Mars to Earth Hohmann Elliptical Transfer.

Figure A.1 Difference between the ellipse equation and the computed integral equation.

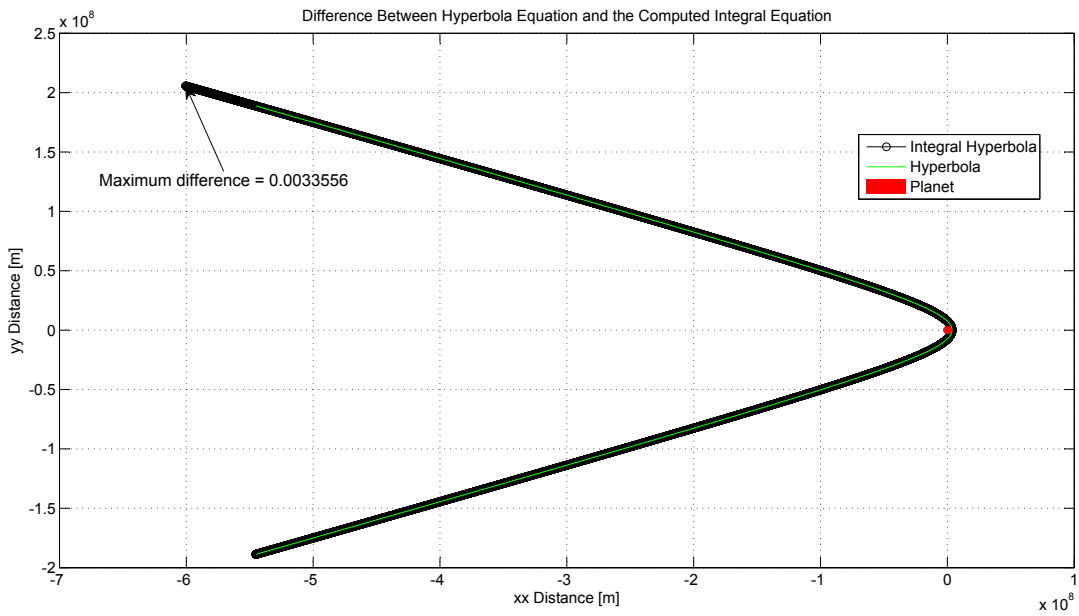

Figure A.2 Difference between the hyperbolic equation and the computed integral equation.

A.3 MATLAB Code

In this section the code developed in MATLAB® for the numerical integration is presented. Some of the code was adapted from [38].

```
function [tout, yout, h, end_type] = Runge_Kutta(method, constants, spacecraft_engine, ...
    initial_vector, initial_time, stop_dim, tolerance)
% This function solves computes the trajectory using the
% Runge-Kutta-Fehlberg method.
% Inputs:
%   method - Runge-Kutta-Fehlberg method to use (RKF4(5) or RKF7(8))
%   constants - Vector containing the gravitational parameter of the
%     central body ([m^3/s^2]) and Earth gravity at sea level ([m/s^2])
%   spacecraft_engine - vector with characteristics of the engine (thrust
%     [N], Isp [s] or Power [W], fuel type and thrust direction [rad])
%   initial_vector - vector with initial position [m], velocity [m/s] and
%     mass [kg] of the spacecraft
%   initial_time - vector with the initial time ([s]) and step
%   stop_dim - maximum time [s]
%   tolerance - tolerance for an accepted step
% Outputs:
%   tout - final time [s]
%   yout - vector with final position [m], velocity [m/s] and mass [kg] of
%     the spacecraft
% User M-functions required: derivatives and step_update

% Author: André Guerra (N° 54763)
```

```
% Instituto Superior Técnico, Mestrado Integrado de Engenharia Aeroespacial
% email address: andre.guerra@ist.utl.pt
% April 2012; Last revision: June 2012
%------------- BEGIN CODE --------------
%% Number of Arguments
N_arg = 6;

%% Coefficients Vector/Matrix
a_45 = [0 1/4 3/8 12/13 1 1/2];
a_78 = [0 2/27 1/9 1/6 5/12 1/2 5/6 1/6 2/3 1/3 1 0 1];

b_45 = [    0          0         0         0        0
           1/4         0         0         0        0
           3/32       9/32       0         0        0
        1932/2197 -7200/2197 7296/2197     0        0
         439/216      -8     3680/513  -845/4104    0
          -8/27        2    -3544/2565 1859/4104 -11/40];

b_78 = [     0       0       0       0          0           0         0         0       0 ...
           0     0  0
            2/27     0       0       0          0           0         0         0       0 ...
                       0     0  0
            1/36    1/12     0       0          0           0         0         0       0 ...
                       0     0  0
            1/24     0     1/8       0          0           0         0         0       0 ...
                       0     0  0
            5/12     0   -25/16   25/16        0           0         0         0       0 ...
                       0     0  0
            1/20     0       0      1/4        1/5          0         0         0       0 ...
                       0     0  0
          -25/108    0       0    125/108    -65/27      125/54      0         0       0 ...
                     0     0  0
           31/300    0       0       0        61/225      -2/9      13/900      0       0 ...
                     0     0  0
             2       0       0    -53/6      704/45     -107/9      67/90       3       0 ...
                       0     0  0
          -91/108    0       0     23/108   -976/135     311/54    -19/60     17/6    -1/12 ...
                   0     0  0
         2383/4100   0       0   -341/164   4496/1025   -301/82   2133/4100   45/82   ...
             45/164   18/41   0  0
            3/205    0       0       0          0         -6/41     -3/205    -3/41    3/41 ...
                    6/41   0  0
        -1777/4100   0       0   -341/164   4496/1025   -289/82   2193/4100   51/82   ...
            33/164   19/41   0  1];

c4 = [25/216 0 1408/2565   2197/4104  -1/5   0];
c5 = [16/135 0 6656/12825 28561/56430 -9/50 2/55];

c7 = [41/840   0   0   0   0   34/105  9/35  9/35  9/280  9/280  41/840   0       0];
```

```
c8 = [  0      0   0   0   0   34/105  9/35  9/35  9/280  9/280    0    41/840  41/840];

%% Method to use (RKF4(5) or RKF7(8))
if method == 45
    a = a_45;
    b = b_45;
    cp_1 = c4;
    cp = c5;
    p = 5;
    stage = 6;
else
    a = a_78;
    b = b_78;
    cp_1 = c7;
    cp = c8;
    p = 8;
    stage = 13;
end

%% Tolerance
if nargin < N_arg
    tol = 1.e-8;
else
    tol = tolerance;
end

%% Variables
% Time and Position
t = initial_time(1);
y = initial_vector;

% Initial Step
h = initial_time(2);

% Maximum time
tf = stop_dim(1);

% Derivatives vector
f = zeros (7,stage);

%% Integration
while t < tf
    t_iter = t;
    y_iter = y;

    %% Evaluate time derivatives at each stage
    for i = 1:stage
        t_i = t_iter + a(i)*h;
        y_i = y_iter;
```

```
        for j = 1:i-1
            y_i = y_i + h*b(i,j)*f(:,j);
        end

        f(:,i) = derivatives(constants,spacecraft_engine,t_i, y_i);
    end

    %% Compute maximum truncation error
    % Difference between (p)th and (p+1)th order solutions
    e = h*f*(cp_1' - cp');
    % Maximum
    e_max = max(abs(e));

    %% Compute allowable truncation error
    ymax = max(abs(y));
    e_allowed = tol*max(ymax,1.0);

    %% Compute fractional change in step size
    Δ = (e_allowed/(e_max + eps))^(1/5);

    %% If the truncation error is in bounds -> update the solution
    if e_max ≤ e_allowed
        t = t + h;
        y = y_iter + h*f*cp';

        % Time and Position Output
        tout = t;
        yout = y;

        % Update the Step
        facmax = 1.5;
        h = step_update(p, e_allowed, facmax, Δ, t, h, tolerance);

        % End Function Type
        end_type = 'Good';
        return;
    else
        % Update the Step
        facmax = 1;
        h = step_update(p, e_allowed, facmax, Δ, t, h, tolerance);
    end
end

%% Verification
if t ≥ tf
    fprintf('\n\n Warning: End time inputed reached! Time = %g s = %g days\n\n', t, ...
        ((t/3600)/24));
    end_type = 'Over_time';
```

```
    tout = 0;
    yout = 0;
end
end
%------------- END OF CODE --------------
```

```
function dfdt = derivatives(constants,spacecraft_engine,f)
% This function computes the derivatives for the Runge-Kutta-Fehlberg.
% Inputs:
%   constants - Vector containing the gravitational parameter of the
%     central body ([m^3/s^2]) and Earth gravity at sea level ([m/s^2])
%   spacecraft_engine - vector with characteristics of the engine (thrust
%     [N], Isp [s] or Power [W], fuel type and thrust direction [rad])
%   f - vector with position [m], velocity [m/s] and mass [kg]
% Outputs:
%   dfdt - vector with derivatives value
% User M-functions required: none

% Author: André Guerra (Nº 54763)
% Instituto Superior Técnico, Mestrado Integrado de Engenharia Aeroespacial
% email address: andre.guerra@ist.utl.pt
% April 2012; Last revision: June 2012
%------------- BEGIN CODE --------------
%% Constants
mu = constants(1); % Gravitational Parameter [m^3/s^2]
g0 = constants(2); % Earth Gravity at Sea Level [m/s^2]

% Spacecraft
T = spacecraft_engine(1);           % Thrust [N]
Type = spacecraft_engine(3);        % Engine type
if Type == 1
    Isp = spacecraft_engine(2);     % Isp [s]
else
    Power = spacecraft_engine(2);   % Power [W]
end
% If specified use a certain angle on the thrust direction
if size(spacecraft_engine,2) ~= 3
    teta = spacecraft_engine(4);    % Thrust Direction [rad]
end

%% Position [m]
x = f(1);
y = f(2);
z = f(3);

%% Velocity [m/s]
vx = f(4);
vy = f(5);
vz = f(6);
```

```
%% Mass [kg]
m = f(7);

%% Norms of position and velocity
r = norm([x y z]);
v = norm([vx vy vz]);

%%  Acceleration (F = m a)
if size(spacecraft_engine,2) ~= 3   % If a certain angle was specified
    if size(spacecraft_engine,1) ~= 1   % A fix angle to the Sun
        dir_T = (([cos(teta), -sin(teta), 0; sin(teta), cos(teta), 0; 0, 0, 1])*[0 ...
            spacecraft_engine(2,1) 0].');
    else                                % An angle to spacecraft velocity
        dir_T = (([cos(teta), -sin(teta), 0; sin(teta), cos(teta), 0; 0, 0, 1])*[vx vy ...
            vz].').'/v;
    end
    ax = -mu*x/r^3 + T/m*(dir_T(1));
    ay = -mu*y/r^3 + T/m*(dir_T(2));
    %az = -mu*z/r^3 + T/m*vz/v;
    az = 0;
else
    ax = -mu*x/r^3 + T/m*vx/v;
    ay = -mu*y/r^3 + T/m*vy/v;
    %az = -mu*z/r^3 + T/m*vz/v;
    az = 0;
end

%% Mass
if Type == 1    % Engine which expels mass
    mdot = -abs(T)/(g0*Isp);
else            % Nuclear engine
    mdot = -(Power*(1/(3600*24)))/(950e9)*1e3;
    %     mdot = 0;
end

%% Return Values
dfdt = [vx vy vz ax ay az mdot]';
end
%------------- END OF CODE --------------
```

```
function h_new = step_update(p, e_allowed, facmax, Δ, t, h_old, tolerance)
% This updates the step for the Runge-Kutta-Fehlberg.
% Inputs:
%   p - maximum order of the Runge-Kutta-Fehlberg
%   e_allowed - allowable truncation error
%   facmax - maximum growth factor
%   Δ - fractional change in step size
%   t - time [s]
```

```
%   h_old - old step
%   tolerance - tolerance for an accepted step
% Outputs:
%   h_new - new step
% User M-functions required: none

% Author: André Guerra (Nº 54763)
% Instituto Superior Técnico, Mestrado Integrado de Engenharia Aeroespacial
% email address: andre.guerra@ist.utl.pt
% April 2012; Last revision: June 2012
%------------- BEGIN CODE --------------
%% Minimum Step
hmin = 16*eps(t);

%% Above and bellow interval limits
int_min = 1-e_allowed;
int_max = 1+e_allowed;

%% Growth factor
if (Δ*0.25^(1/p) < int_min && Δ < 1) || (Δ*0.25^(1/p) > int_max && Δ > 1)
    factor = Δ*0.25^(1/p);
elseif (Δ*0.38^(1/p) < 1 && Δ < 1) || (Δ*0.38^(1/p) > int_max && Δ > 1)
    factor = Δ*0.38^(1/p);
elseif (Δ*0.8 < 1 && Δ < 1) || (Δ*0.8 > int_max && Δ > 1)
    factor = Δ*0.8;
elseif (Δ*0.9 < 1 && Δ < 1) || (Δ*0.9 > int_max && Δ > 1)
    factor = Δ*0.9;
else
    factor = Δ;
end

%% Step Update
if h_old > 0
    if tolerance == 1.e-11
        h_new = min(min(h_old*factor, h_old*facmax), 1e3);
    else
        h_new = min(h_old*factor, h_old*facmax);
    end
elseif h_old < 0
    h_new = max(h_old*factor, h_old*facmax);
end

%% Minimal Condition Verification
if abs(h_new) < hmin
    fprintf('\n\n Warning: Step size fell below its minimum\n allowable value (%g) at time ...
        %g.\n\n', hmin, t)
end
end
%------------- END OF CODE --------------
```